

Chapter 2

Core Monitoring

Abstract Reactor parameters subjected to limitations are continually monitored. Reactor operation is based on a number of parameters characterizing the distribution of coolant temperature, power profiles in the fuel assemblies, power density distribution. In-core instrumentation supplies raw data, which are processed, and finally reactor operator is provided with maps and logs. The present chapter describes detection methods, the elaboration of the detector signals, and the main steps of signal processing. The presented methods are used typically in pressurized water reactors (PWRs) and boiling water reactors. The emphasis is on the applied mathematical and physical methods as well as considerations.

For a given reactor type, an operational envelop is defined. In the operational envelop, limit values are given for all measurable reactor parameters, and core monitoring continually records the operational parameters subjected to limitation, thus making it possible to enunciate if a parameter is approaching or exceeding its limit value. The number of implementable measurements is limited by technology.

Limit violation must be observed at any location inside the reactor core although there are technical constraints on the number of implementable in-core measurements. Limit violation is rarely detected directly, at most a reasonable estimation can be given based on the measured values. Safe operation sets the critical power ratio (CPR), see (2.106), which can be estimated from the maximal power in a fuel pin. The instrumentation supplies temperature rise and power release in measured assemblies. But an assembly may host more than a hundred of fuel pins, thus there is a power profile inside an assembly. Chapter 4 discusses how can the analyst use the computational model to acquire various corrections on the measured values to estimate the maximal value from the measured value.

Usually the cold leg temperature of each loop of the primary circuit is measured yet the coolant temperature entering a fuel assembly is not known exactly. At most a mixing matrix is given which specifies the contributions of the loops to the entering flow rate of a given assembly. As a consequence, the individual entering temperature of a fuel assembly is known only approximately.

The power distribution in the core is well approximated by the solution of the actual diffusion equation; in the diffusion equation fuel assemblies are represented by homogenized fuel assemblies. The diffusion code is validated against measurements.

Notwithstanding, the actual core parameters (reactor power, actual control rod positions, actual boron concentration, assembly-wise coolant flow rates and burnups to mention a few) should always be known in a power plant. A calculated power distribution of the actual core makes a good service in restoring the power distribution in the entire core from the measured values.

The problem of restoring the power distribution is actually an interpolation problem. First we need to find suitable and effective interpolating functions. The next step is to establish an interpolation method tailored to the given reactor type, and finally the interpolation should be adjusted to the actual reactor state. The related problems are discussed in the next three Sections.

Safety limits concern with thermal hydraulics (e.g. temperature increase in an assembly or in a sub-channel) and neutronics (e.g. power local density and burnup). But other info, like trends of given parameters, or distributions in the core, may be also relevant for the operator.

2.1 Role of Models in Reactor Operation

A power reactor is similar to other devices of contemporary industry: a complex structure is built so that by appropriate cooperation of its parts make it capable of completing a given function. There are, however, remarkable differences:

1. the used materials should be described in unprecedented details, for example the material composition should be given including the isotopic composition.
2. the components should work on an unprecedented wide time scale, from milliseconds to several weeks.
3. the interacting components are described by a wide range of sciences, including branches of mathematics, physics, and several modern engineering sciences.

One may like or dislike but science works with models, and results obtained from a model are applicable only within the range of the model. Furthermore, most models involve parameters and constants to be determined by experiments.

Under the mentioned circumstances, we have no other choice but the validation and verification (V & V) of the models against measurements. We deal only with the topics directly connected to reactor operation and within that solely with the relationship of the calculational model and the in-core measurements. The calculational model is the subject of Chap. 4, here we gratify with the input-output aspect of the computational model, which is a computer program transforming input into output. Evidently input should describe the reactor, the output should provide technical data needed for reactor operation.

Input data are classified as quantities describing reactor components (e.g. geometry, material composition and property) and parameters depending on the actual

state of the reactor. To be specific, the parameters include W -the actual power of the reactor, c_B -the boric acid concentration, H_c -position of the control rods, B -burnup level. As to the coolant, when mentioned, the inlet temperature T_{in} , the exit temperature T_{out} and the coolant flow rate G may be used. When speaking of loop data, the mentioned quantities are supplied by a loop subscript. The reactor model takes the following symbolic form:

$$\mathbf{y} = \mathbf{f}(\mathbf{x}), \quad (2.1)$$

meaning that the reactor model maps the input data \mathbf{x} into the output \mathbf{y} when the reactor is in stationary regime. Except Sect. 4.4.2.1 in Chap. 4, throughout the present work we deal with the stationary regime.¹

The analysis should be prepared for two aspects. The first one is the uncertainty of the input data. If a data is measured, like c_B or W , the result of a measurement is a random variable, with a given mean value and variance. The former is considered as “THE MEASURED” value, the latter as the error of the measurement. Another problem is that the measurement takes place in a noisy industrial ambience, after electronic processing of the measured signal, and the measured value may be in error, and, the functional relation between \mathbf{x} and \mathbf{y} is often of approximate nature. It is more realistic to replace (2.1) with

$$\eta = \phi(\xi), \quad (2.2)$$

where Greek letters stand for random counterparts of the deterministic variables.

The first thing in this situation is to ensure that we are on the right track. To this and we need a large number of observations, handle input, output, and model as random and to see the statistics if it supports the correctness of our model. This step is called verification and validation $V\&V$. After $V\&V$, we have a reliable model with estimated mean values and variances. It should be noted that the validation is valid only to a given interval of the input and the output. Physical considerations help judge if a given change is outside the validity range.

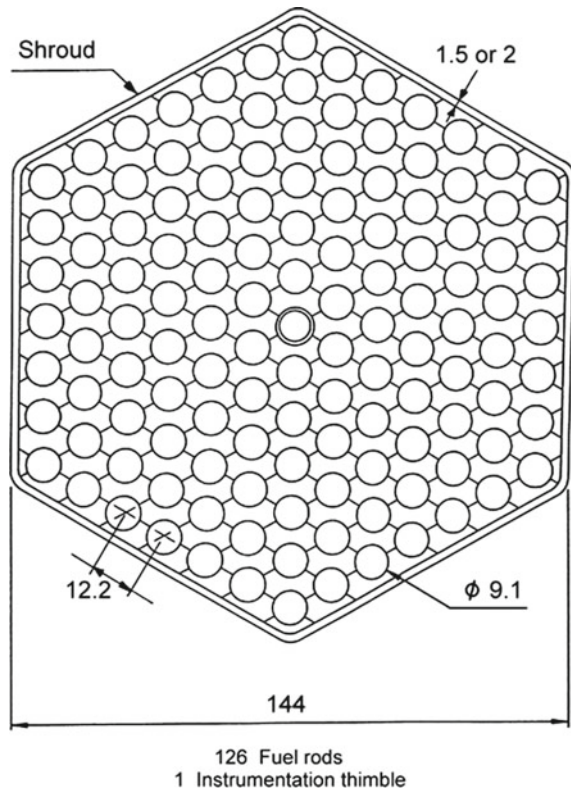
In reactor operation, the question is if a reactor state used in the calculational model accords with the actual state of the core.

2.2 Basic Functions and Services of Core Monitoring Systems

A nuclear reactor core consists of interchangeable fuel assemblies thus the outer geometry of assemblies must be the same whereas the internal geometries and material compositions may differ. The reactor core is surrounded by a reflector region to reduce the number of neutrons escaping the core. There are two types of

¹The in-core system samples the data with cycle time ~ 1 s, so the reactor can be considered as stationary most of the time.

Fig. 2.1 Hexagonal fuel assembly



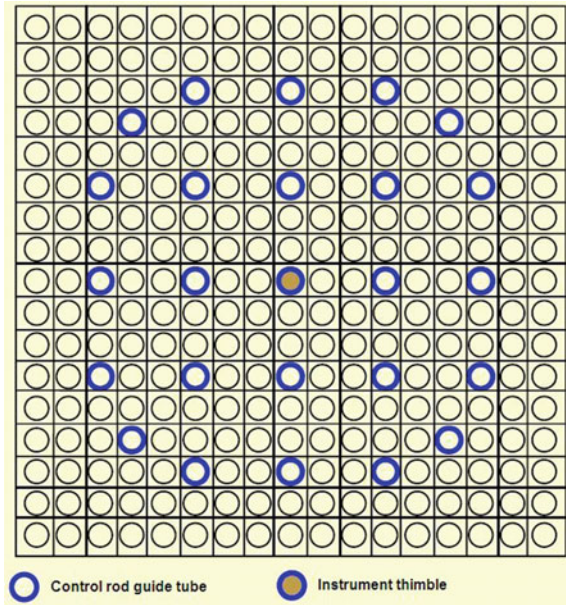
assemblies, the first one is called fuel assembly, it contains fuel pins arranged in a regular geometry. A fuel pin is surrounded by coolant, which is usually water. The second assembly type is called control assembly because it contains neutron absorbing material, usually a boron compound, e.g. borated steel or boron carbide.

If an assembly is equipped with measurement, the detector material is placed in a tube positioned at the geometrical center of the assembly. That tube contains also the cable forwarding the detector signals to electronic processing. Usually control assemblies do not host any detector or other measurement support. Fuel assemblies often form a regular hexagonal or square pile, see Figs. 2.1. and 2.2.

The basic functions of a core monitoring are as follows:

1. To give a realistic estimate of the assembly power distribution;
2. To give a realistic estimate of the pin power distribution in any given assembly;
3. To estimate the DNBR value, see Sect. 2.3.9, in any fuel assembly;
4. To estimate the assembly power for any assembly;
5. To provide parameters needed for the reactor operation;
6. To detect departure from the planned operation.

Fig. 2.2 Square fuel assembly, see Ref. [12]



Core monitoring data are usually shown on displays in a form easily comprehensible for the operators.

Throughout the following two Subsections, we are using several terms relating calculated and measured quantities in a reactor core. The basic terms are used in the sense given in Ref. [19], including cell, assembly, supercell, calculation of neutron flux or power distribution.

In connection with measured values, one should mention the accuracy of the measured value. The terminology to be applied throughout the present work is standard but for the readers' convenience a short summary is given in Sect. 6.2.1 of Chap. 6.

2.2.1 SPN Detectors (SPNDs)

We start with the interpretation of the measurement. The detector wire produces electric charge due to nuclear reactions. The detector material should absorb a neutron from the neutron gas in the assembly, and emit charged particle when nucleus formed after neutron absorption decays. Detector materials may include among others rhodium, platinum, vanadium. Typically several isotopes of a given detector material absorb neutrons, see Fig. 2.3, where decays of rhodium isotopes are shown. As we see, isotope ^{103}Rh absorbs neutrons resulting in two possible excited states: 7% forms an excited state of ^{104m}Rh , which is a meta stable nucleus and releases its excess energy in two ways: 0.18% in two steps emits a β particle to arrive at

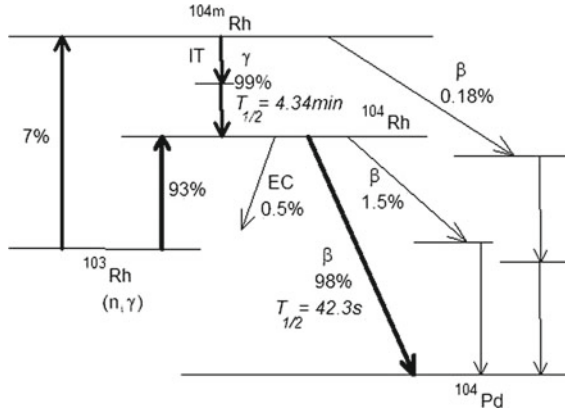


Fig. 2.3 Decay scheme of rhodium isotopes

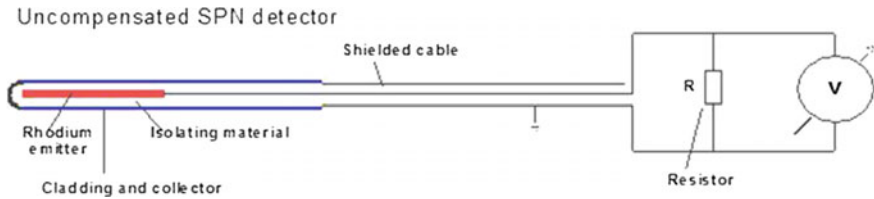


Fig. 2.4 Scheme of SPND detector

the ground state of nucleus ^{104}Pd . On the other branch, ^{104}Rh emitting a β particle reaches the ground state of nucleus ^{104}Pd . Note the β particle is emitted after 42 s delay.

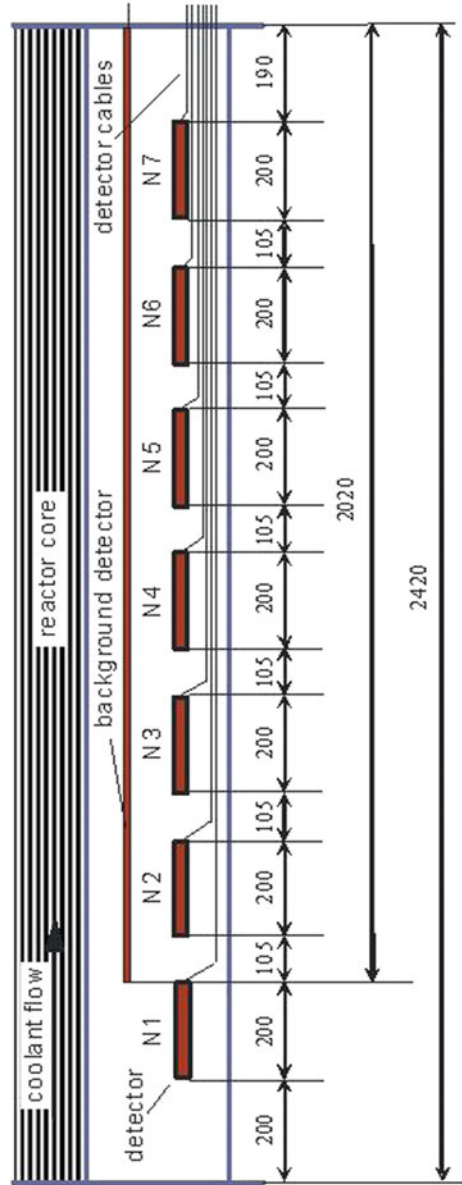
Detectors are usually arranged into chains, as in a PWR, like the VVER-440/213 reactor. The scheme of the detector is shown in Fig. 2.4, the detector itself is placed in a tube, see Fig. 2.5. The SPND requires a given volume, usually it is implemented in the central tube of the fuel assembly. In VVER-440, an SPND has seven detectors positioned equidistantly, plus a cable to measure the current induced outside the detector. The tube is separated into two parts by a stainless steel positioning plate, the upper part in Fig. 2.5 hosts the cable of detector No. 7, the lower part hosts the cables of detectors No. 1–6, and a cable.

From the SPND current, the number of absorptions per unit time can be estimated. Let Σ_d be the detector cross-section, Φ the neutron flux at the detector, then the current I_d is given by

$$I_d = \int_{V_d} \int_E \Sigma_d(\mathbf{r}, E) \Phi(\mathbf{r}, E) dE d\mathbf{r}. \quad (2.3)$$

Note, that here Φ is the neutron flux at the detector and not the average flux of the assembly, see Sect. 2.3.7. The assembly power ψ_{ass} is

Fig. 2.5 Geometry of the SPND detector



$$\psi_{ass} = \sum_{k=1}^{N_{pin}} \int_{V_k} \int_E \psi_k(\mathbf{r}, E) dE d\mathbf{r}. \quad (2.4)$$

The number of fuel cells in an assembly is large $N_{pin} \gg 1$. Flux and power are related as

$$\Psi_k(\mathbf{r}, E) = \Sigma_f(\mathbf{r}, E) \varepsilon \Phi(\mathbf{r}, E) \quad (2.5)$$

where $\Sigma_f(\mathbf{r}, E)$ is the fission cross-section, ε is the amount of energy released in a fission act. Unfortunately $\Sigma_f(\mathbf{r}, E)$ and ε differ for various fissionable isotopes, and being macroscopic data, depend on the nuclide density distribution within a fuel pin. The isotope composition varies in time and also varies with the power level. To cut the Gordian knot, a linear relation is assumed between assembly power Ψ_{ass} and detector current I_d :

$$\Psi_{ass} = C(\mathbf{p}) I_d, \quad (2.6)$$

and the conversion factor $C(\mathbf{p})$ is assumed to depend on a parameter vector \mathbf{p} . The following parameters are usually included in \mathbf{p} : reactor power, control rod position, boron concentration, isotope composition of the fuel. The actual form of function $C_{i,j}(\mathbf{p})$ is determined by fitting a suitable function to observed assembly powers as function of detector currents at various situations.

The following expression is minimized:

$$\sum_{i,j} (\Psi_{ass,i,j} - C_{i,j}(\mathbf{p}) I_{d,i,j})^2 = \min_{C_{i,j}}. \quad (2.7)$$

Here the data base is subdivided into classes, which are similar with respect to the detector current I_d and assembly power Ψ_{ass} , a given class is identified by subscripts i, j . Expert eyes are needed to choose appropriate classes and to classify the operational data. As a given unit operates, the data base is enlarged by novel operational data, and the fitting is repeated from time to time.

The main function of the SPND is to provide information on²:

1. the axial power distribution in the reactor core;
2. the maximal, axial power peaking factor k_z , see Eq. (2.14);
3. the assembly power peaking factor k_q , see Eq. (2.15);
4. the 3D power peaking factor k_v , see Eq. (2.16);
5. a check on power asymmetry in the core.

Combining k_q , k_k , and k_z , one obtains an estimate for the maximal power density and the CRP, which is an important design safety criterion.

An alternative solution is the aeroball system. The current generated by the beta particles is transmitted to be processed, more precisely: noise filtering and amplifying. Further details are given in Sect. 2.3.

²The equations to be quoted below refer to assembly No. i , added as a subscript to the corresponding expression.

2.2.2 *In-core Temperature Measurements*

Local temperatures in the core are not measured directly but in a number of positions coolant exit temperatures are measured. Supplementing that information with the axial power distribution from the SPND data, one obtains an estimate of main features of the heat transfer process to be discussed in Sect. 2.3.9.

A thermocouple exploits the thermoelectric effect. When a conductor is subjected to a thermal gradient, it will generate a voltage. This phenomenon is termed the thermoelectric effect or Seebeck effect [10, 11]. Measuring this voltage necessarily involves connecting another conductor to the “hot” leg. Thus a thermocouple is connected to a reference “cold” leg of temperature T_0 , and to the site where temperature T is to be measured (hot leg). The metal connecting the hot leg to the cold leg will experience a temperature gradient, and for a given metal, the voltage and the temperature difference are in a known functional relationship. Over the typical temperature range in a reactor, the thermal voltage U is a cubic function of the temperature difference $(T - T_0)$:

$$U(T) = A_1(T - T_0) + A_2(T - T_0)^2 + A_3(T - T_0)^3. \quad (2.8)$$

Coefficients A_i are determined in a calibration step.

In a power reactor the thermocouple should, obviously, be resistant to neutron radiation. In the core, the spatial variation of the gamma radiation is less than, for example, that of the thermal neutron flux. That observation has lead to a so-called gamma-temperature measurement method.

The γ thermometer (GT) is a solid stainless steel rod with argon-filled annular chambers located at various levels. Differential thermocouples are embedded in the rod at each level so that a temperature difference, proportional to the gamma flux impinging on the rod, is effected between the thermocouple junctions. The gamma thermometer consists of a hollow, cylindrical stainless steel rod of length roughly equal to the reactor core height.

Annuli of material are removed at intervals along the rod, and a cladding is swaged onto the exterior in an inert atmosphere. The thermocouple set and associated leads are contained in the rods central core. Basically, the idea behind the dual-purpose application of the gamma thermometer is to utilize the temperature difference between the hot and cold junctions as an indication of the local heat generation rate, and to utilize the shape of the temperature distribution to infer the thermal hydraulic environment exterior to the device.

To determine the thermal power of assembly k we calculate the (thermal) enthalpy rise W_k^T by (2.73) that we repeat here

$$W_k^T = G_0(J_k^{hot} - J_{cold}). \quad (2.9)$$

Note that (2.9) involves technology dependent data like G_0 , the average coolant flow rate in an assembly.

2.3 Physical and Mathematical Basis of Core Monitoring

Core monitoring is based on physical laws formulated as functional relation among measurable physical quantities. For example, the temperature of the coolant is measured by an imbedded thermocouple producing voltage between the cold point and the hot point of the thermocouple positioned in the reactor core. That voltage is transformed into temperature after calibration.

Similarly an SPND gives a detector current that should be transformed into power density. Let us label the assemblies with SPND by subscript i , and subscript ℓ labels the elevation in the chain, see Fig. 2.5. We seek a conversion factor $\varepsilon_{\ell i}$ transforming measured detector current $I_{\ell i}$ into assembly power. Assuming seven axial detector positions, with the help of sensitivity $\varepsilon_{\ell i}$, the power density $w_{\ell i}$ at the detector elevation ℓ is determined by

$$w_{\ell i} = \varepsilon_{\ell i}(I_{\ell i} - \alpha_{\ell i} I_{8i}). \quad (2.10)$$

Here $\varepsilon_{\ell i}$ is a conversion factor, $I_{\ell i}$ is the measured current. Expression (2.10) takes into account that a fraction of the current comes from the cable, not from the detector, the correction is proportional to the dummy cable current I_{8i} , the proportionality factor being $\alpha_{\ell i}$. The proportionality factor $\alpha_{\ell i}$ is linear in the cable length counted from the position of detector at the i -th elevation. When the background cable does not work, a surrogate background current is used, it is taken to be proportional to the thermal assembly power W_i^T :

$$I_{8i} = \beta_{di} W_i^T \quad (2.11)$$

As to β_{di} , it is derived from W_i^T and I_{8i} of assemblies with working background cables. W_i^T is available either from direct measurements or from estimations described in Sects. 2.3.4, 2.3.5, and 2.3.7. Subscript d refers to enrichment as the approximation works adequately only for assemblies of identical enrichment. The proportionality factor is obtained from least square approximation as

$$\beta_d = \frac{\sum_i I_{8i} W_i^T}{\sum_i I_{8i}^2}. \quad (2.12)$$

Summation runs for assemblies with a given enrichment d and with reliable background cable current. In this procedure we lose information: all assemblies of enrichment d share a common β_d factor.

As to $\alpha_{\ell i}$, it is proportional to the flux integral over the length of detector i :

$$\alpha_{\ell i} = c \int_{H_1}^{H_z} \Phi(z) dz, \quad (2.13)$$

where H_1 is the lowest cable position in the SPND chain, and H_z is the highest position. The problem is that the SPND is used just to measure the flux (or power).

The cycle design calculations require a reliable calculational model, it can be used to determine the integral in (2.13). The calculational model determines axial flux and power profiles in discretized forms, continuous distribution is obtained for example by cubic spline interpolation, see Appendix D.

The power w_i of assembly i estimated from SPND measurements. In core design calculations, the maximum power density should be determined. To this end several power peaking factors are applied: the axial power peaking factor is the maximum of

$$k_{iz} = \frac{\max \tilde{w}_i}{\tilde{w}_i}, \quad (2.14)$$

where k_{iz} - axial power peaking factor of assembly i , \tilde{w}_i is the axial average power in assembly i . The assembly power peaking factor is the maximum of

$$k_{iq} = \frac{w_i^T}{w_{average}^T}, \quad (2.15)$$

here k_{iq} -2D power peaking factor of assembly i . 3D power peaking factor is the maximum of

$$k_{iv} = k_{iz}k_{iq} \quad (2.16)$$

k_{iv} -3D power peaking factor in assembly i .

The computation works with nominal detector positions z_k , the measurements take place at actual positions z'_k . With the help of spline interpolation functions ϕ_j , we derive the following transformation matrix from actual positions z_k to nominal positions z_ℓ :

$$R_{k\ell} = \sum_{j=1}^7 \phi_j(z_k) [\phi_j(z_\ell)]^{-1}. \quad (2.17)$$

In fine tuning we exploit that the integrated assembly power from DPZ currents and from measured ΔT and coolant flow in the assembly, should be the same. This is insured by calibration when all ε_{ik} of assembly i is multiplied by a tuning constant.

In the temperature measurements the thermopower $U(T)$, see Eq. (2.8), involves a common factor A_1 by assuming $A_2 = a_2 A_1$, $A_3 = a_3 A_1$ and during the start-up measurements A_1 is fitted to a stable, known temperature.

To determine the thermal power w_i^T of assembly i , we need the enthalpy rise. We have to take into considerations that there are at least two assembly types: majority is a normal assembly of identical geometry but geometry of control assemblies definitely must differ from the majority. For normal assembly we use

$$w_i^T = G_0 (J_{i,out} - J_{i,in}) \quad (2.18)$$

whereas for control assemblies

$$w_{iC}^T = G_C (J_{i,out} - J_{i,in}) . \quad (2.19)$$

The coolant entropy at entering the assembly is

$$J_{i,in} = J_{in,0} (1 + E_1(T_{i,in} - T_{0a})) , \quad (2.20)$$

here T_{0a} is the nominal temperature of the coolant in the cold leg. $T_{i,in}$ is the inlet coolant temperature in assembly i . Constant E_1 is determined by fitting. The entering coolant temperature is determined from the cold leg temperatures of the loops using the mixing matrices. Here, for the sake of simplicity we assume that assembly inlet temperatures are constants.

As to $J_{i,out}$, the following, analogue to (2.20), expression can be used:

$$J_{i,out} = J_{out,0} (1 + E_2(T_{i,out} - T_{i,0})) , \quad (2.21)$$

where $J_{out,0}$ is the nominal enthalpy of the coolant at exiting assembly i , constant E_2 is determined by fitting, $T_{i,out}$ is the coolant temperature at exiting assembly i .

2.3.1 Relationship Between Measurement and Calculation

By the time we have the first measurements on a unit, several other actions have been done. Using the approved calculation model, several calculations have been carried out to support the licensing process of the reactor and of the actual core. The calculations have been analyzed and criticized by several experts, see the first paragraph in Sect. 2.7.5. Why do we not let the reactor run until the end of the actual fuel cycle once we have invested so much energy into designing the reactor in general and to plan the fuel cycle in special? The answer is the following:

1. Core design codes are based on a large number of data, including scientific models of the nucleus and specific nuclear reactions. Those data are held in huge libraries called evaluated nuclear data library (ENDL). One has to be cautious when working with thousands of measured data.
2. As soon as the reactor is not close to its stationary work regime, we have to remember that basic equations of reactors are nonlinear, see Chap. 4. Some of them tend to stabilize the time dependent processes others do not. We discuss this in Chap. 4 in details.
3. Also in Chap. 4, we point out that each calculation is based on assumptions and the obtained results are correct only if the assumptions hold.

This is the main point in implementing measurements in industrial devices. In every operating power plant data are continually collected and analyzed to make reasonably sure that reactor operates on the designed track, or, if there is a deviation from the plans what kind of correcting actions should be put in effect.

2.3.1.1 Parameters in Calculation

We assume that our computational model has passed the V&V process. Physical models involve constants or parameters, and the theory is often tolerant with their admissible values and we seek methods to improve our otherwise perfect calculations.

In general, we have a mathematical relationship between a measured quantity $\Phi(x_i)$ at position x_i in the core, and we seek a function $f(x, \mathbf{c})$ having a value for every assembly at $x = x_i, i = 1, \dots, N_{as}$ where N_{as} is the number of assemblies in the core. We seek a parameter vector \mathbf{c} such that $f(x_i, \mathbf{c})$ be close to Φ_i when $x = x_i$. The positions in a reactor core are fixed by the design, so it suffices to refer to $\Phi(x_i)$ as Φ_i . When we are interested in the axial position z we use $\Phi_i(z)$. Often we deal with discrete axial positions, then we use Φ_{ij} where the second subscript means the interval $(j - 1)\Delta z \leq z \leq j\Delta z$. Φ_{ij} may be regarded as mean value or the value at the midpoint of interval $[z_{j-1}, z_j]$.

In the ideal case,

$$\Phi_i = f(\mathbf{c}) \quad (2.22)$$

meaning that Φ_i is a function of parameter vector \mathbf{c} . Being measured, Φ_i must carry error. When a measurement is repeated n times, we usually obtain n different values even if the physical circumstances are identical. We say that measured Φ_i is a random variable and (2.22) may hold only for the mean value $E\{\Phi_i\}$:

$$E\{\Phi_i\} = f(\mathbf{c}). \quad (2.23)$$

Equation (2.22) is often called physical model. Such models are discussed in Chap. 4. Note that there are several models, and the analyst should choose the one which is the best to describe the problem under consideration. Assume that the measured Φ_i is free from systematic error. Then, it is possible that Φ_i determines \mathbf{c} . The parameter vector obtained this way is a random vector $\boldsymbol{\gamma}$ and $E\{\boldsymbol{\gamma}\} = \mathbf{c}$. The estimate is called unbiased if

$$\delta\mathbf{c} = E\{\boldsymbol{\gamma}\} - E\{\mathbf{c}\} = 0. \quad (2.24)$$

Here $\delta\mathbf{c}$ is the bias of the parameter vector and it is the systematic error of the estimation. Parameter vector $\boldsymbol{\gamma}$ that we obtain by fitting deterministic basis functions to measured values must be random. When several measurements are carried out, the mean value and variance are obtained by standard statistical tools [13, 43]. In practice, a measured value is described by its mean value and its standard deviation, or, by its probability distribution.

We investigate a reactor core with N_{as} fuel assemblies, the physical distribution to be monitored is $\boldsymbol{\Phi} = (\Phi_1, \dots, \Phi_{N_m})$, where N_m , that may not exceed N_{as} , is the number of assemblies implemented with measurement. We express $\boldsymbol{\Phi}$ as a linear expression of N_m precalculated and deterministic basis vectors $\mathbf{B}_k = (B_{k1}, \dots, B_{k,N_m})$ and $k = 1, \dots, N_{as}$. The coefficients are determined from the condition that the

interpolated flux should be as close as possible to the Φ_j measured values at measured positions:

$$Q(\mathbf{c}) = \sum_{j=1}^{N_m} (c_j B_{kj} - \Phi_j)^2. \quad (2.25)$$

Here B_{kj} is the k -th basis function at assembly j used in the interpolation; $1 \leq j \leq N_{as}$. Coefficients $\mathbf{c} = c_1, \dots, c_{N_b}$ are to be chosen so that Q be minimal. Since Φ_j is random, Q is also random³ Furthermore, as elements of \mathbf{c} depend on random variables $\Phi(x_j)$, they must be random, so we replace \mathbf{c} by $\boldsymbol{\gamma}$. We have to solve the following set of equations for $\boldsymbol{\gamma} = (\gamma_1, \dots, \gamma_{N_m})$:

$$\sum_{j=1}^{N_m} \sum_{k=1}^{N_b} B_{rj} B_{kj} \gamma_k = \sum_{j=1}^{N_m} \Phi_j B_{rj}, \quad r = 1, \dots, N_b. \quad (2.26)$$

Let

$$P_{kr} = \sum_{j=1}^{N_b} B_{rj} B_{kj}; \quad r = 1, \dots, N_b; \quad k = 1, \dots, N_b. \quad (2.27)$$

and

$$f_r = \sum_{j=1}^{N_b} \Phi_j B_{rj}; \quad r = 1, \dots, N_b. \quad (2.28)$$

Then we have to solve

$$\sum_{k=1}^{N_b} P_{kr} \gamma_k = f_r; \quad r = 1, \dots, N_b. \quad (2.29)$$

for γ_k . Equation (2.29) is solvable if the basis functions $B_k(x_j)$, $j = 1, \dots, N_{as}$ are linearly independent thus N_b , the number of basis functions may not exceed the number of measured assemblies. When $\boldsymbol{\gamma}$ is determined, the following estimation is at our disposal in assembly k :

$$\Phi_k = \sum_{r=1}^{N_m} \gamma_r B_{rk}; \quad 1 \leq k \leq N_{as}. \quad (2.30)$$

A random variable is described by its distribution function. Below we quote statements which are well known in statistics. Details are available e.g. in [14, 15].

The minimum of Q is proportional to an $n - m$ degree of freedom chi-square random variable:

$$Q_{min} = \sigma^2 \chi_{n-m}^2. \quad (2.31)$$

³Yet we preserve the traditional notation Q although it is a random variable.

The mean of a χ_{n-m}^2 is $(n - m)$ therefore

$$\sigma^2 = \frac{Q_{min}}{n - m} \quad (2.32)$$

can be used.

Now we determine the distribution function of $\boldsymbol{\gamma}$, to this end we solve (2.29) for $\boldsymbol{\gamma} = (\gamma_1, \dots, \gamma_{N_b})$:

$$\boldsymbol{\gamma} = \mathbf{P}^{-1} \mathbf{f}, \quad (2.33)$$

where

$$f_r = \sum_{j=1}^{N_b} \Phi_j B_{rj}; \quad r = 1, 2, \dots, N_b. \quad (2.34)$$

therefore elements of vector \mathbf{f} are linear in Φ_j . The distribution function of a linear combination

$$\eta = \sum_{j=1}^{N_b} a_j \Phi_j \quad (2.35)$$

is normal, as Φ_j are statistically independent random variables, their mean and sum are again normally distributed, the mean of the sum being linear combinations of the means of the involved random variables distributed normally, and the variance is a linear combination of the variances [28]. Let $\mu = a\xi + b$, and $E\{\xi\} = m$ then $E\{\mu\} = am + b$ and $E\{\mu^2\} = E\{(a\xi + b)^2\} = E\{a^2\xi^2 + 2ab\xi + b^2\}$ and $E\{\mu^2\} = a^2 E\{\xi^2\} + 2abm + b^2$. The variance of μ is

$$\sigma_\mu^2 = E\{\mu^2\} - E\{\mu\}^2 = a^2 E\{\xi^2\} + 2abm + b^2 - (am + b)^2 = a^2 (E\{\xi^2\} - m^2) = a^2 \sigma_\xi^2,$$

and finally the variance of μ is given by

$$\sigma_\mu^2 = a^2 (E\{\xi^2\} - m^2). \quad (2.36)$$

In Eq. (2.30) the γ_k numbers are linear combinations of the normally distributed Φ_j measured values, and are themselves also normally distributed. The usual notation for the variance of a general random variable ξ is $\sigma_\xi^2 = E\{\xi^2\} - E\{\xi\}^2$. Using this notation for γ_k we arrive at

$$\sigma_{\gamma_k}^2 = \sum_{j=1}^{N_b} \left(\sum_{r=1}^{N_b} \mathbf{P}_{kr}^{-1} B_{rj} \right)^2 \sigma_{\Phi_j}^2 \quad (2.37)$$

In conclusion:

1. Q_{min} is a measure of the goodness of fit. If Q_{min} is too large (that conclusion may be obtained from analyzing the chi-square statistical table available in textbooks and codes such as MATHEMATICA, MAPLE, or MATLAB), something must be wrong. Possible reasons are: failure in the measurement or improper trial functions, unexpected change of the core state (control rod position, coolant flow distribution, boron concentration, etc.).
2. Using the variances of the fitted γ_k coefficients, one can easily determine the variance of the fitted map. When the difference at position x_i , which is a measured assembly, exceeds three-times the standard deviation, the measured value should be checked, see Sect. 6.4.
3. When there are several independent in-core measurements implemented, the measurements and the obtained map should be cross-checked. This may reveal several early stage problems.

Usually the number N_b of basis functions is smaller than the number N_m of measured positions. Below we investigate how to select the basis functions.

In a VVER-440 core, the number of assemblies is 349, the outlet temperature is measured above 210 assemblies. The measured positions are predetermined. In this case $N_{as} = 349$, $N_m = 210$. There are at most 210 basis functions, whereas the dimension of the temperature field is 349. In principle there are

$$\binom{N_{as}}{N_m} = \frac{N_{as}!}{N_m!(N_{as} - N_m)!} \approx 3.4710^{100}$$

possible choices.

The basis vectors $B_{1i}, \dots, B_{N_m,i}$ can be ranked, according to increasing contribution to the measured values:

$$\sum_{i=1}^{N_m} \Phi_i B_{1i} > \sum_{i=1}^{N_m} \Phi_i B_{2i} > \dots > \sum_{i=1}^{N_m} \Phi_i B_{N_m,i}, \quad (2.38)$$

and the first basis function is the most valuable. Assume the basis functions \mathbf{B}_k to be orthogonal. Then, expression (2.26) can be rewritten as

$$\gamma_k = \frac{\Phi \mathbf{B}_k}{\mathbf{B}_k \mathbf{B}_k}, k = 1, \dots, N_b, \quad (2.39)$$

meaning that basis functions \mathbf{B}_k describe more of Φ when γ_k is large. The approximation quality by a linear expression recurs in the principal component method (PCM), see Sect. 6.3 in Chap. 6, and global sensitivity method in F.2.

2.3.2 Check on Measured Values

In-core measurements fall into two categories. The SPND or air-ball measurements⁴ provide the only measured information on the axial distribution of the power in the reactor core. The coolant temperature increase provides detailed information on the radial distribution of the core power. The two kinds of measured powers carry different information: the temperature increase of the coolant and the flow rate allow estimating the enthalpy rise of the coolant and is determined dominantly by thermal properties (heat conductance, heat transfer coefficient, temperature of fuel, clad and coolant etc.) of the fuel assembly. SPNDs measure the local neutron flux or power. It is known that a part of the energy released in fission appears in forms differing from heat (e.g. excitation energy of fission products, gamma radiation). Geometry of an SPND chain can be seen in Fig. 2.5. One string contains seven detectors located at seven elevations. Cables of the detectors should be isolated by an insulator layer. Unfortunately in the insulator also may occur electric charge producing nuclear reaction and that parasitic current should be corrected for. To this end a cable without detector is also placed into the SPND. Geometry of the SPND has been shown in Fig. 2.5. The magnitude of the current induced in the cable depends on H , the length of the cable and on the flux integral over the cable length:

$$I_{corr} = \frac{\int_{H_{det}}^H \Phi(z) dz}{\int_0^H \Phi(z) dz}. \quad (2.40)$$

Here I_{corr} is the current correction; H_{det} -lower elevation of the detector cable; H -is the uppermost point of the detector cable. The actual detector current is proportional to $I - I_{corr}$:

$$I_d = \frac{C_1}{(1 - C_2 Q)^{C_3}} (I - I_{corr}). \quad (2.41)$$

Here Q is the total charge having emitted by the detector. On the average, a given nuclide captures only one neutron and emits only one electron, so the denominator accounts for the “detector burnup”. The constants in (2.41) are determined by studying the behavior of the detector.

As we see, when background current is in error, it is impossible to carry out the background correction. To avoid throwing out good measured currents, it is possible to subdivide the thermal assembly power into parts proportional to the power integrated into the length of the corresponding background cable, see (2.11).

The converting factor $C(\mathbf{p})$ in (2.6) depends on the state of the fuel assembly, which in turn depends on local and global quantities, for example, burnup, coolant temperature and power density are local parameters but boron concentration is a global parameter. In general,

⁴Henceforth we use the term SPND for both measurements.

$$C(\mathbf{p}) \equiv C(B, T, P, c_B, \dots) \quad (2.42)$$

where B -burnup; T -coolant temperature; P power density; c_B -boron concentration. Just like in a parametrized cross-section library, the parameter dependence is a low order polynomial of the difference from a nominal state. The required number of parameters can reach 20.

Assume that $C(\mathbf{p})$ has been determined from (2.7), and the SPND current is converted into assembly power by (2.6). Detector currents are periodically read out automatically, and the measured power is also re-estimated by the same period. We have seen that SPND signal has its inertia, the signal may not change arbitrarily in time.

Note that the relaxation time includes the inertia of the electronic processing as well. It is a good practice to compare the measured detector current $I_d(t)$ at time t with the previous value and filter out changes caused by state variation caused by an electronic contact or operation error. A simple formulation of the mentioned condition is: check if the condition

$$|I_d(t + \Delta t) - I_d(t)| < \varepsilon, \quad (2.43)$$

holds where ε may depend on the reactor state, and is different for various reactor types. It is a good idea to compare time variation with time variations of other detectors in the same detector chain.

The neutron flux at a given core point of the reactor varies with time. Where the neutron flux is large, there more fuel is consumed in unit time, where the neutron flux is smaller, less fuel is consumed, consequently the neutron flux tends to diminish flux differences. From the core design calculations, the operator has a prediction what kind of variations are possible and expectable in a given core. Below we focus on the axial power distribution, which is measured either by an air-ball system or by SPND chains. We address the following sample problem: given an axial power profile $\Psi(z)$, measured values are at our disposal at K positions: $P_k = \Psi(z_k)$, $k = 1, \dots, K$. The questions to be answered are:

1. what is the error of the axially integrated power?
2. how changes the estimated maximal power density and its position if some of the detectors fail?
3. how to use the SPND measurements if only a part of the measurements can be used?

As we see in Fig. 2.5, the detectors do not cover the total height of the core and current I_d is proportional to the average power over the detector length. The axial power profile is obtained after interpolation. The actual detector lengths are unequal, the vendor may deliver the correct lengths in the fuel passport. When this is not the case, the SPND assemblies should be screened.

When we have obtained the average power w_k , $k = 1, \dots, K$ at the center of each detector. The axial power profile is a smooth function, thus spline interpolation can be used. Spline interpolation requires one additional value above the core and one

under the core⁵. As the material distribution in the mentioned regions is known only approximately, and the solution of the diffusion equation in a homogeneous material predicts a cosine-like axial shape, it suffices to know the upper $z_0 = \ell_u$ and lower $z_{K+1} = \ell_l$ extrapolation distances, where the power is zero. The power profile is approximated by third order splines, see Appendix D, as

$$\Psi_m(z) = c_{m0} + c_{m1}(z - z_m) + c_{m2}(z - z_m)^2 + c_{m3}(z - z_m)^3; \quad z_{m-1} \leq z < z_m; \\ m = 1, \dots, K.$$

z_0 and z_{K+1} have been determined, the midpoint of interval $[z_m, z_{m+1})$ is the midpoint of the m -th detector and there the interpolant should have the value w_m . Every detector center lies in one and only one interval. There are $K + 2$ points, $K + 1$ intervals involved in the interpolation. The flux must vary axially smoothly, so we may use the smoothness to reduce the number of unknowns. The needed equations automatically emerge from the continuity of the flux at the end points of the interval:

1. $\Psi_1(\ell_l) = 0$ and $\Psi_K(\ell_u) = 0$ at the lower and upper extrapolation points the interpolated power be zero.
2. $\Psi_m(z_m) = \Psi_{m+1}(z_m)$, $m = 1, \dots, K$, i.e. the interpolation polynomial is continuous;
3. $d\Psi_m(z_m)/dz = d\Psi_{m+1}(z_m)/dz$, $m = 1, \dots, K$, i.e. the derivative of the interpolation polynomial is continuous;
4. $d^2\Psi_m(z_m)/dz^2 = d^2\Psi_{m+1}(z_m)/dz^2$, $m = 2, 3, \dots, K$, i.e. the second derivative of the interpolation polynomial is continuous.

The above restrictions represent $3K + 2$ conditions, the remaining K conditions are obtained from requiring the measured values to be given at the midpoints of every interval. The $3K + 2$ conditions form a homogeneous linear equation set. As the measured powers are $\mathbf{w} = (w_1, w_2, \dots, w_K)$, the coefficients depend on the measured values and the interpolant takes the following form:

$$\Psi(z) = \sum_{m=1}^{K+2} (c_{m0}(\mathbf{w}) + c_{m1}(\mathbf{w})(z - z_m) + c_{m2}(\mathbf{w})(z - z_m)^2 + c_{m3}(\mathbf{w})(z - z_m)^3). \quad (2.44)$$

As the interpolated $\Psi(z)$ is linear in the measured powers \mathbf{w} , any linear function $L(\Psi(x))$ is also linear in \mathbf{w} . For example, the assembly power

$$W = \int_0^H \Psi(z) dz = \mathbf{M}_W^+ \mathbf{w} \quad (2.45)$$

where elements of the adjoint vector \mathbf{M}_W^+ give the contributions of the SPND powers to the axially integrated power given by:

⁵Extrapolated upper and lower end of the axial power profile.

$$\sum_{m=1}^{K+2} \sum_{j=0}^3 c_{mj} \int_0^H (z - z_m)^j dz. \quad (2.46)$$

The linearity allows for precalculating every indispensable matrix needed in signal processing.

It is clear from (2.45) that effect of mis-positioned detectors is nonlinear. Let the position of detector m change be $z_m \rightarrow z_m + \delta z_m$. Then the power distribution changes by

$$\begin{aligned} \delta \Psi(z) = & \sum_{m=1}^{K+2} c_{m1}(\mathbf{w})(z - \delta z_m) + c_{m2}(\mathbf{w}) (2(z - z_m)\delta z_m + (\delta z_m)^2) + \\ & c_{m3}(\mathbf{w}) (3(z - z_m)^2 \delta z_m + 3(z - z_m)(\delta z_m)^2). \end{aligned} \quad (2.47)$$

Finally, note that error in the core height should also be investigated. The core height is not a simple technical data that can be read out. There are gaps among fuel pellets, the pellets expand with temperature, the axial length of the pellets may vary from pin to pin and from assembly to assembly. It is reasonable to regard core height H as a random parameter known with some error.

The analyst should bear in mind that the goal of in-core instrumentation is monitoring safety limits. As to SPND, to monitor the local power density peaks. As burnup progresses, the maximum of power density may change, first the only maximum appears somewhere in the middle of the core height, later on two maxima may appear. Fortunately the detector position is constant until the SPND is not disassembled, but sensitivity analysis may be expedient if some detector reading is obstinately misfits to others.

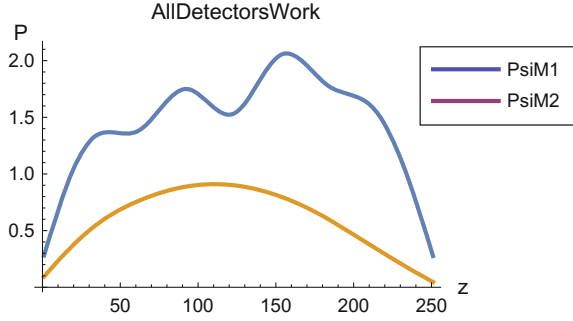
2.3.3 Axial Power Profile

The axial power profile is given by (2.44) provided all the K measured detector currents are reliable. Sensitivity analysis readily provides information on the error of the measured power value created by error in either detector position or reading. To this, the structure of expression (2.44) should be investigated. There are $K + 1$ axial intervals determined by $K + 2$ axial points. Two points, viz. z_0 and z_{K+1} are extrapolated endpoints, where the flux (and also the power) is zero. Let us call those two points external, the remaining K points internal. In interval $z_{m-1} \leq z < z_m$ the power is assumed to have the form of (2.44).

Tools of calculating features of neutron gas are discussed in Sect. 4.3. Calculational tools amenable to determine the axial profile use the following assets:

- a parametrized cross-section library in which the actual cross-section set can be looked up as function of the moderator temperature, the boron concentration, the

Fig. 2.6 Interpolated power profile when all detectors work (PsiM1-old core; PsiM2-fresh core)



power level and the burnup level. The actual cross-sections are determined by such engineering tools like interpolation in a large library.

- A computer code to solve the few-group diffusion equation. The number of energy groups is usually 2 or 4.
- In power reactors the temperature feed-back is taken into account in a coupled calculation, where the neutron flux and fuel, as well as moderator temperature are calculated in a coupled core.

The above mentioned sophisticated tools are not needed to get a general picture of the power distribution along a fuel assembly. In a fresh core, the shape of the axial power can be estimated by solving the one-dimensional diffusion equation:

$$D \frac{d^2 \Phi}{dz^2} + \Sigma \Phi(z) = 0, \quad (2.48)$$

where diffusion constant D and cross section Σ are constant. Solution of (2.48) is $\Phi(z) = \cos(Bz)$ where B is constant and can be determined from the core height, as the neutron flux vanishes at the top and bottom of the core. The maximum of power is at about the midpoint of the core height. Σ has two components: the fission produces neutrons, the absorption consumes them and Σ is their difference. As time passes, the number of fissionable nuclei in the fuel diminishes and there appear strong absorbers (xenon, samarium for example) among the fission products. Thus the cosine form (cf. curve PsiM2) tends to alter into a curve with two or more maxima (cf. curve PsiM1) in Fig. 2.6. shows such curves when every detector signal can be used. Note the differences between the areas under the respective curves: the area is proportional to the assembly power, it is one of the key safety parameters. In operating PWRs SPND chains include between 4 and 7 detectors. There is no essential difference [27] between safety parameters of reactors with 4 or 7 detectors. At the same time it should be noted that the accuracy of the estimated assembly power may depend on the number of detectors. Below we shortly revisit the question.

Reliability of the SPND measurements is influenced by the following key factors:

1. Number and position of the working SPNDs in the detector chain.
2. The axial power profile.

3. Processing of the measured signals.

First, note that if one detector of a detector chain fails the uncertainty of the estimated assembly power depends not only on the axial profile but also on the position of the false detector. It happens, however, that a given detector fails and the axial power profile deteriorates. Below we study the consequence of deterioration. In Fig. 2.7 we show the two curves of the axial shapes in Fig. 2.6 but this time we neglected the SPND at elevation 60 cm. In the fresh core we obtain curve e PsiM2, the change is modest whereas curve PsiM1 has changed remarkably, it is less bumpy. Of course it would be a naive approach to neglect the missing measurement, instead we had to re-evaluate the axial shape. To do so, we study the interpolating polynomial, see Figs. 2.8, 2.9, 2.10 and 2.11. The interpolating polynomial is a smooth curve which takes value unity a given detector elevation and zero at all the other elevations. When

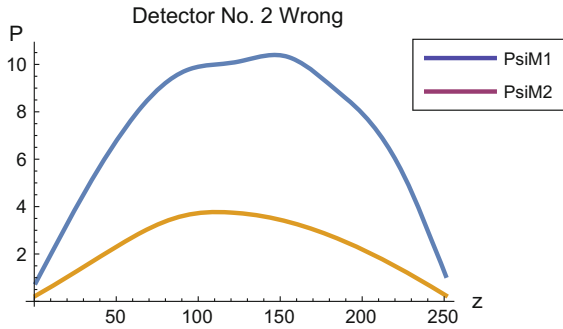


Fig. 2.7 Interpolated power profile when detector at 60 cm is wrong (PsiM1-old core; PsiM2-fresh core)

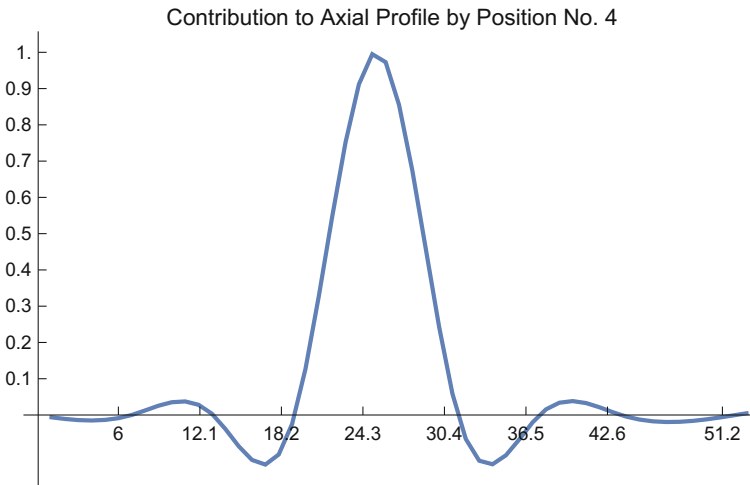


Fig. 2.8 Interpolating functions associated with internal Positions No. 4 in Assembly No. 33

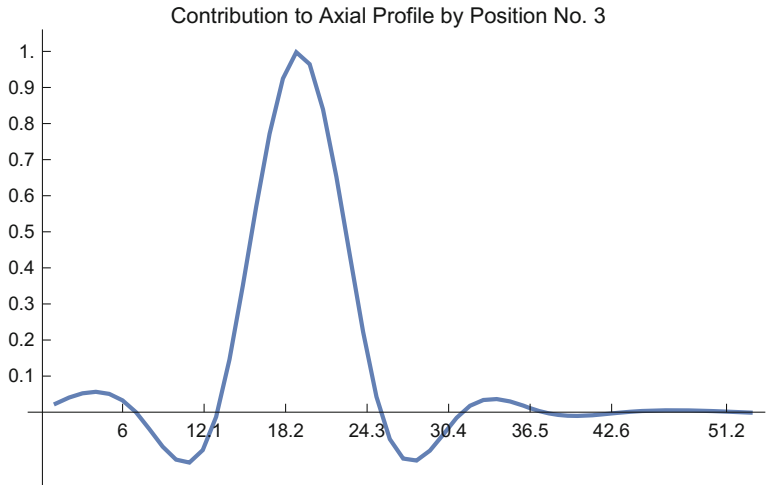


Fig. 2.9 Interpolating functions associated with internal Positions 3 in Assembly No. 33

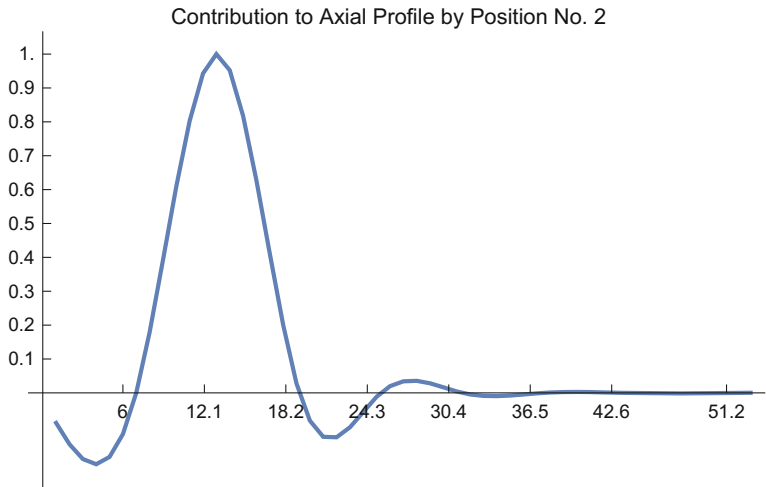


Fig. 2.10 Interpolating functions associated with internal Positions 2 in Assembly No. 33

one measurement is missing, we lose information and that is reflected in the changed curve.

Of course it is possible to reduce the lost information. There is no wonder in a wrong detector being less harmful when the axial power is smooth. As burnup progresses, the peak in the axial shape tends to flatten, see the left and right side of Fig. 2.7, where curve PsiM2 is an axial shape in a fresh core and PsiM1 is in the second fuel cycle.

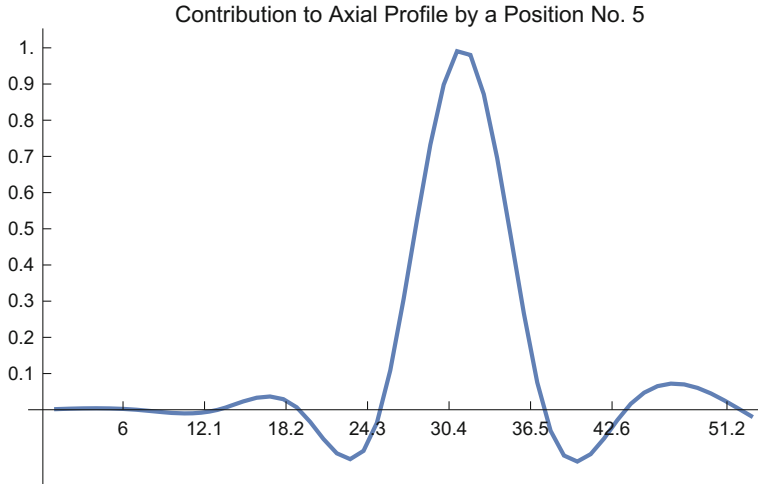


Fig. 2.11 Interpolating functions associated with internal Positions 5 in Assembly No. 33

Below we study the influence of detector positions on the axial power shape. SPND chains are made in the fuel factory, the detector data (positions, detector lengths) are provided by the fuel factory with a given accuracy.⁶ Below we demonstrate possible effects of mis-positioned SPNDs in a numerical analysis. Let the nominal detector positions in centimeters be

$$\mathbf{z} = (-6, 30, 50.5, 71, 91.5, 112, 132.5, 159, 250 + 6), \quad (2.49)$$

where we assumed seven detector positions and two extrapolation distances where the extrapolated flux is zero. The extrapolation distance, here 6 cm, is estimated therefore each element of vector \mathbf{z} is taken as random. We assume the random position of the detectors to be independent and normally distributed with the nominal position as mean value and the variance be 0.2 cm. As to the axial power shape, we assume a typical second fuel-cycle profile:

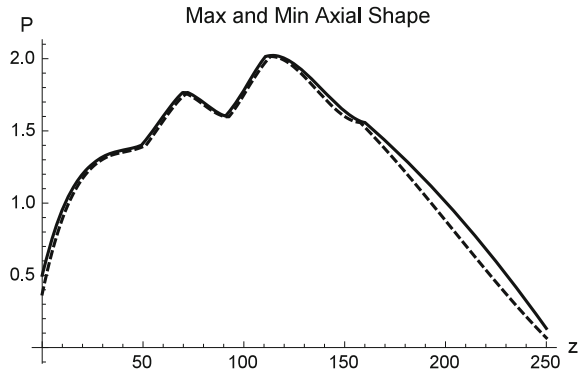
$$P = (0, 1.312, 1.401, 1.765, 1.598, 2.015, 1.858, 1.558, 0) \quad (2.50)$$

and determine a random sample of 100 elements of the power profile, see Fig. 2.12. First let us assess the error sources. 0.2 cm error in the detector position is an under-estimation, the detector length also has an error as a wire is cut to a more or less given length. Diameter and density of the detector wire represent further error source. All the mentioned error sources but the nominal detector is considered as an error source.

As shown in Appendix D, interpolating functions are expressions (that are) linear in the measured values Ψ_i . Thus the contribution of measured value Ψ_i to the

⁶The mentioned data are in the fuel passport.

Fig. 2.12 Position sensitivity of the axial power profile



interpolated value can be determined. This decomposition allows us to estimate the uncertainty of the axial power profile directly. Firstly, because of the linearity, the measurement errors add up. Secondly, the uncertainty of the measuring position can be estimated through the first derivative of the interpolating function. The reason is that we must use an interpolation method to reconstruct the axial power profile. When a measurement fails, a portion of the axial region remains without measurement.

When speaking of measured and calculated values in a core, the coordinates should be fixed. In the VVER-440 type PWRs the assembly positions are numbered as shown in Fig. 2.18.

The position error influences maxima of the axial power profile but the effect is rather small. We note that the axial shape under consideration is unspecific, usually the axial distribution is a simple but always a smooth curve. Large deviations (above 10%) occur only at the top and bottom of the core where the power density is small. The difference in the integrated power is $\sim 4.3\%$. This is a numerical estimate of the σ of the assembly power is a metered assembly. In a PWR, there are 36 SPND chains, as the probability of a σ random error is ~ 0.045 at absolutely normal regime the error of the SPND based power in one of the metered assemblies may exceed 8%. This error includes solely the contribution of the error in the detector position.

When in a PWR there are $36 \times 7 = 252$ SPNDs, there is a chance of a detector failure, see the last paragraph in Sect. 2.3.1.1. It is clear that a wrong detector means loss of information and the accuracy of the measured value(s) must decrease. We have seen the interpolating functions can not be used to decrease the error. What information source may be at our disposal? The answer is found in studying the reactor core. When the load is symmetric, it is possible to compare the total power of symmetrically located assemblies. Fortunately although the axial distribution may depend on control rod positions but only within a distance of a few assembly size, henceforth the axial power profile is almost the same in assemblies of symmetric positions.

That observation can be utilized as follows. The axial profile is determined in a two-stage procedure, in the first step the power profiles are studied in the core under consideration and a few typical profiles are determined [20]. In the second step, the

Fig. 2.13 Effect of failure of DPZ No. 1 in Assembly No. 33 Det-1 Inop: with Detector No. 1 inoperable; all det: all detector operable; ref-calculated axial shape

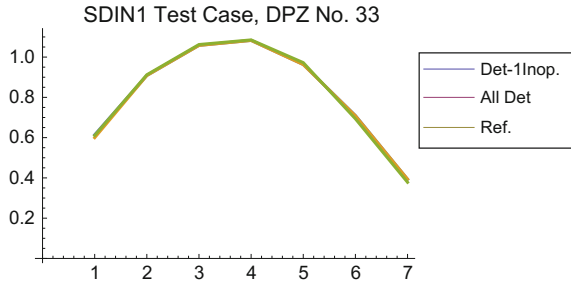
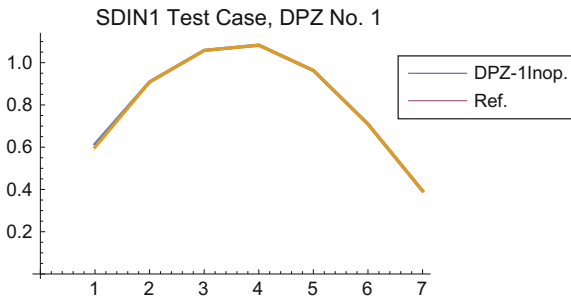


Fig. 2.14 Effect of failures of Detectors No. 1 and 5 in Assembly No. 9



measured but incomplete axial distribution is expressed as a linear combination of the typical profiles selected in the previous step. That procedure is based on the collective features of the axial profiles in the studied core and the information missing from the measurement due to a false detector is provided by the above mentioned linear combination. In statistics, the procedure is called principal component method [22] and is described and an application is given in Sect. 6.3.2. Engineering applications emphasize that feature of the method that a reduced amount of information may suffice to restore for example a picture, thus the name Reduced Order Method (ROM) is also encountered.

Below examples are presented to demonstrate the PCM method. The studied core is identified as SDIN1, see Chap. 6. First we deal with failure of a single DPZ detector. The axial power profile is determined by cubic spline interpolation, see Appendix D, the interpolation is based on the measured values at the seven axial detector positions. The effect of missing measurement can be studied by comparing the restored seven values at the seven axial detector positions. Detector No. 1 being inoperable is used to study the effect of a missing measurement in a region where the gradient is large, see Fig. 2.13. The restored values are connected by a straight line and are compared to the seven measured values serving as reference.

In DPZ Chain No. 7, in assembly No. 9, the detector No. 5 is inoperable, now excluding also detector No. 1, we study the effect of two inoperable detectors, see Fig. 2.14. Two missing detectors cause only a slight error in the restored axial profile.

Instead of presenting further examples, we show the summary of all the 36 assemblies with at least two inoperable detectors. To this end detectors 3 and 4 have been

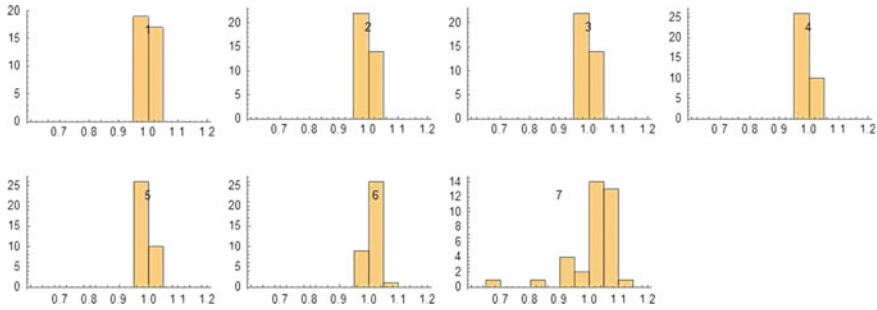


Fig. 2.15 Statistics of error caused by inoperable detectors *Vertical axis* No. of cases; *horizontal axis* deviation from the mean value

discarded everywhere in the evaluation. The comparison shows the ratio approximation/reference in Fig. 2.15. In the figure statistics of the seven axial metered positions appear separately. On level 1 all the restored values agree within a few percent. The only difference is on level 7, where large relative deviations can be observed. Note however, that the absolute power values are small at the level of detector No. 7. The chance of having in one SPND chain more than three inoperable detector is neglected.

2.3.4 Non-metered Assemblies

Because of technical limitations, the number of assemblies equipped with a measurement is limited and there is a need to estimate the would be measured values in those core positions. The neutron flux is the solution of the diffusion equation. The power distribution is derived from the neutron flux thus the measured ΔT_i in assembly i is not arbitrary. The power of a non-metered assembly can be calculated by a suitable model provided the model input is known. Let us summarize the calculations in an operator \mathcal{T} that we apply on the power distribution:

$$\mathcal{T}(p)\Psi = \Psi. \quad (2.51)$$

Actually \mathcal{T} is a computer code, its input being the parameter set describing the core, the fuel, and the coolant. As to parameter vector p , we may use the same vector as in the SPND signal processing.

Equation (2.51) is invariant under the geometric symmetries of the core provided that material distribution and coolant flow pattern are symmetric. Two reactor cores are shown in Figs. 2.16. and 2.17. In Fig. 2.16. the ATMEA1 reactor in-core measuring system, where the fuel assemblies are squares, in Fig. 2.17 the AES-2006 core monitoring system is shown. In the latter fuel assemblies are hexagonal. In the ATMEA core, rows are labeled by numbered from 1 to 14, the column labels go from

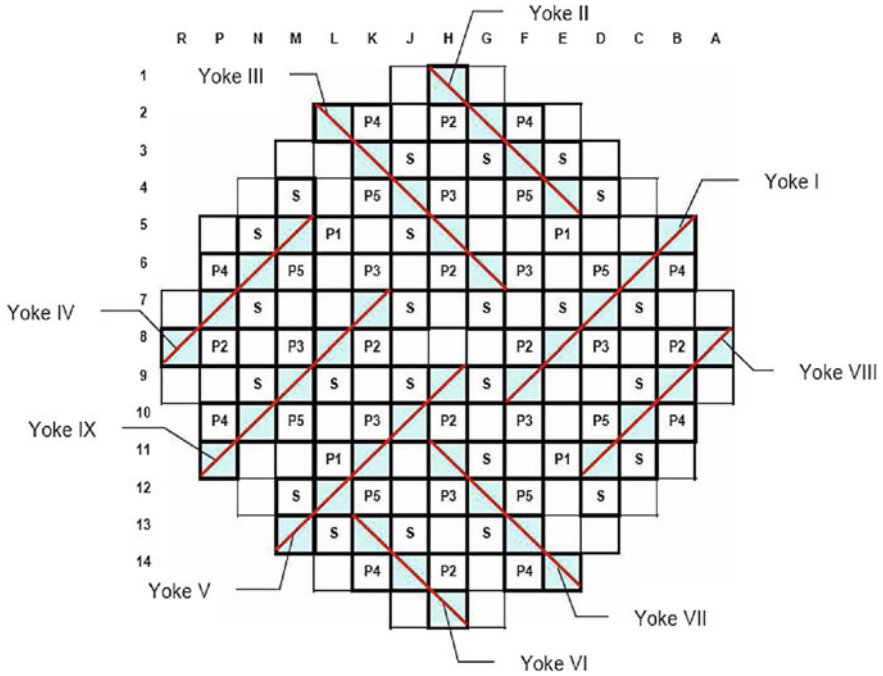


Fig. 2.16 ATMEA1 core monitoring system

A to R. An assembly position is given by a pair, e.g. (1, J) refers to the upper leftmost assembly. The central assembly is (8, H), the core geometry shows 45° rotational or reflective symmetry if assembly properties in symmetric positions are identical. The symmetry center is the midpoint of assembly (8, H).

In the AES-2006 core, which is shown in Fig. 2.17, hexagonal assemblies are loaded. An assembly is identified by a row and column number pair. The center of the core is assembly (8, 29), the core includes six geometrically identical sectors. Remember, geometrical symmetry is only one component of the core description and if the burnup, the coolant flow distribution or the cold leg temperatures, or the flow rates of the loops differ, the symmetry may deteriorate.

One of the functions of in-core instrumentation is to check the flow distribution and assembly reload symmetries. First we refrain from using geometrical core symmetry. Assume the core to be invariant under a given rotation. Then the power distribution⁷ would be

$$\Psi_{s,i} = a_s \psi_i, \quad (2.52)$$

where subscript s refers to sectors, i to positions within the sector. First we have to check whether the assembly powers show that symmetry. To this end we regard

⁷Detailed discussion of probability distributions is available in symbolic mathematics and statistics softwares like MATHEMATICA, MATLAB, MAPLE etc.

$$\frac{\partial Q}{\partial \psi_i} = 2 \sum_s (\Psi_{s,i} - a_s \psi_i) a_s = 0, \quad i = 1, 2, \dots \quad (2.56)$$

Equations (2.55) and (2.56) are nonlinear in a_s s and ψ_i s. Such equations are solved by iteration. The number of unknowns is one a_s per sector and one ψ_i per position.

Q_{min} is a random variable as (2.55) and (2.56) involve the measured power $\Psi_{s,i}$. The probability distribution of Q_{min} is the well known chi-squared distribution, and the expectation value of Q_{min} is given by

$$E\{Q_{min}\} = \sigma^2 \chi_{n-m}^2, \quad (2.57)$$

where χ_{n-m}^2 stands for a random variable distributed as χ^2 with degree of freedom $n - m$. Furthermore, n is the number of points where $\Psi_{s,i}$ are known, and m is the number of fitted parameters. σ^2 is the variance of the measured powers. Since the expectation of χ^2 is $n - m$, the following estimation is obtained for the variance of the measured powers:

$$\sigma^2 = \frac{Q_{min}}{n - m}. \quad (2.58)$$

The actual Q_{min} is a random variable determined by (2.54), and by looking up the chi-squared distribution in a statistics software (like MATHEMATICA, MATLAB or MAPLE), we can determine the probability that the power distribution can be expressed as a product of a sector dependent amplitude a_s and a position dependent ψ_i .

Solving (2.55) and (2.56), we immediately obtain the sector amplitudes a_s and the sector power distribution ψ_i . There is one sector amplitude for each sector, and one power for each sector position, i.e. $s = 1, \dots, N_s$ and $i = 1, \dots, N_p$ where N_s -number of sector positions, N_p -number of positions in a sector.

Q_{min} qualifies the global fit. There may be individual positions, called out-layers, where the general relation breaks down. In those positions another statistical variable, the Student fraction can be used. The Student fraction τ_i is a random variable given by, see [15] [Chapter III.]:

$$\tau_i = \frac{\Psi_{s,i} - a_s \psi_i}{\sqrt{\frac{Q_{min}}{(n-m)}}}, \quad (2.59)$$

its distribution is normal, with zero mean value and unity variance. Note the nominator in (2.59) to be the difference between the measured power and the prediction of our simple model used in (2.55) and (2.56). The denominator is the standard deviation of the fit.

From the point of view of statistics, we have set up a typical statistical hypothesis: the measured power $\Psi_{s,i}$ is expressible as a product of two terms, a sector dependent a_s and a position dependent ψ_i . We test our hypotheses by comparing the measured values and the estimated values. When Q_{min} , which is a χ^2 random variable takes

a value indicating that the probability that our hypothesis is true, and that value is close to one, say 0.95.⁸

The local difference between the measured value and the predicted value is also a random variable, see (2.59), its distribution is known to be normal. A normally distributed random variable takes values around the mean value by high probability but difference about 3σ occurs with probability ~ 0.05 . The probability of the following event: in a core where there are 100 measured positions, and at three positions we observe $5 \tau_i > 3$, is close to unity, so not unusual. On the following pages we are going to present various statistical methods to analyze measurements or to assign a value to a non-metered assembly.

Looking at the power map of a reactor, it is not easy to discover some internal structure in the data. The root of power distribution is the neutron flux obeying the diffusion equation, see Sect. 4.3 in Chap. 4, the solution of which is a slowly varying function. That immediately addresses the question: are there typical micro structures in the power distribution? If yes, is it possible to find them? Can we work out effective tools to analyze the measured power distribution and to assign estimated values to non-metered assemblies? Mathematical statistics has the mentioned means [20]. Recently the mentioned technique has been known as reduced order model (ROM), see [23, 24].

It has been mentioned that the power distribution can be approximated by linear combinations of properly chosen trial functions, see (2.30); we have exploited a special trial function in (2.52), where the trial function has been chosen as a sector amplitude a_s multiplied by a position dependent ψ_i . In mathematical sense this is equivalent to assuming that we have six sectors that may include only an amplitude. Lets generalize the idea in the following way: let us subdivide the core into regions of equal size and let each sector have free amplitudes. Formally [25]: the power distribution is

$$\Phi = (\Phi_1, \dots, \Phi_{N_{as}}), \quad (2.60)$$

and the core is considered as set of N_{el} elements with m assembly in each element. Overlapping elements are allowed therefore $N_{el}m \geq N_{as}$. The elements are of identical geometry. The elements are used as follows.

In the first, learning step, we study a reference power distribution that we subdivide into elements and form the following matrix:

$$\mathbf{A} = (\mathbf{y}_1, \dots, \mathbf{y}_{N_{el}}). \quad (2.61)$$

Here \mathbf{A} is a rectangular matrix with N_{el} columns and m rows. From \mathbf{A} , we form the $m \times m$ observation matrix \mathbf{S} :

$$\mathbf{S} = \mathbf{A}\mathbf{A}^T. \quad (2.62)$$

It can be shown that \mathbf{S} is symmetric and positive definite matrix. At the end of the first step, we determine the eigenvalues and eigenvectors of \mathbf{S} :

⁸That number is called confidence level.

$$\mathbf{S}\mathbf{z}_i = \lambda_i \mathbf{z}_i; \quad i = 1, \dots, m, \quad (2.63)$$

and order the eigenvalues in a decreasing order: $\lambda_1 > \lambda_2 > \dots > \lambda_m$. The eigenvectors are orthogonal.

2.3.5 Trial Functions

An obvious generalization of (2.52) is to regard functions ψ_i as trial functions and to interpret its amplitude as the weight of ψ_i in the actual core. Through appropriate selection of ψ_i it is possible to follow the development of an evolution: when its amplitude increases with time, the physical process attached to it has gaining importance. Usually the amplitude starts from a small value but if it surmounts above the noise level, we may catch a dangerous process still in its egg form. We suggest useful trial functions in Chap. 5.

We seek a vector $\Psi_i, i = 1, N_{as}$ representing an assembly-wise distribution in the core. Given are the measured values at N_{meas} points, where $N_{meas} < N_{as}$ to reconstruct the Ψ_i values. To this end we use basis functions and expand the unknown distribution as a linear expression of the basis functions. In the practice it suffices to use a few trial functions. We use here a variant of the principal component method, see Sect. 6.3.

When the analyst investigates a map of measured values $y_i, i = 1, \dots, N_m$, the first thing to do is to find out if there is any symmetry in the core. Say the answer is: the core has an n_s fold symmetry. The next step is to order the measured values into one of the n_s sectors. After that, one collects the measured values of a given position in all the sectors and makes a miniature statistics: determine the mean value and the variance.

In the next step the difference between the variances is studied. Are there outliers? What is in the vicinity of a given outlier? That kind of analysis is usually fruitful. Formally, the above mentioned analysis corresponds to (2.54) with $\Psi_{s,i}$ being the measured value in position i of sector j . It is possible to find out-layer positions by studying the Student fractions (2.59).

It should be emphasized that the measured values belong to a given core state and if we have a core-follow calculation, the calculated distribution refers to a presumed state. Operational parameters, like power, boron concentration, control rod position, or flow rate distribution in the core, the temperature of the entering coolant differ from their presumed values. Yet, the precalculated distribution must be a nice guess of the actual core state. This is why the calculated distribution is chosen to be the number one trial function.

Using the calculated distribution, one can derive further trial functions. For example, a trial function to represent the power map change can be obtained from the difference of two calculated distributions with slightly differing control rod positions.

Similarly, if the flow rates vary in the loops, the result will be a tilt in the temperature distribution. Two more trial functions, one with a tilt in direction x and one

with a tilt in direction y suffice as their linear combination is able to model any flow tilt.

When the boron concentration contains systematic error, the neutron spectrum will be somewhat harder and results in an error depending on the enrichment.

2.3.6 Computation Model

As in fundamental science, without an appropriate model and appropriate measurements no reactor would work. One component of reactor calculations is a bunch of computer programs, which determine for example the power distribution, the amount of fission products, or the coolant temperature distribution in the reactor core. Those computations⁹ need a large amount of data including (see also Chap. 4):

1. Material properties (densities, heat conduction, isotopic composition, viscosity etc.);
2. Nuclear properties (cross-sections, resonance parameters, etc.);
3. Description of the technology (mechanical, electric, material connections, propagation of failures etc.);
4. Connections between parts and components of the technology (equipment may work continually, others operate only on demand);
5. Operation of a power plant may require feed back between primary and secondary circuit.

By now it may have become clear that calculations by reactor models and measurements represent two sides of reactor description.

The computational model is representable as an input-output relationship. Input assumes all parameters that determine the state of the core state. This huge amount of information must be condensed, for example the isotope composition is not given for each pin individually but a simplified construction is in use: material composition and cross sections are combined in macroscopic cross sections and exploiting the homogenization c.f. Sect. 4.3, a cross-section library is created in which the actual cross sections are calculated by interpolation as function of a few well selected parameters. Actually, the input of reactor calculation is composed of a parametrized library and the actual parameters. As parametrized library is updated only when a new fuel is used, we consider it given.

Another component of the input is the core description. The geometry is usually constant¹⁰ Load pattern is renewed only at the end of a fuel cycle therefore the core pattern is fixed in a fuel cycle. Finally, the following data identify the core:

1. power;
2. control rod positions;

⁹Here we deal only with normal operation.

¹⁰As far as the authors note, it has happened that to reduce the irradiation of the reactor vessel, a VVER-440/213 core geometry has been changed.

3. boron concentration;
4. coolant inlet temperature;
5. burnup;
6. coolant flow rate.

Some of the above given parameters are global, like control rod position, boron concentration, others may be either global or local (e.g. power, inlet coolant temperature). Finally, the computer model is a set of computer programs fed by a parameter vector \mathbf{p} and producing a distribution \mathbf{y}_i :

$$\mathbf{y}_i = \mathbf{f}_i(\mathbf{p}). \quad (2.64)$$

Here vector notation refers to distributions. A possible casting of outputs may be: \mathbf{y}_1 : flux, $\mathbf{y}_2 = \mathbf{W}_{ass}$: power, $\mathbf{y}_3 = \mathbf{T}_{out}$, $\mathbf{y}_4 = \Delta\mathbf{T}$.

Usually a computational model works with data provided by the designer, the power plant staff. We mention two examples. The first one is the assembly geometry. Most program assumes the fuel assembly to be the same for all the core. At the same time, it is clear that the geometries of a control assembly and a fuel assembly do differ and this is taken into account by correction factors. The second one is the inlet temperature distribution. Usually the cold leg loop temperatures differ by a few degrees, and the inlet temperature of assembly i is to be calculated from the formula

$$T_{in,i} = \sum_k M_{ik} T_{c,k}, \quad (2.65)$$

where $T_{in,i}$ is the inlet temperature of assembly i , M_{ik} is the mixing matrix, $T_{c,k}$ -cold leg temperature in loop k .

First we study the sensitivity of the calculated distributions in terms of uncertainties of input data.

$$\delta\mathbf{y}_i = \sum_k \frac{\partial \mathbf{f}_i}{\partial p_k} \delta p_k. \quad (2.66)$$

Uncertainties are usually considered to be statistically independent. Let us estimate the number of elements in parameter vector \mathbf{p} ! We have N_{as} coolant inlet temperatures, the same number of coolant flow rates, and inlet temperatures. In a VVER-440, $N_{as} = 349$, therefore more than one thousand small, statistically independent contributions should be summed up to get $\delta\mathbf{y}_i$. Statistics provides us with means to assess statistical features of $\delta\mathbf{y}_i$, see Section G.1 in Appendix F. Conclusions are summarized as follows:

- distribution tends to the normal distribution, with appr. 20 terms in (2.66), application of the normal distribution is acceptable.
- variance is monotonously increasing with the number of terms. When variances of δp_k do not depend on k , variance of $\delta\mathbf{y}_i$ increases as \sqrt{K} where K is the number of parameters.

To assess the accuracy of a calculated distribution, the computation should be tested carefully [18]. This is done in a procedure called validation and verification (V&V). Usually the well selected test cases include simple problems with known exact solution, a set of more complex problems [44], including measurements on test facilities [45]. Similar benchmark compilation [46] exists for thermal hydraulics as well including loss of coolant accident tests [47] and measurements on scaled-down model [48]. In power plants measured data are collected for testing computations and the involved models.

Measured values may be used to test the operational parameters used in the calculational model. Calculated fields power distribution and ΔT distribution can be compared with calculated results. Let us seek the optimal parameter vector \mathbf{p} that minimizes the expression

$$Q(\mathbf{p}) = \sum_i (\mathbf{y}_i - \mathbf{f}_i(\mathbf{p}))^2 \quad (2.67)$$

where the summation runs only over the measured positions. This results in the following non-linear equation for the parameter vector \mathbf{p} :

$$\sum_i \sum_k (\mathbf{y}_i - \mathbf{f}_i(\mathbf{p})) \frac{\partial \mathbf{f}_i}{\partial p_k} = 0. \quad (2.68)$$

We have as many equations as many parameters p_k are involved in the fit. The derivative can be calculated only numerically since $\mathbf{f}_i(\mathbf{p})$ is provided by a computer program. Note that \mathbf{f}_i has as many elements as the number of measured positions. Before going into details of the fitting, we observe that some elements of \mathbf{p} have global effect: control rod positions and boron concentration change the reactivity, the fitting always should be done in a critical reactor state.

When the calculational model is exact, and the numerically calculated derivatives are sufficiently accurate, we have to build up a numerical method to minimize (2.67). The available procedures fall into two categories. The first categories finds the minimum of (2.67) without derivation, such a method is the simplex method. The second family uses derivatives, and includes gradient methods, steepest descent and many other.

Minimum of $Q(\mathbf{p})$ can not be zero because the measured vector \mathbf{y}_i involves measurement errors. Let $\mathbf{y}_i = \mathbf{y}_{i0} + \delta \mathbf{y}_i$ where $\delta \mathbf{y}_i$ is the error. When the measurement is unbiased $E\{\delta \mathbf{y}_i\} = 0$ and its distribution is normal with $D\{\delta \mathbf{y}_i\}$ standard deviation.¹¹ The obtained Q_{min} value is used to estimate the variance of the measured values. That value may depend on i .

Measured values can be used to tune the computational model. By analyzing the distribution between calculated and measured values one may observe special differences. It may happen that large deviations are associated with a given enrichment, or, a given region, say near the reflector or around a control rod. Then by tuning

¹¹Note that from 100 points two or three points always fall outside the 3σ limit.

parameters of assemblies with a given enrichment, or in the vicinity of the control rod, or the control rod parameters, may bring calculated distribution closer to measurements. On the contrary, if large deviations occur at fuel assemblies associated with a common cold point improving evaluation of measured temperatures may be improved.

A Student fraction map may indicate clearly the mentioned anomalies. Unfortunately there is no automatic limit indicating an anomaly. It is a long learning process that leads the analyst to recognize the mentioned phenomena. The observations may help adjoin novel trial functions to the fitting. By introducing such a novel basis function into expression (2.25) that is capable of describing a part of the difference between measurement and calculation, Q_{min} will be reduced.

2.3.7 Assembly Power Estimation

In a nuclear reactor, energy is released in the fuel pins, which are packed into fuel assemblies ready to be moved as one unit in the refueling process. The geometry of fuel assemblies is identical. One of the main goals of the in-core instrumentation is to check on the spatial distribution of the released power in the core.

Unfortunately it is not possible to measure the assembly power directly but through models. The measurement methods fall into two main categories: thermal measurements estimate the thermal energy taken by the coolant; nuclear power measurements estimate the power released in the fuel. Obviously the two kinds of measurements measure different energies. Either measurement directly relates to safety:

- When the released nuclear energy density exceeds a safety limit, the fuel may overheat, that may result in clad dehermetization and partial release of radioactive gases such as xenon or iodine.
- Another possible consequence of fuel overheating is occurrence of heat transfer crisis at the external boundary of the fuel pin. That may deteriorate heat removal from the fuel.

In a fuel assembly, the number of fuel pins is 126 in a VVER-440 reactor, the measurement must be local so we need a physical model to relate the local measurement to the assembly power. Such a model is elaborated after analysis of a large amount of operational data of a given power reactor type [16]. The work may consist of the following steps:

1. Large amount of data are collected in which the measured signal (usually detector currents and assembly powers). The assembly power should be determined from the power distribution in the core, the detector currents are taken from the measurement. Both are collected on a well equipped industrial reactor in the design phase. The collected data should cover the entire life of the assembly (fresh fuel, few burn-up stages, few operational regimes including various coolant flow regimes, control rod positions, etc.).

2. The collected data are ordered into classes a given class involving a characteristic operational mode. Within a class a model and a functional relationship are elaborated, the latter between the assembly powers of measured assemblies and the measured currents.
3. The next step is to fit the free parameters of the model to the measured values. In the fitting an approximate form of the detector current–assembly power relationship may be assumed and the constants of the fitted functions are determined.

The assembly power is easy to be determined in metered assemblies. Consider an assembly with temperature measurement. The thermal energy released in the fuel heats up the coolant flowing through the assembly and the amount of released thermal energy equals the enthalpy rise, the latter equals the mass of the coolant multiplied by the temperature increase and the specific heat capacity. The calculation must involve quantities measured by the technology. The technology provides the following measured quantities:

1. Q_j —coolant volume rate in loop j , given for all j .
2. ΔP_j —pressure drop of Main Circulating Pump (MCP) j .
3. Characteristics of MCP j .
4. ρ_j —coolant density in loop j .
5. T_j^c —coolant temperature in the cold leg of loop j .

The hot-leg enthalpy is calculated by the formula

$$J_k^{hot} = J_0^{hot} (1 + A_1(T_k^{hot} - T_0^{hot})) \quad (2.69)$$

where J_0^{hot} is the specific enthalpy of the coolant; T_k^{hot} —hot leg temperature of loop k ; A_1 —constant to be obtained by fitting; T_0^{hot} —nominal temperature of coolant in the hot leg. The thermal power W_k^P of loop j is determined as

$$W_k^P = G_k(J_k^{hot} - J_k^{cold}), \quad (2.70)$$

G_k —mass flow rate in loop k , and J_k is specific enthalpy in loop k , in the cold and hot leg, respectively.

A fraction of the coolant may flow bypassing the heated core. The so called gap fraction is estimated as

$$G_{gap} = G \frac{T_{mix} - T_{hot}^{ave}}{T_{mix} - T_{cold}}, \quad (2.71)$$

where G —total coolant flow of the loops; T_{mix} is the average temperature in the “mixing area”, T_{hot}^{ave} —average of the loop hot-leg temperatures. The cold-leg enthalpy J_0^{cold} enthalpy is determined analogously to (2.69):

$$J_k^{cold} = J_0^{hot} (1 + A_2(T_k^{cold} - T_0^{cold})). \quad (2.72)$$

There is no measurement in any control assembly, so there the flow rate and the enthalpy is only estimated. In an assembly equipped with exit temperature

measurement, the released power is calculated as

$$W_k^T = G_0(J_k^{hot} - J_{cold}) \quad (2.73)$$

with

$$J_k^{hot} = J_{k0}^{hot} (1 + E_2(T_{in} - T_0^{hot})) \quad (2.74)$$

and

$$J_k^{cold} = J_{k0}^{cold} (1 + E_1(T_{in} - T_0^{cold})). \quad (2.75)$$

In the last two equations constants E_1, E_2 are determined by fitting, $J_{k0}^{hot}, J_{k0}^{cold}, T_0^{hot}, T_0^{cold}$ are nominal values. It must be noted that the nominal values depend on the data of the MCPs, if the flow rates are different, if the entering temperatures do differ in the loops, corrections should be used.

Thus far we discussed the approximations from the point of view of technology. Now we pass on to the problem of assigning power to non-metered assemblies. We address the following questions:

1. How to compare the temperature rises in two or more different fuel assemblies?
2. How to assign a temperature rise to a non-metered assembly?

Using the readings provided by technology, we are able to determine the enthalpy rise in the metered assemblies. Some limits are formulated from the maximal temperature in the core, see Sects. 2.3.9 and 2.3.8.2, and with the help of the known coolant flow rates in the assembly, the released thermal energy corresponds a temperature rise. It is customary to use ΔT_i , the temperature rise in assembly i to assess the temperature distribution in the core. In the rest of the present Subsection we study the problem of estimating ΔT_i for non-metered assemblies.

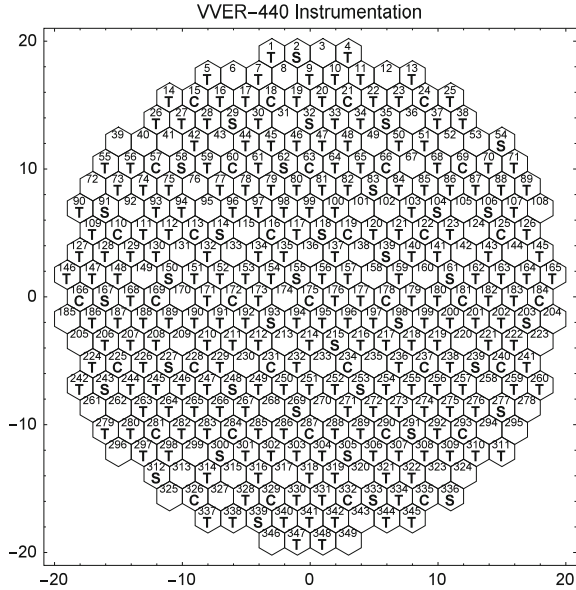
The first step is analyzing the in-core instrumentation with the goal of comprehending the concept of the designer.¹² The following questions need to be answered:

1. What is the portion of the metered assemblies?
2. Can a concept be seen from the distribution of the measured assemblies in the core?
3. What kind of anomalies can be detected by the implemented instrumentation?
4. How large is the area of the core not having any measurement?
5. Does the technology provide any additional information concerning the flow-rate distribution, the assembly in-let temperature distribution?

As an example, we analyze the VVER-440 core, see Fig. 2.18. The core has 349 hexagonal fuel assemblies, 210 of them implemented with exit temperature measurements, 36 with SPND chains, in each chain there are 7 rhodium detectors. There are 36 control assemblies located symmetrically plus the central assembly. There are 6 loops in the primary circuit, the reactor core is cooled a flow supplied by 6 MCP, arranged in 60° symmetry. There are temperature and flow-rate measurements in

¹²A lucky analyst may have a document where the concept is clearly formulated.

Fig. 2.18 Instrumentation in VVER-440 Core (C control assembly; T Thermocouple; S SPND chain)



each loop. Criticality is maintained either by boric acid solved in the coolant water or by moving control rods. There is a group of 7 control rods for fine criticality regulation.

The fraction of the measured assemblies is $(210 + 36)/349 = 0.704$. If 230 measurement works, $2/3$ of the core is measured. When the flow rates or inlet temperatures differ in the six loops, the difference may initiate flow rate and coolant temperature variations in the 60° sectors. Even small variations can be detected first by the loop instrumentation, or by the in-core instrumentation. The instrumentation is almost symmetrically implemented.

At the same time no control assembly has any implemented measurement. Usually the vendor provides data, for example the flow rate in a control assembly. The coolant exit temperature is usually measured over the fuel assembly and the coolant flow is turbulent, resulting in fluctuating measured temperature. The relaxation time can be estimated from thermal hydraulics model calculations and compared to the sampling cycle.

Temperature measurement is based on Eq. 2.8, which needs a reference cold point, which is a large metal mass kept in an isolated place to minimize possible temperature variations. Actually, there are several cold points, so a typical situation is shown in Fig. 2.19, which is one of the screens that the operator can see. The central part of the screen shows the assemblies equipped with temperature measurements. Each one is connected to one of the 12 cold points. Every in-core temperature measurement and loop thermometer is connected to two, different cold points. The cold points are redundant and independent. When the first cold point is not realistic, the evaluation

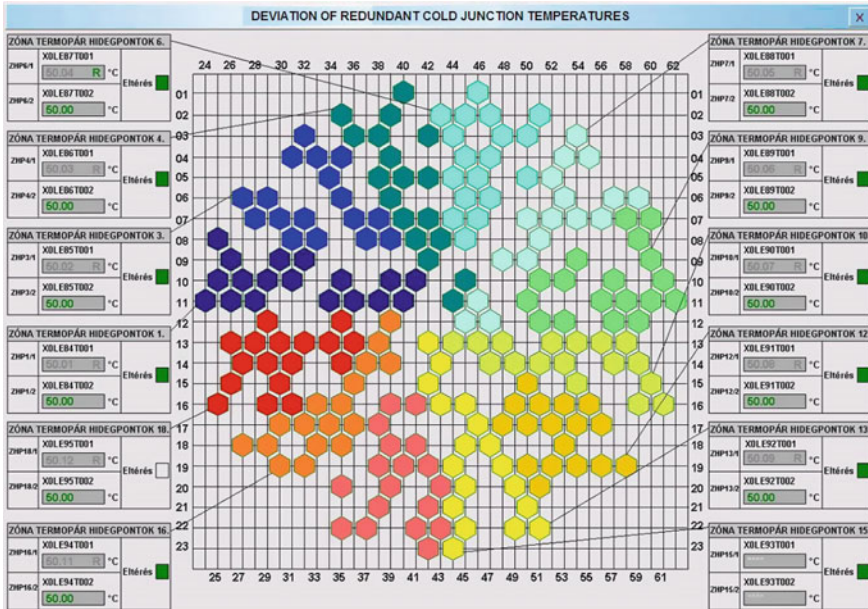


Fig. 2.19 Deviation of redundant cold junction temperatures in a PWR (Paks NPP, Hungary)

automatically switches to the other cold point. Figure 2.19. shows the differences between the first and second cold point temperatures.

Color code shows the locations of the thermocouples in the core, assemblies of a given color are assigned to the same cold point. Actual temperatures of the cold points are shown on the left and right side of the figure. Thermocouples are identified by a code X0LEXXTYYY, where XX is a number, YYY is 001 or 002. Under the code the temperature of the cold point is displayed. After the temperature a color code shows the status of the cold point values, green is OK, red is too high.

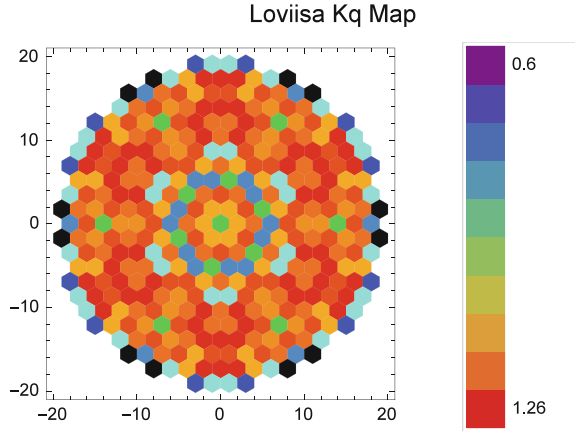
It is important that a cold point problem always effects a given group of assemblies as indicated in Fig. 2.19. Similarly, detector signals are processed by an electronics and knowing which measurements belong to a given electronics may help in identifying electronics failure. Such cases will be discussed in Chaps. 6 and 7.

The symmetric locations of loops, the symmetric core load suggests application of statistical model such as Eq. (2.54). The fitted sector amplitudes, the distribution of the Student fraction often may indicate flow anomalies.

Information of the axial variations comes exclusively from SPND chains. To provide the reader with an impression, what is the 210 thermocouple in a PWR core of 349 fuel assemblies, we present a measurement,¹³ see Fig. 2.20, on a PWR at Loviisa [27] NPP. Not the temperature increase is given but its relative value, the so-called k_q , which is the ratio of the assembly power to the average assembly power. As

¹³Actually, the data serve comparing measured and calculated values.

Fig. 2.20 Assembly-wise power distribution based on core outlet temperature measurements and calculations



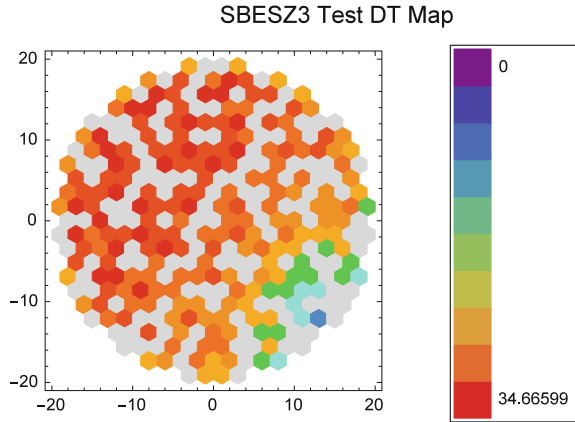
you have seen before, assembly positions should be defined unequivocally, and this is achieved in various ways. In Fig. 2.17 two coordinates are used, the horizontal one starts at 16, the vertical one at 1. In Fig. 2.16, the vertical positions are numbered, the horizontal ones are marked by letters from A to R. Our notation is more practical: the assembly centers are labeled, coordinates of the central assembly are (0, 0). This is practical since transformations like rotations and reflections are easy to be programmed. Assemblies are numbered consecutively starting from the uppermost left assembly and the numbers increase from left to right. In Fig. 2.19 we see another numbering, rows are numbered from top to bottom and positions within a row are numbered from 24 to 62.

The cold leg temperatures are important because their errors directly appear in the measured temperatures consequently in temperature differences the error is nearly doubled because the variance of the difference is the sum of the variances of the terms.

The calculations show 60° symmetry of the core. The face-to-face assembly size is $d = 14.7$ cm, compared to the thermal diffusion length λ_t we see $d \sim 8 - 10\lambda_t$. As diffusion length λ_f is greater in the fast energy groups, cf. Sect. 4.3, $d \sim 3 - 4\lambda_f$. These data suggest that strong difference in material composition (think of a control assembly) can be felt in the first neighbor assembly but rather weakly in the second neighbor.

In general, it is a good idea to study the measured field, see Fig. 2.21. We follow the major steps on the test case SBESZ3. The measurement is from a PWR of type VVER-440/213 at Paks NPP. All the 210 thermocouples work, the preprocessing indicated no problem, neither with the cold points nor with the electronic preprocessing. Yet a closer look at the temperature field shows a unusual temperature distribution. In assembly No. 74 we see $\Delta T = 33.5^\circ\text{C}$ but in the first neighbor assemblies we find 32.6°C at position 56, 34.7°C at position 93, and only 29.5°C at assembly 94. In the almost diametrically opposite positions we find 14 and 14.1°C at assemblies

Fig. 2.21 ΔT map at measured positions (SBESZ3 Test)



No. 259 and 241. In Chap. 3, we show that this may indicate the presence of a local perturbation in the core, see Eq. (3.12).

Location of the thermocouples does not allow for comparing exactly opposite positions thus a better picture is obtained after a more detailed temperature distribution. It is important not to add any additional information to the measured field. As far as we know, the core is symmetric, coolant flow rates do not indicate any essential difference in the flow rate distribution. Thus we may assume more or less symmetric power distribution in the core. In such situation factorization (2.51) must be a good approximation. We use (2.55) and (2.56) to find sector amplitudes a_s , $s = 1, \dots, 6$ and sector distribution ψ_i , $i = 1, \dots, 59$. Details of fitting in is discussed in Appendix G. The sector amplitudes are, after appropriate normalization, as listed below:

$$0.9822, 1.149, 1.1971, 1.1431, 0.8961, 0.632498 \quad (2.76)$$

Sector 1 is North-East, and sectors are numbered counter clock wise. Amplitude of the Nord-East sector (0.632498) is approximately half of the amplitude of the Nord-West sector (1.1971). This corroborate the first observation: there is a strong flux gradient in the core.

The next step is to compare the measured and fitted values in the measured positions, see Fig. 2.22. There is no doubt: there is a North-West to South-East flux tilt in the measured data. We go on analyzing the Student fraction map, which is a statistical characteristics of the fit, see Fig. 2.23. Roughly Student fractions in the interval $[-3, +3]$ are acceptable but 2–4 outlier points are still within the statistical error. Frequencies of Student fractions are shown in Fig. 2.24. In the large number of zeros take into account that the 139 non-metered positions are marked by zero on Fig. 2.24. This concludes the statistical analysis. Certainly, the final goal is to find out how to interpret the anomaly. For example, the observed data may be caused by a coolant flow anomaly, a wrong control rod position and so on. Further analysis methods are discussed in Chaps. 5–7. Time series analysis of the thermocouples may also reveal

Fig. 2.22 Measured-reconstructed ΔT maps at measured positions (SBESZ3 test)

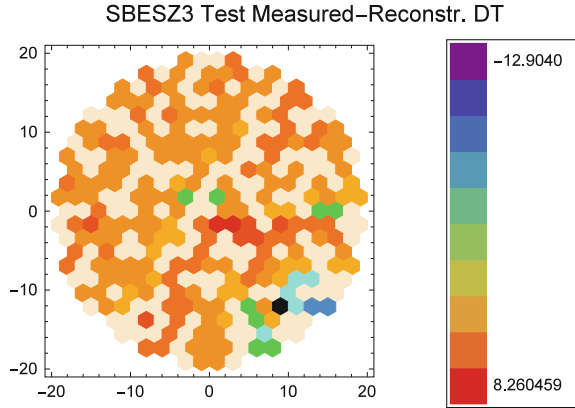
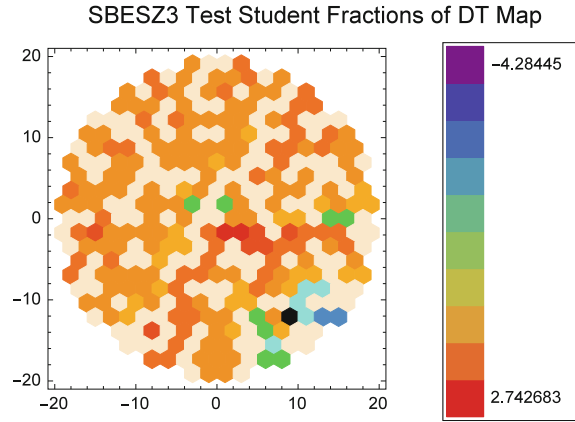


Fig. 2.23 Student fractions of ΔT map at measured positions (SBESZ3 test)



technical problems. Simple indicators like mean value and variance may indicate signal processing problems, see Fig. 2.25, where the variance is too large compared to variance of other detectors. The reason is that a bit of the analogue-digital converter “flip-flops”, randomly varies between two states. The length of the investigated period is 1500 s, during that interval flip-flop of at least three bits can be observed. Let p stand for the probability of a measurement failure. Let p be the probability of a failure. Assuming failures to be independent, the probability that 16 measurements fail is

$$\binom{246}{16} p^{16} (1-p)^{230} \sim 5.2 * 10^{24} p^{16}. \quad (2.77)$$

When $p = 0.01$, and detector signals are read out in a cycle of 16 s, the mean value of the time between two failures of 16 detectors is appr. 185 days.

The first question is: can we give an estimation for the non-metered assemblies? To answer, a simple and effective approximation discussed in connection with Eq. (2.67) will be used. Usually, it is a good idea to assume core symmetry. When there is some

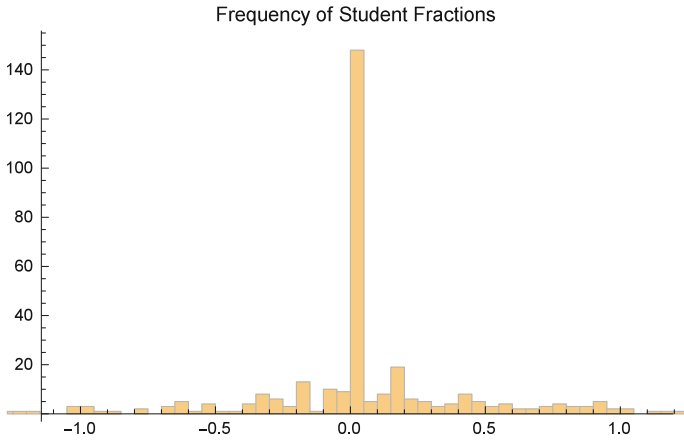


Fig. 2.24 Frequencies of Student fractions (SBESZ3 test)

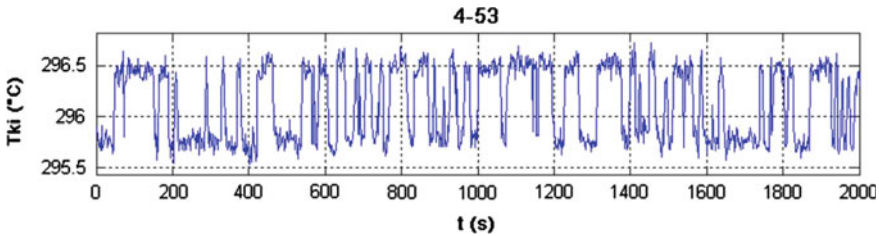


Fig. 2.25 Unstable signal in assembly at coordinates (4–53)

slight asymmetry, the difference in the sector amplitudes will reflect it. When the core is symmetric, it is possible to divide the core into sectors, e.g. 60°, 120° or 180° symmetry sectors can be observed in Fig. 2.20. The simplest solution is to find orbits, elements of which are transformed into each other by core symmetries, and the missing positions are filled up by rotations. Most core processing code has that option. Chapter 6 provides more sophisticated methods.

If the Reader doubts whether or not it is economic to implement a complicated and expensive in-core instrumentation, the answer is given in an EPRI study, see Ref. [17].

2.3.8 Pin Power Estimation

Safety limits bound the maximal pin power value and maximum pin linear power, too. We have given methods for obtaining assembly power in Sect. 2.2. The power distribution inside an assembly may vary if the moderator-to-fuel ratio depends on position within an assembly or if the assembly contains absorber pins. An assembly

located near to the core edge contains a power gradient because of the different surroundings. Unfortunately there exists no instrumentation to measure pin powers in a fuel assembly. That problem must be studied by numerical models.

2.3.8.1 Intra-Assembly Power Distribution Determination

The intra-assembly power distribution is determined using results of the assembly powers determined in the core. When the diameter of a fuel cell is of the order of a typical thermal mean free path, usually a few-group diffusion equation is solved for example by the finite difference method, Monte Carlo (see MCU code [54]) or collision probability method (WIMS code [55]). As to thermal hydraulics codes, see [6, 29].

2.3.8.2 Intra-Assembly Sub-Channel Temperature Determination

At the stage of sub-channel calculation, the assembly powers have been determined. The assembly powers are either assembly integrated or averaged. The structure of the assembly fixes the geometry of the sub-channel structure and the task is to determine the flow rates, coolant temperature distributions, and the power profiles in the sub-channels. The physical problem is to determine the distributions of mass, energy and momentum in the assembly. To carry out the calculations, we formulate the conservation equations to see what kind of physical parameters are required to lay down the conservation equations, and to assess the complexity of the problem. Right at the beginning, we note that two approaches are used in the problem formulation: the first one is called porous model, the second one is called sub-channel model. The latter is used in the BWRs and PWRs. For readers interested in the approach of the first model, we mention a few code names: THINC-1 [1], JOYO [2], MISTRAL [4], TEMP [5], POUCHOK [8], FLICA [7]. The porous model is compared to the sub-channel model in Ref. [9].

We write the balance equations into the following form. The starting point is the formulation used in non-equilibrium statistical physics [10] but we change the notation to the form used in Ref. [29]. We start with the mass conservation:

$$\frac{\partial \rho(\mathbf{r}, t)}{\partial t} + \nabla(\rho \mathbf{V}) = 0, \quad (2.78)$$

where ρ is the fluid density, \mathbf{V} is the coolant velocity, \mathbf{r} and t are the space variable and the time, respectively. ∇ is the Nabla operator. We introduce the so-called substantial time derivative:

$$\frac{D}{Dt} = \partial t + \mathbf{V} \nabla. \quad (2.79)$$

The momentum balance of the fluid takes the following form:

$$\partial \rho \mathbf{V} t + \nabla(\rho \mathbf{V} \mathbf{V}) = -\nabla P + \nabla \tau + \rho \mathbf{g}. \quad (2.80)$$

Here P is the pressure, τ is the shear stress in the fluid, \mathbf{g} is the gravitation force.

Balance of the internal energy u of the fluid reads as

$$\partial \rho u t + \nabla(\rho u \mathbf{V}) = -\nabla \mathbf{q}'' + q''' + P \nabla \mathbf{V} + \Phi_\mu, \quad (2.81)$$

where q'' is the conduction of heat in the fluid, q''' is the volumetric heat deposit directly into the fluid due to neutrons escaping from the fuel rods; Φ_μ is the dissipation due to viscous stresses in the fluid. The heat conduction vector \mathbf{q}'' is proportional to the temperature gradient:

$$\mathbf{q}'' = -k \nabla T, \quad (2.82)$$

therefore $\nabla \mathbf{q}'' = -k \Delta T$. With the help of fluid enthalpy h the internal energy equation can be written as

$$\frac{\partial \rho h}{\partial t} + \nabla(\rho h \mathbf{V}) = -\nabla \mathbf{q}'' + q''' + \frac{\partial P}{\partial t} + \mathbf{v} \nabla P. \quad (2.83)$$

Note that here viscous dissipation has been dropped as it is neglected in the COBRA model [29].

Enthalpy can be used also in the energy conservation resulting in

$$\rho \frac{Dh}{Dt} = -\nabla \mathbf{q}'' + q'''. \quad (2.84)$$

The above given equations are supplemented with the following equation of state expressions:

$$\rho = \rho(P, h), \quad (2.85)$$

$$T = T(P, h), \quad (2.86)$$

$$\mu = \mu(P, T), \quad (2.87)$$

here μ is the viscosity, and

$$k = k(P, T), \quad (2.88)$$

k is the thermal conductivity.

Since there may be liquid and vapor in the coolant channels, it is reasonable to use the two-phase mixture balance equations. An arbitrary volume V is bounded by a surface A and in V vapor and liquid occupies volume V_v and V_l , respectively. The mixture of liquid and vapor flows past fuel rods of diameter D_f . The fuel-mixture boundary is either a heated surface or a wetted perimeter P_H . Vapor and liquid are assumed to be uniformly distributed throughout the flow field and variations of the fluid properties are neglected. We take the flow direction x upward along the channel

wall. The volume fraction occupied by the vapor per unit volume of the mixture in the control volume, the void fraction, is denoted by α_v :

$$\alpha_v = \frac{V_v}{V}. \quad (2.89)$$

Here V_v is the volume occupied by vapor, and V is the total volume occupied by vapor and liquid. Consequently, the volume fraction occupied by the liquid is

$$\alpha_l = 1 - \alpha_v. \quad (2.90)$$

The next important term is called flow quality, written as χ , and is the ratio

$$\chi = \frac{F_v}{F}, \quad (2.91)$$

and $0 \leq \chi \leq 1$.

Finally, we arrive at the following conservation equations used in the COBRA model [29, Sect. 2.2.3]:

1. Mass conservation:

$$A \frac{\partial}{\partial t} \rho + \frac{\partial}{\partial x} F + \sum_{k \in i} e_{ik} w = 0. \quad (2.92)$$

Here A is the subchannel flow area, w -mass flow per unit length in the lateral direction through the gaps. e_{ik} -subchannel index.

2. Axial momentum balance equation:

$$\begin{aligned} A \frac{\partial \rho U}{\partial t} + \frac{\partial \rho U^2 A}{\partial x} + \sum_{k \in i} e_{ik} \rho U V s = & -A \frac{\partial P}{\partial x} - \frac{1}{2} \left(\frac{f_w}{D_{hy}} + K_{ll'} \right) \rho U |U| A \\ & - C_T \sum_{k \in i} w'(\Delta U) - A \rho g \cos \theta. \end{aligned} \quad (2.93)$$

Here U is the flow velocity of the two-phase mixture, g is the gravitation constant.

3. Lateral balance equation

$$s \frac{\partial \rho V}{\partial t} + s \frac{\partial \rho V U}{\partial x} = \frac{s}{l} [P_{l+\Delta l} - P_l] - \frac{1}{2} \frac{s}{l} K_G \rho V |V| \quad (2.94)$$

Here K_G is the loss coefficient.

4. Subchannel energy conservation equation:

$$A \frac{\partial \rho h}{\partial t} + \frac{\partial \rho U h A}{\partial x} + \sum_{k \in i} e_{ik} \rho V h s = \sum_{m \in i} \phi_{im} P_H q_W'' + \sum_{m \in i} C_Q \phi_{im} q' - \sum_{k \in i} w'(\Delta h), \quad (2.95)$$

where C_Q is the fraction of the rod power generated directly in the coolant.

5. Equations of state. The enthalpy of each phase and the saturation temperature are:

$$h_l = h_f(P); \quad h_v = h_g(P); \quad T = T_{sat} P \quad (2.96)$$

the phase density is

$$\rho_l = \rho_f(h_l); \quad \rho_v = \rho_g(h_v). \quad (2.97)$$

The transport properties are:

$$\mu_l = \mu_f(h_l); \quad \mu_v = \mu_g(h_v); \quad k_v = k_g(h_v); \quad k_l = k_f(h_l). \quad (2.98)$$

The surface tension is

$$\sigma = \sigma(P). \quad (2.99)$$

The specific heat at constant pressure is:

$$C_{pl} = \left(\frac{\partial h_l}{\partial T_l} \right)_P \quad (2.100)$$

The mixture quality is

$$\chi = \frac{h - h_l}{h_v - h_l}. \quad (2.101)$$

In COBRA, the vapor void fraction is obtained from an empirical correlation relating the void fraction to the quality and transport properties. The correlation is written in the form of

$$\alpha_v = \alpha_v(\chi, \rho_v, \rho_l, \sigma, \dots). \quad (2.102)$$

In the numerical model, the fuel assembly is usually represented by a regular fuel array and the coolant flows in sub-channels between the fuel rods. Heat is generated in the fuel and a heat flux is given along the surface of fuel rods. A simplified geometry is shown in Figs. 2.26 and 2.27 for a square and triangular assembly, respectively. In Fig. 2.26, four fuel pins determine a subchannel, which is called control volume and is indicated by a thick line. Boundary of a subchannel consists of four arches A_w and four straight lines A_t . The diameter of a fuel pin is D_r . A 60° sector of the elementary volume in a hexagonal assembly is shown in Figure 2.27. Positions in the control volume are given by coordinates U, V , the height of the control volume ΔX , the area at $U = \text{const}$ is A and the area is determined by S , the distance between perimeters of two neighboring fuel rods.

Before setting out for the numerical methods, the analyst has to decide what is the goal of the assembly calculation. A few of the possible options:

1. To analyze the safety margins. One topic is the power peaking factor in the assembly, a second topic is the maximal coolant and fuel temperatures. The H/U

increases with the complexity of the calculational model. The model determines the number of unknowns in the problem as fine details can not be deduced from a coarse discretization. The calculation is usually carried out in 3D, the structure of the assembly determines the number of discretized elements. An important issue is the number of axial layers which may increase the computation time considerably.

A numerical procedure, in which the above derived variables can be used includes the following steps:

- discretization: usually one can choose an appropriate geometrical model ranging from the 3D full core calculation to a symmetry element of an assembly. At the boundary of the chosen geometry an appropriate boundary condition should be fixed.
- choosing an appropriate numerical method;
- setting up an iterative scheme;
- acceleration of the solution.

In a production code, like COBRA, the mentioned elements have been elaborated carefully and in accordance with each other. Below we assess some of the above mentioned elements in connection with a practical problem.

At a recent revision [3] of the simulator code RETINA, the impact of the increased H/U ratio on the power at the assembly corner, see Fig. 2.1, has been investigated. There is no measurement implemented to study the intra assembly power distribution, so the effect has been studied by numerical models. The number of sub-channels is 264. The numerical study started with a refinement of the spatial discretization, see Fig. 2.28. In COBRA, corner sub-channels are represented by one element but to improve the model each corner sub-channel has been divided into two parts. For example at the left-top corner elements No. 1 and No. 202, at the topmost corner No. 8 and No. 263 replace one COBRA channels, respectively. Later on the averages of the elements are used in the calculation. Pins in the vicinity of the assembly boundary and especially the corners have been modeled by a more refined mesh.

To minimize the error due to the external boundary condition, the studied area included the central assembly to be analyzed and its six neighbors, see Fig. 2.29. There is a central tube at the center of fuel assembly increasing the local H/U ratio. In code testing, a simplified power has been used, see Fig. 2.30, to model power distribution inside a PWR assembly. Powers of fuel pins adjacent to the central tube were set to 2.2 kW, whereas powers of other fuel pins were set to 1.5 kW. The calculated axial power distribution is expected to reflect the lateral mixing inside the assembly, and that can be seen in the axial temperature profile.

In the assembly under consideration, the power and temperature distributions have been determined by FE method using triangular elements inside the assembly. Note the special discretization at the assembly corners in Fig. 2.31. The model also served studying the coolant mixing effect in a PWR simulator. Figures 2.31 and 2.32 show the sub-channel temperature values in layer No. 2 and 6, respectively. In Fig. 2.31, the lateral temperature distribution at level 2 shows sharp variations, notwithstanding in Fig. 2.32 the temperature distribution is less sharp.

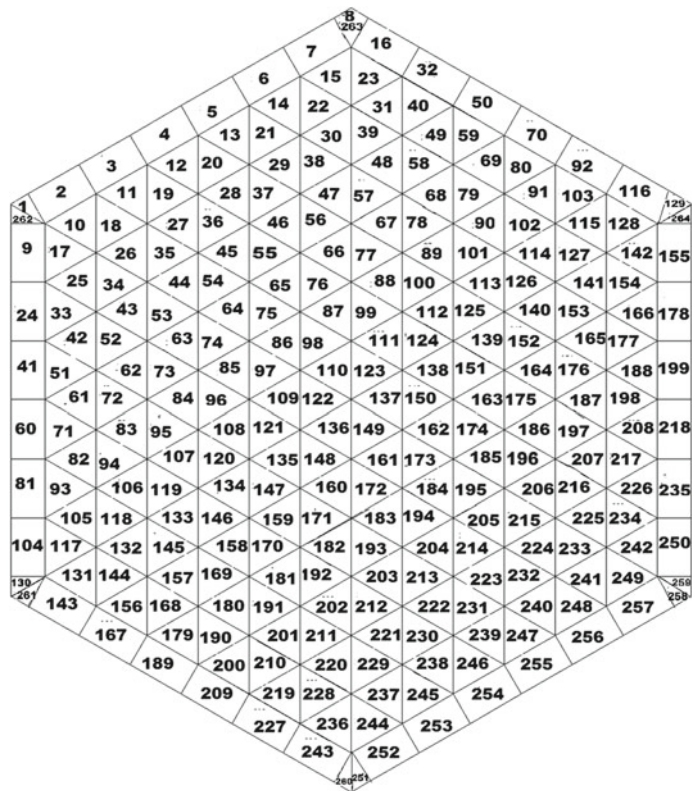
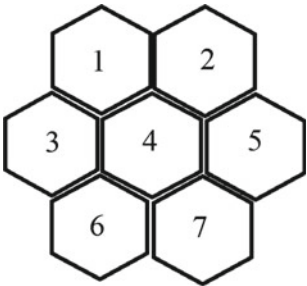


Fig. 2.28 Discretization in a hexagonal assembly [3]

Fig. 2.29 Surroundings and boundary condition [3]



Let us stop for a moment, and look back in time. Technical development has made it possible to refine the mesh structure. In the sixties quite modest geometrical representations had been used, see [6]. In general, the geometrical model is determined by the structure of the assembly. Merging geometrical elements accelerates, subdividing

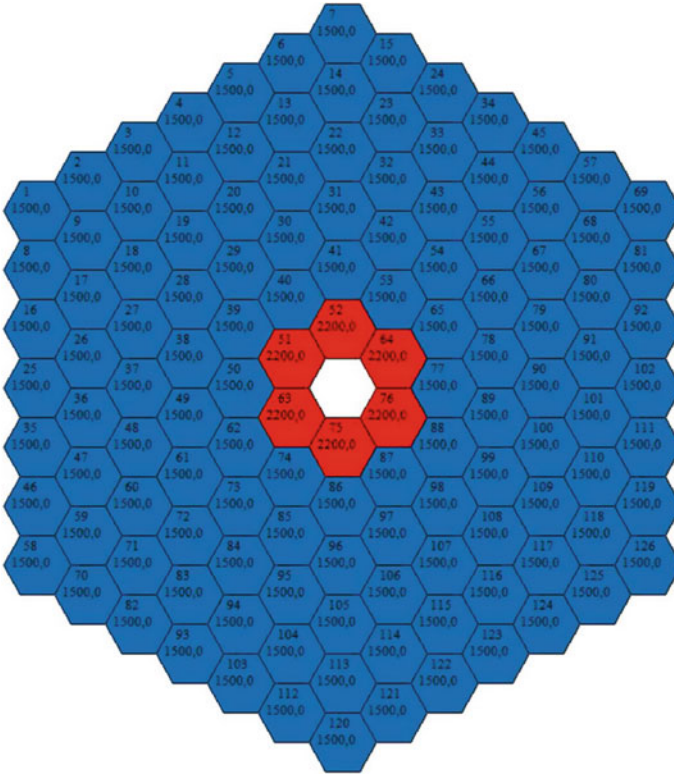


Fig. 2.30 Cells and initial pin powers in a hexagonal assembly [3]

slows down the calculation. From the sixties, a typical discretization of a hexagonal and a square assembly are shown in Fig. 2.33 reproduced after [31] and Fig. 2.34 after [30], respectively. In Fig. 2.34 gap numbers are in boxes, channel numbers are simple numbers.

The two most often used numerical methods are the finite difference and finite element methods. In general, the finite difference method is simpler to implement and the finite element method is more efficient. For details, see Sect. A.1. It is important that the geometry in thermal hydraulics problems differs from the geometry in neutronics problems. The reason is that in neutronics problems the assembly is treated as a unit, whereas in thermal-hydraulics the coolant description may vary from sub channel to sub channel.

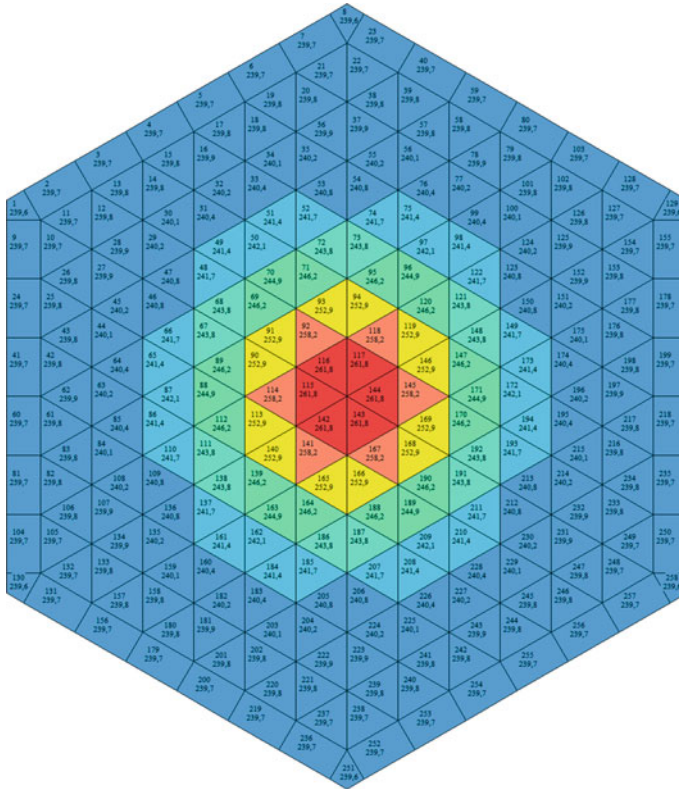


Fig. 2.31 Sub-channel temperatures calculated by FEM at axial level no. 2 [3]

2.3.9 DNBR Estimation

Fission produces heat in the fuel pins, the released heat is transferred to the coolant streaming around the fuel pin. When the heat flux is increased so much that the heated surface can no longer maintain continuous liquid contact, boiling crisis occurs. The heat flux when boiling crisis occurs is called critical heat flux (CHF). Actually, the transferred amount of heat depends on the flow regime of the coolant. A rough subdivision of flow regimes is:

- the heated surface is surrounded by coolant in liquid state. The coolant flow may be laminar or turbulent, the heat transfer is larger in turbulent flow.
- steam bubbles appear in the coolant. The heat conductance of bubbles is small, the energy transfer is worse than in flow regime.
- when the number of bubbles grows, the bubbles may form a stable bubble film, or slugs. That regime of flow may lead to local overheating of the clad.
- the flow may take annular form, that may transform into dispersed flow of coolant and bubbles.

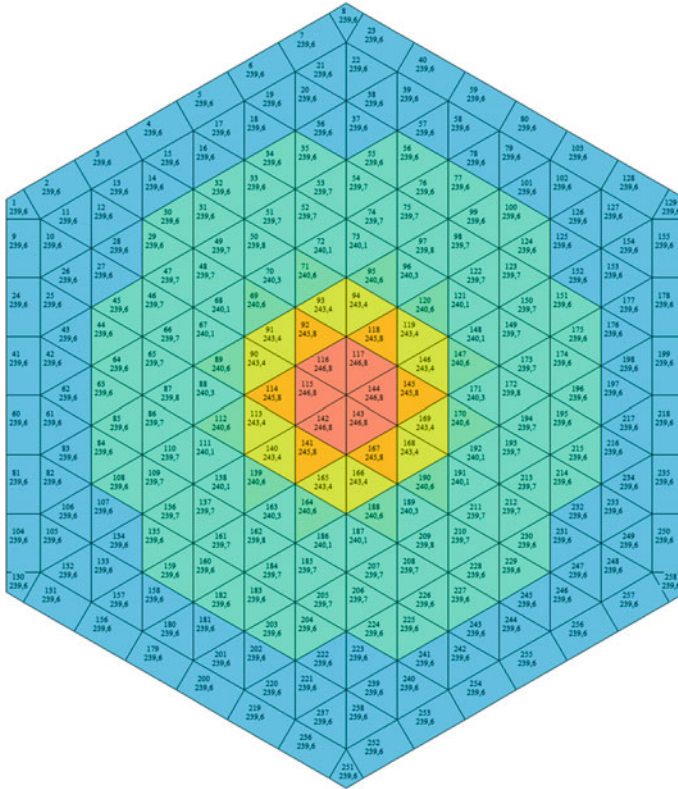


Fig. 2.32 Sub-channel temperatures calculated by FEM at axial level no. 9 [3]

The quality of heat transfer depends on the surface features [21]. For example the RELAP code has an input parameter describing the surface quality of the heated volume.

Once the predicted CHF is known, it may be used to express the local heat flux divided by CHF, see Fig. 2.35. Notations on the figure: G -mass flux P -pressure, T_{in} -inlet temperature.

The CHF sets a limit to the amount of power transferred and may lead to heated surface damage. The CHF depends on the flow regime, and the presence of steam phase. The following scenarios are distinguished:

1. Departure from Nucleate Boiling (DNB).
 - a. *Nucleation induced*. At high subcooling, when mostly nucleate boiling transfers the heat, that type of CHF is often encountered. Bubbles grow and collapse at the wall, and convection takes place between bubbles. DNB occurs at very high surface heat fluxes. CHF occurrence depends on local heat surface flux and flow conditions.

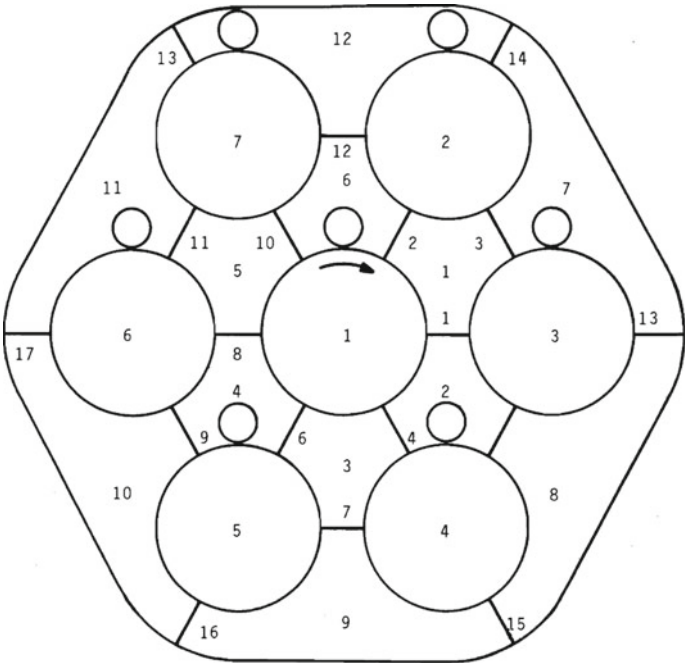
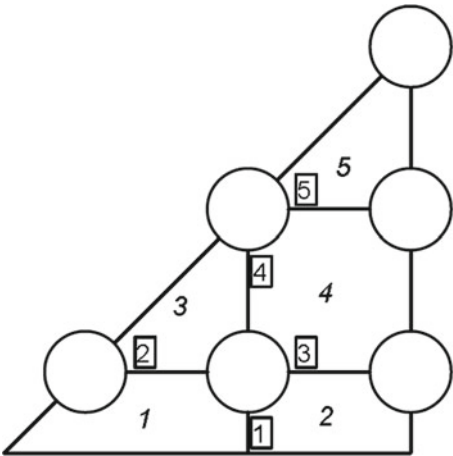


Fig. 2.33 Discretization in a hexagonal assembly [6]

Fig. 2.34 Discretization in a square assembly [6]



- b. *Bubble clouding*. [20] The number of bubbles generated in subcooled and saturated nucleate boiling depends on the heat flux and bulk temperature. The bubble population density near the heated surface increases with heat flux and often a so-called bubble boundary layer forms a short distance away from the surface. If this layer is sufficiently thick it can impede the flow of coolant to the heated surface. This in turn leads to a further increase in bubble population until the wall becomes so hot that a vapor patch forms over the heated surface. This type of boiling crisis is also characterized by a fast rise of the heated surface temperature (fast dryout). Physical failure of the heated surface frequently occurs under these conditions.
2. Helmholtz instability. In saturated pool boiling, the CHF is limited by the maximum vapor removal rate. Ultimately at very high heat flux levels, the relative velocity between liquid and vapor will be so high that an unstable flow situation is created, resulting in a CHF condition. A similar situation can be considered at very low flow rates or flow stagnation conditions. This type of CHF is accompanied by a rapid rise in surface temperature (fast dryout).
3. annular film dryout.
4. unstable or periodic dryout.
5. slow dryout.

Methods for predicting CHF. Because of the many possible fuel bundle geometric shapes, a wide range of possible flow conditions and the various flux distributions, it is impossible to predict the CHF for all cases with a single CHF prediction method and a reasonable degree of accuracy. The complexity of predicting the CHF in a nuclear fuel bundle may be best understood by first considering the prediction of CHF of a simplest experimental setup; a uniformly heated tube cooled internally by a fluid flowing at a steady rate vertically upwards. Here the CHF is a function of the following independent variables:

$$CHF = f(L_H, D_\ell, G, \Delta H_{in}, P, E) \quad (2.103)$$

where L_H is the heated length, D_ℓ -diameter, G -mass flux, ΔH_{in} -enthalpy, P -pressure, and E is the global quality of the surface including: roughness, thermal conductivity and wall thickness. For further models and details see Refs. [20, 26].

Design criteria aim at providing

“adequate heat transfer which is compatible with the heat generation distribution in the core such that heat removal by the Reactor Coolant System or the Emergency Core Cooling System (when applicable) assures that the following performance and safety criteria requirements are met:

1. *Fuel damage¹⁴ is not expected during normal operation and operational transients (Condition I) or any transient conditions arising from faults of moderate frequency (Condition II). It is not possible, however, to preclude a very small*

¹⁴Fuel damage as used here is defined as penetration of the fission products barrier (i.e. the fuel rod clad).

number of rod failures. These will be within the capability of the plant cleanup system and are consistent with the plant design bases.

2. *The reactor can be brought to a safe state following a Condition III event with only a small fraction of fuel rods damaged although sufficient fuel damage might occur to preclude resumption of operation without considerable outage time.*
3. *The reactor can be brought to a safe state and the core can be kept subcritical with acceptable heat transfer geometry following transients arising from Condition IV events."*

As to CHF or DNB, it is assumed that exceeding DNB or CHF leads to fuel damage. Thermal hydraulic design criteria are formulated in terms of confidence level for the departure from nucleate boiling ratio (DNBR) or critical heat flux ratio. Sometimes also the critical power ratio (CPR) is used. The mentioned terms are defined as

$$DNBR = \frac{\text{DNB heat flux at a location}}{\text{local heat flux at the same location}} \quad (2.104)$$

$$CHFR = \frac{\text{CHF heat flux at a location}}{\text{local heat flux at the same location}} \quad (2.105)$$

$$CPR = \frac{\text{Power level to produce CHF}}{\text{fuel assembly power level}} \quad (2.106)$$

As CPR depends on the pressure, temperature and the inlet flow, either one should be taken the value at the CHF.

Some care is needed when dimensionless parameters are used in a thermal hydraulics problem. Note that "characteristic distance" and other engineering parameters are not well defined. In such a simple geometry as a cylindrical pipe a characteristic distance may be the diameter or the length of the pipe, depending on the problem under investigation. Furthermore, the subject of thermal hydraulics analysis is often a complex problem, where in various regions different characteristic distances, velocities etc. can be given. Below we give a list of frequently encountered problems in nuclear engineering amenable to thermal hydraulics analysis. Most of the problems adhere to the technology of the power plant:

1. Heat transfer models in the core;
2. Anticipated transients without SCRAM¹⁵;
3. containment transient analysis;
4. turbine transients, such as turbine trip;
5. steam generator transients;
6. loss of feedwater transients;
7. loss of off-site power;
8. core modeling;
9. coupling core and coolant system;
10. transient analysis;

¹⁵SCRAM-System Control Rod Automatic Motion.

11. component analysis;
12. safety analysis;
13. severe accident analysis;
14. loss-of-coolant-accident (LOCA) analysis.

When regarding the thermal hydraulics of the reactor core, we encounter the following problems:

1. Two-phase flow;
2. Heat transfer;
3. Phase change;
4. Coolant dynamics;
5. Sub-channel analysis.

System codes have been developed for solving the above problems. We only mention only a few generally used system codes: ATHLET, CATHARE, COBRA, MEL-CORE, RELAP. These codes have been developed at large research centers, and are carefully tested. Notwithstanding CATHAR has been designed for severe accident modeling, RELAP is a best estimate code to analyze transients and postulated accidents in LWR systems. COBRA has been developed for transient analysis and LOCA analysis. MELCOR is a severe accident analysis code.

2.3.10 Further Parameters

Thus far we have been discussing continually working core monitoring. There is however, a measurement to monitor degradation of the reactor vessel. The material of the reactor vessel is a special steel alloy. The venue of the energy release is inside the reactor core. The maximal temperature in the core may exceed 330°C during energy production, the pressure is about 155 bar . At the end of a fuel cycle, the steel temperature may be considerably lower. The design life time of a reactor is 30–60 fuel cycle.

Alloys are overcooled liquids, with a grain structure. It means that the steel is composed of domains of a few micrometer size. Within a domain atomic components (iron, carbon, complementers in low concentration like cobalt, phosphor, and impurity) are arranged in a more or less regular and stable order. It is important that the domain structure is stable, at normal reactor temperature the atoms do not change their respective positions. At domain boundaries the equilibrium is fragile, different forces act on atoms at domain boundaries and slow processes, like diffusion may result in slow variation of the domain boundary. Temperature or concentration gradient speed up migration of atoms trapped in interstitial positions. When the reactor vessel is warmed up and cooled down, thermal stress may cause migration of atoms near domain boundaries.

Reactor pressure vessel is subject to radioactive radiation. The fission process in the fuel assemblies next to the reactor pressure vessel provides among others

high energy neutron and gamma radiation. A collision with a high energy particle may create new vacancies and interstitial lattice disorders. These may deteriorate the mechanical properties of the vessel.

To monitor mechanical properties of the reactor pressure vessel, a sample set is located in the vicinity of the core barrel. Samples have been made from the same material as the core barrel, and at the end of a fuel cycle some of the samples are analyzed to check on the progress of the reactor vessel degradation.

2.4 Safety Aspects of Core Monitoring

As mentioned in Sect. 1.1, safety analysis fixes limits for the key reactor parameters insuring safe operation. Now we discuss the role of in-core instrumentation in reactor safety.

Reactor operation rests on two pillars: calculational methods and measurements. None of them is perfect as calculation uses a large amount of measured parameters like cross-sections, material properties like heat conductance, heat capacity, specific heat, and models like diffusion approximation, transport theory, flow regime of the coolant, heat exchange models and many others. Why do reactor designers, constructors, operators and safety instructors believe that such a complex system is reasonably safe?

The present chapter discusses the in-core measurements. We did not discuss the loop measurements which also serve as a cross-check of safety parameters. The ionization chambers, the coolant loop energy balances serve as independent measurements of the key measured values in the core. Calculational models are surveyed in Chap. 4 and provide adequate means to solve practical problems in the field of reactor operation. All these provide a sound basis for safe reactor operation.

The present Section is a short detour to basic terms of safety assessment based on statistical considerations [49, 56]. We assume the existence of a calculational model, which may contain approximations, whose results need not be exact but reasonably accurate. Neither the input of the calculational model nor the calculational model is assumed to be perfect. Statistical foundation has been elaborated in Refs. [50–53]. In our analysis the computer model is a code running on a computer, it is actually a function

$$y = f(x_1, x_2, \dots) \quad (2.107)$$

mapping a given x_1, \dots input into output y . When the input variables are considered deterministic, y is also deterministic: when we repeat the calculation we get the same result.

Usually input parameters are obtained either from measurement, or from other models. For example the neutron flux is calculated from geometry data, material compositions and cross-section data of the involved isotopes. Even a deterministic calculation includes random elements, therefore it is reasonable to carry out several

calculations with possible inputs and estimate the most unfavorable y even in a deterministic model.

Running model (2.107) N times, we get y_1, \dots, y_N output values. From the output values it is possible to construct functions $L(y_1, \dots, y_N)$ and $U(y_1, \dots, y_N)$ such that the majority of the calculated values are in the interval $[L, U]$. If the unknown distribution function $g(y)$ of the calculated value were known then

$$\int_L^U g(y)dy > \gamma \quad (2.108)$$

would hold, where $\gamma < 1$ but is close to one. The probability $\beta < 1$ that (2.108) holds can be given:

$$\beta = \sum_{j=0}^{s-r-1} \binom{N}{j} \gamma^j (1-\gamma)^{N-j} \quad (2.109)$$

with

$$L = y(r), U = y(s), \quad (2.110)$$

provided the calculated outputs are ordered in monotonously: $y_i < y_{i+1}$, $1 \leq i \leq N-1$. Clearly $\gamma \leq 1$ and $\beta \leq 1$. Having any finite number of output, only a statistical statement can be formulated. When U is the largest calculated output y_N , we have

$$\beta = 1 - \gamma^N. \quad (2.111)$$

Since one finds misinterpretations in the engineering practice, it is not superfluous to underline the proven notion of formula 2.111: β is the probability that the largest value $y(N)$ of a sample comprising N observations is greater then the γ quantile of the unknown distribution of output variable y . Another formulation asserts that γ is the probability that the interval $(-\infty, y(N)]$ covers a larger than γ portion of the unknown distribution $g(y)$ of the output variable y .

It should be emphasized again and again: there exists only relatively safe operation of any industrial device. The goal in design and operation of a device should be content with a given risk. Acceptable risk is determined by mechanisms of the society often formulated as laws, regulations etc. Experts' duty is to point out risks, to suggest risk reduction.

In practice, the number of output parameters is larger than one as it should include maximum power rates in fuel assemblies and pins, exit assembly temperatures and so on. When several output variables should be accounted for, the problem becomes more complex because the output variables may be correlated. The problem is analyzed in Sect. 5.2.1.1.

2.5 Characteristic Approaches Used in Various Systems

The first question to be answered in a core monitoring system is what is the system based on? Possible answers range from the measured values to the calculated distribution with a weighted sum of the two in between. We assess the mentioned possibilities one after the other.

1. Measurement based approach. It is natural that measured values should not be altered without a reasonable cause. But what to do with the positions without measurement? When the core symmetry has been confirmed, within one orbit the assembly powers can be restored by using core symmetry.
2. Calculation based approach. Once we have a well tested calculation model why not base the interpolation on it? That attractive idea may hinder another goal of in-core instrumentation: to check if the actual reactor state has departed from the planned state. Comparing measured powers and calculated powers may lead to discovery of measurement errors, misloaded fuel assemblies.
3. Mix of measurement and calculation. It is reasonable to use the reliable measured values and use the calculated values at unmeasured positions.

First the in-core instrumentation should be studied. Distribution of the metered assemblies speaks of the intention of the designer. The measurement pattern should serve among others unveiling a wrong measuring device (cold point, electronic contact error, electronic processing error, etc.), check core load symmetry. On the other hand remember, individual entering coolant temperatures are not measured thus local flow pattern anomalies (e.g. due to crud) are mostly detected by local temperature measurements.

Even when the calculational model has proved rather accurate at tests, remember that the accuracy depends also on the input data. In a stationary reactor state it is not a problem to provide good quality input but in a transient this is not so. A reactor is almost always in a stationary state so first we assess the input needed for a calculational model in stationary state.

1. Fuel assembly parameters. Good calculation needs good input. Fuel assembly parameters include enrichment, burnup level,¹⁶ isotopic composition as required by the calculational model.¹⁷
2. Global parameters of the reactor: assembly wise coolant flow rates, positions of the control rods, boron concentration, reactor power.
3. Core geometry. Fuel assemblies geometry should be given with adequate accuracy. Computations are usually based on simplified models so do not use individual assembly height.
4. Boundary conditions. The albedo to be used at the reflector boundary has been studied carefully usually at the code development stage. The albedo to be used at

¹⁶This is especially important when there are assemblies with burning poison in the core.

¹⁷This depends on the goal of the calculation. A number of codes put up with one initial enrichment and one burnup level, others may require a number of fissionable isotopes or fission products.

the top of a PWR is usually established by fitting the calculated criticality to the observed criticality.

5. Initial conditions. As a code used in core monitoring calculates one given core which changes rather slowly, the first core state can be taken from the core design calculation.

A calculational model to be used in core monitoring considerably differs from the models used in core design or economic calculations. Core state is updated relatively slowly, and there is an excellent initial guess: the previous calculation. Slow variations, like burnup or slow transients may be neglected.

2.6 Core Monitoring in Various Reactor Operation States

Measured values are displayed at the operator's board after signal processing. The operator should have a chance to notice if the measured value is "strange" and the operator should be provided by means to solve the riddle: how to resolve the observed contradiction. That requires a careful signal processing, but failures may not be excluded. Manuals should prefer operator's action towards the safer direction in unclear situations.

In over 91% of the time reactors operate in nearly stationary regime. Automatic regulation maintains the critical state, only fluctuations may occur. Criticality control is based on ionization chambers not on in-core instrumentation. As we have seen it in Fig. 2.3 in Sect. 2.2.1, the SPNDs are too slow to be used in transient handling. Thermocouples are faster but there is one more aspect of the instrumentation that has to be taken into account. In-core signals are handled in a single data sampling technology. It means that a signal is sent to the sensors when the read-out process is initiated. It is the frequency of the multiplexer that determines the data sampling period, which is usually in the order of 2 s. Signals of the ionization chamber are analogous (or of considerably higher frequency) than read-out of the in-core signals.

Manuals prescribe the range of stationary, transient or trip conditions. The operator is informed on the actual state of the reactor, and built in mechanism regulate minor transients. In a reactor trip, the operator may need to get a proposed work plan to restore stationary regime without violating any regulation limit. That problem is beyond the limits of the present work.

2.7 Core Monitoring Systems

As it may have become clear, a core monitoring system may be based on different considerations depending on the instrumentation, the experience with the given reactor type, its usage in normal and abnormal reactor regimes.

The basic functions of a core monitoring system can be formulated as follows:

1. Core monitoring is essential in verifying the safe operation of a NPP. Do not forget, regulations formulate limits to the maximal power density, the maximal fuel and moderator temperature as well as the avoidance of boiling crisis in the reactor core. It is not possible to measure the fuel temperature, therefore indirect methods are used. The moderator temperature continually grows as the coolant elevates along the fuel assembly. If the axial power profile is adequately measured and the coolant temperature is measured just above the top of the fuel assembly, fuel damage can be excluded by high probability.
2. Since we have no means to measure neither the coolant temperature in control volumes, nor the fuel temperature in fuel pins, safety of reactor operation relies on secondary evidence. This is why safety limits bear a given amount of reserve.
3. There is a not negligible probability that limit violation occurs in a nonmetered assembly therefore correct estimation of coolant temperature as well as the maximum power rate in an assembly are equally important.
4. Experience in power reactor operation is of outmost importance. This is why operational data should be collected and analyzed continually to find weak points in reactor calculation and operation.

Basic functions of core monitoring are:

1. Estimate the axial power profile and the maximal power density and maximal ΔT in each assembly. Not only limit violations but also unusual behavior should be investigated. Keep in mind that in any reactor type there are fuel assemblies without instrumentation.
2. Continually analyze flow anomalies and detect them as soon as possible.
3. Continually monitor unusual behavior to detect early misloaded fuel assembly.

The power plant should possess a core calculation system (a continually running computer code), which is provided with the actual parameters of the core. That code is the cornerstone of the in-core signal processing. A validated code may be able to provide the information missing from the measured data. For simple technical reasons it is impossible to supplement every fuel pin and every control channel with measurement. A technical thing always may go wrong, the in-core evaluation system and the operator should recognize such a situation and actuate an adequate repair or preventive action.

In-core instrumentation involves the following actions:

1. In the reactor start-up period check if everything operates normally. Think of possible errors like false fuel assembly mark which is very far from any analyst.
2. Test if any element of the instrumentation fails. Remember, hidden failures are not always realized by the technique. Usually a few wrong measurement causes no problem in reactor operation.
3. Provide reactor operator with adequate information on the reactor state.
4. Observe tendencies in the state of the reactor core. Coolant flow anomalies, appearance of anomalies may become clear only after a long and careful study of the information provided for the operator. Most of the mentioned problems are slow and there is time to analyze the situation.

Some methods applicable in the actions have been mentioned through Sections of the present chapter. Regulations prescribe precisely for example what kind of information must be provided for the operator. It is evident that assembly-wise data must be given for each assembly. There are conventional assumptions at each unit, for example it may be assumed that the entering coolant temperature is the same for each assembly. It is a good idea to compare the loop flow rates and cold-leg temperatures to check if the assumption may be accepted.

Processing of the in-core signals should involve the following steps:

1. Compare the measured data with each other.
2. Compare the measured data with the predictions of your computational model.
3. Use your computer model to determine the parameters subjected to limitations.
4. When calculated and measured data differ try to find out what may be behind the difference.
5. Try to place any observed anomaly in the context of the data you trust.

The defense of depth principle requires to have information on the following parameters during reactor operation:

1. Neutron flux and distribution (startup, intermediate and operating power ranges);
2. Rate of change of neutron flux;
3. Axial power distribution factor;
4. Power oscillation;
5. Reactivity control devices;
6. Temperatures of fuel cladding or fuel channel coolant;
7. Temperature of reactor coolant;
8. Rate of change of temperature of reactor coolant;
9. Pressure of the reactor coolant system (including cold overpressure settings);
10. Water level in reactor vessel or pressurizer (varying with plant state and differing with reactor type);
11. Reactor coolant flow;
12. Rate of change of reactor coolant flow;
13. Tripping of primary coolant circulation pump;
14. Intermediate cooling and ultimate heat sink;
15. Water level in the steam generator;
16. Inlet water temperature for the steam generator;
17. Outlet steam temperature for the steam generator;
18. Steam flow;
19. Steam pressure;
20. Settings provided to initiate steam line isolation, turbine trip and feedwater isolation;
21. Closure of isolation valve for the main steam line;
22. Injection of emergency coolant;
23. Containment pressure;
24. Settings provided to initiate startup of spray systems, cooling systems and isolation systems for the containment;

25. Dry well pressure (only for PWRs);
26. Control and injection systems for coolant poison;
27. Radioactivity levels in the primary circuit;
28. Radioactivity levels in the steam line;
29. Radioactivity levels and levels of atmospheric contamination in the reactor building;
30. Loss of normal electrical power supply;
31. Emergency power supply.

Some of the above parameters are simple, like the loss of electrical supply; others are difficult to be measured. For example, temperature of fuel cladding is a number for each fuel pin in each fuel assembly. Most of the parameter is actually a function of space and time. Engineering considerations limit the measurement in the reactor core therefore some of the limited values are obtained from models.

As we have seen on the previous pages, the models include measured values and distributions obtained by a validated and licensed core calculation. The recently available computer capacity allows for a frequent core calculation based on measured values of the core state, i.e. actual reactor power, boron concentration, control rod positions, burnup distribution.¹⁸ It is possible to base reactor operation on calculations. At the same time, differences between calculated and measured power distributions may provide additional information on the measurement system, or the reactor actual state.

Difference between calculated and measured distributions carry important information when the reactor is in a transient state, is at power transients, start-up period.

Throughout the following subsections, we present shortly in-core systems that have been used for a longer time.

2.7.1 BEACON

BEACON has been developed by Westinghouse. The original BEACON has been elaborated for a core made up from square fuel assemblies although later modifications have made it possible to be used in hexagonal fuel assemblies with rhodium self-powered in-core detectors [65]. The below presented summary is based on Ref. [66].

The BEACON (Best Estimate Analyzer for Core Operations Nuclear) system is an advanced core monitoring and support system which uses existing instrumentation data in conjunction with an analytical methodology for on-line generation and evaluation of 3D core power distributions. The system provides the tools for core monitoring of the power limits delineated in the Technical Specification, core follow, core measurement reductions and core predictions. The system was initially developed in the early 1990s and approved by the USNRC for continuous on-line core monitoring in 1994.

¹⁸Burnup varies very slowly in time.

The development of BEACON version 7.0 as part of the WhiteStar project will be another major upgrade of the system that is designed to incorporate and support the following goals.

1. Integrate the new and advanced nodal solution methods and data management being implemented in the Westinghouse core design codes
2. Add features and functions to support the zero by ten (zero fuel failures by 2010) initiatives by utilities in the US.
3. Support the new plant features and requirements for the Westinghouse AP1000 reactor design.
4. Provide better and easier to use reactivity management and data interfacing tools to support the reactor operations staff.

To reduce fuel failures to their lowest possible level the US nuclear industry has been collectively working on a zero by ten fuel initiative. To support this initiative the BEACON 7 system will include the capability to monitor and predict local ramp rates, fuel conditioned powers and local fuel limits. A 3D core monitoring system is ideally suited to this task because of the detailed information it has on each assemblies pin power distribution. Predictive calculations can be used before startups or planned power maneuvers to predict local fuel ramp rates for different scenarios which can then be evaluated to determine which power maneuvers meet the operational goals with the most ramp rate margins. The improvements in system data management and storage capacity have made it easier and faster to save and track large amounts of data needed for this type of analysis over an operating core cycle.

2.7.1.1 Software Development Methodologies

The development of ANC and the integration with BEACON follow an iterative software development methodology and a phased development strategy. The project was broken into three distinct development phases, each of which with defined deliverables. The first phase of development of the project included the development of ANC 9.1, NEXUS and the integration of these components. The methodology updates to ANC described in this paper are also part of the first phase of development. The integration with PIP, DEPORT and CoreStore was also completed in the first phase of the project. The first phase of the project has completed. The second phase of the project included the feature development to support analysis needed for AP1000 core design. These features include limits and margin calculations, features to support the 3DFAC analysis as well as integration with the VIPRE-W code for DNB feedback. In addition, the MSHIM control strategy will be coded into ANC in the second phase of the project. The third phase of the project includes the integration of ANC and BEACON to support online core monitoring for both AP1000 and non-AP1000 cores.

2.7.2 GARDEL

Below we present highlights of a two-page leaflet on GARDEL, which can be implemented on any BWR.¹⁹ GARDEL is an advanced on-line core monitoring suite with built-in reactivity management tools. Combining Studsviks state-of-the-art reactor analysis methods with efficient database technology and a customizable graphical user interface, GARDEL can help reduce uncertainties and conservatism that limit reactor operating efficiency.

GARDEL can be deployed throughout the entire organization, allowing view-only displays for operators in the control room, while providing engineers with advanced operational planning functionality. Featuring an easy-to-use graphical interface that allows reactor engineers to easily perform accurate, reliable planning calculations, GARDEL offers enhanced reactivity management functions and can support site-wide operations.

With several powerful engineering features to analyze past conditions or plan for future operations, GARDEL gives you the ability to quickly respond to unexpected operational needs or events.

GARDELs data acquisition methods can be implemented at any BWR plant. Using detailed, real-time signals from the plant process computer, GARDEL explicitly calculates global and local core surveillance quantities down to the pin level.

The accuracy of the 3D core simulation, combined with built-in adaption to detector signals, provides reliable tracking and prediction of the core operation even under off-rated conditions.

GARDEL extends Studsviks reactor analysis capabilities to the control room using the core model generated by core designers and engineers to allow streamlined data sharing between all areas of the plant.

Regulators worldwide have approved GARDELs powerful administrative controls, which ensure secure collection and archival of all plant signals and calculation results while granting authorized users full access to data and automated calculation tools. The high degree of automation in the built-in support calculation functions prevent potential user input errors when performing operational support calculations.

GARDEL automatically generates periodic, daily, and monthly core follow and isotopic reports, which can be easily customized to fit the specific reporting needs.

Many additional reports can be generated on demand with the click of a button and exported outside the system in a variety of formats.

GARDEL includes several built-in functions to provide support for core operations.

1. Shutdown Margin: Determines high worth rod and assesses shutdown margin.
2. Critical Control Rod Pattern Searches: within a defined sequence to find the critical control rod pattern.
3. High Notch Worth: Moves through control rod sequences to find high notch worth patterns.

¹⁹On a similar other leaflet PWR.

4. Cold Criticals: Evaluates in-sequence or local criticals using Studsviks exclusive temperature dependence and period correction capabilities.
5. Reanalysis of Past Operational Events: Allows the user to recalculate past operating event and analyze data down to the pin level.
6. User-Specified Predictions: Allows the user to create projections of future operations for planning and guidance.

GARDEL manages data flow from the plant computer and automatically activates neutronic calculations based on changing reactor conditions.

The GARDEL system continuously compares calculated-to-measured values for core thermal quantities and in-core detector readings, using automatic signal-to-power conversion.

GARDEL helps utilities ensure conformance to training simulator performance objectives, standards, and regulations including those expressed in 10CFR55.46, SOER 96-02, and the ANSI 3.5 Standard.

Since the GARDEL core neutronic model is cycle-specific and always reflects the actual operating history of the plant, it can be used to maintain an S3R training simulator core model with no additional resources.

Additionally, plant support personnel can use GARDEL to export a snapshot of the current core conditions for just-in-time (JIT) simulator training.

As to the PWR version of GARDEL [67], its heart is SIMULATE-3 neutronics model, which has been used in 15 countries, licensed in six countries, used by safety authorities in several countries. According to the authors of [67], the code has been applied to virtually all existing PWR fuel and core design including include ultra low leakage loading patterns, both UO_2 and MOX lattices, burnable poisons containing boron as well as integrated absorbers including erbium, gadolinia, and boron coating, and a variety of incore detector types; such as U^{235} fission chambers, gamma sensitive platinum emitters, gamma thermometers, fixed rhodium incore detectors, and vanadium aero balls.

2.7.2.1 GARDEL System Configuration

GARDEL does not run on the plant computer. Refreshment of the data archive is periodically conducted (typically every 1–2 min) and data are transferred to the GARDEL server. That data set is a relatively small file containing few parameters such as reactor power, flow, pressure, inlet and outlet conditions, control rod positions, excore and incore signals (when available), etc.

As to signal handling: the plant process computer feeds the plant computer with signals that the process computer stores. These data are then used in the neutronics model for core tracking. The frequency of the data transmission depends on the required monitoring frequency, and is limited only by the speed of the neutronic simulator²⁰ (typically).

²⁰Usually less than 30 s are needed for a full core 3-dimensional SIMULATE-3 calculation.

Periodic controller: it manages data flow from the plant computer to the GARDEL database. It automatically activates neutronic calculations when reactor conditions change when an authorized user demands.

SIMULATE-3: GARDEL accesses the same core monitoring system (CMS) neutronics model that has been developed by the core design group and used for core design calculations. Due to the modularity of GARDEL, several CMS calculations can be conducted simultaneously from different computers within a network.

Database: It archives all results (plant signals as well as calculational results). The database is specifically designed to maximize efficiency in recording and retrieval of plant signals and CMS calculational results.

Graphical User Interface: It is the heart of operator info. It does not only display the current plant status and allows authorized users to access the database but also provides support to the operator among others with reactivity management calculations. Due to the modularity of GARDEL, the graphical user interface (GUI) module can be executed individually for each authorized user on their own desktop. This allows multiple users to simultaneously conduct and share calculations or access plant measured and computational results. Each user can configure the GARDEL display on their desktop independently of another users configuration. User access to various features within the GARDEL system can be controlled by the GARDEL system administrator. Provided users have access to the network where GARDEL resides, they can use GARDEL remotely, e.g., telecommuter support.

2.7.2.2 GARDEL Results

This section provides several specific examples illustrating the accuracy of the system and applicability in resolving operational issues. Since its inception several years ago, GARDEL has been installed at 5 PWRs and several engineering offices throughout the world. These installations comprise fixed and movable, neutron and gamma sensitive, in-core instrumentation devices. GARDEL is used at these installations for a variety of applications from core monitoring to operational support and reactivity management. The description taken from Ref. [67] has been shortened. The first data to be investigated are from the 2-loop Westinghouse Beznau NPP.²¹ The online core monitoring of the units is GARDEL (Fig. 2.36)

Figure 2.37 presents an example of the GARDEL accuracy during several months of a representative cycle for margin to LCO for the calculated integrated radial peaking factor, $F\Delta h$. The figure shows the SIMULATE-3 calculated margin, FDHM0, compared to the margin based on correction factors from the latest flux map (FDHM1) and the margin calculated combining information from the latest flux map with the current thermocouple readings (FDHM2).

The difference between the FDHM0 and FDHM1 is about 2%, which is approximately the accuracy of the calculated reaction rates, compared to measurement. Additional modification based on thermocouple data is negligible and therefore,

²¹The original notation has been retained.

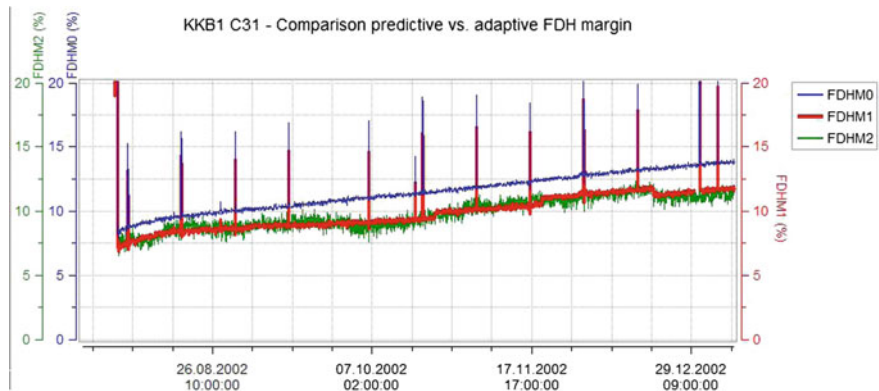


Fig. 2.36 GARDEL comparison of predicted and corrected FΔh margins

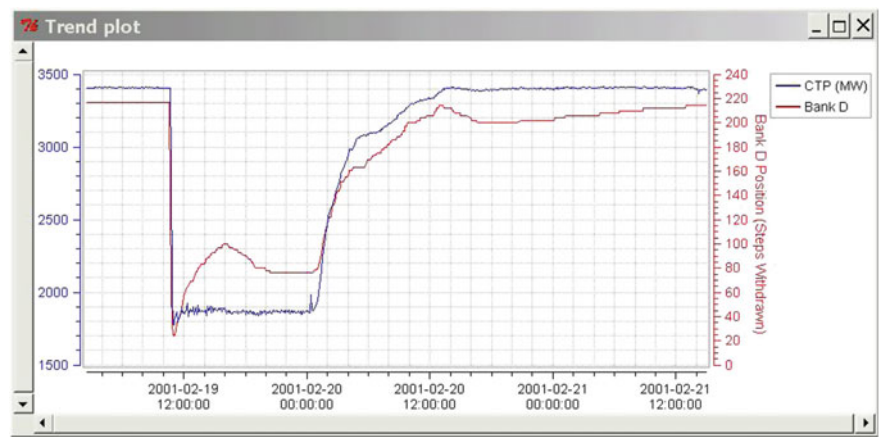


Fig. 2.37 GARDEL trend plot of key parameters during pump trip

Beznavu does not use corrections based on thermocouple data for margin to limits assessment.

Another transient is shown in Fig. 2.37. In a state near to end of cycle of a Westinghouse designed PWR, the McGuire, Unit-1, 4-loop; a main coolant pump trip occurred. This triggered control rod insertion, and reduced the power level. The unit was stabilized at the reduced power level, and the transient initiated a xenon transient. The transient is a good opportunity to study the accuracy of GARDEL.

GARDEL calculated the axial flux imbalance, ΔI , an important parameter for core monitoring and operator guidance during a power maneuver. A graphical summary of power and control rod positions during the event taken directly from GARDEL is presented in Fig. 2.37.

The next example GARDEL performs signal to power conversion with fixed detectors. Since these detectors burn out, compensation is required within GARDEL

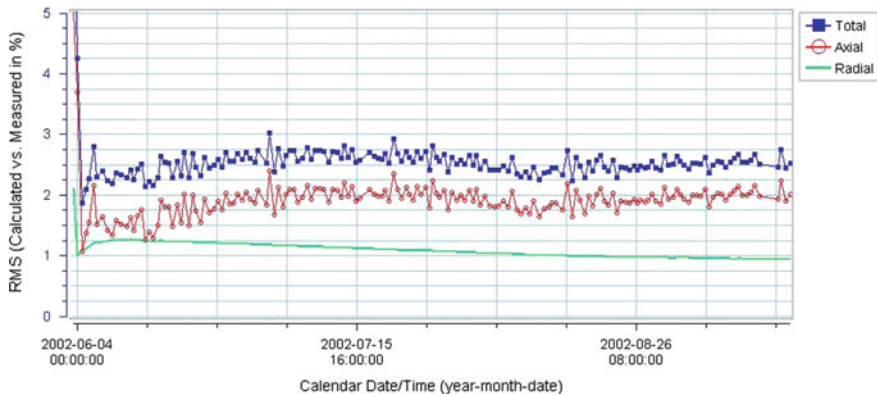


Fig. 2.38 GARDEL reaction rate accuracy for a fix detector system

to update charge accumulation and detector sensitivity for each individual detector. This feature reduces the load on the process computer where the charge accumulation would normally be calculated. Also, as with movable detectors, the signal/power conversion factors are created on demand at the actual plant conditions, eliminating approximations and reducing the resources traditionally required to generate the pre-computed library.

Figure 2.38 shows a trend plot of the radial, axial and total (nodal) RMS between calculated and measured power distributions during the cycle. The overall RMS between the calculated and measured Rhodium reaction rates is 1.0% for the radial (2D integrated) and 2.7% for the total (3D). The results could provide a basis to decrease the current uncertainly factor used in the LCO monitoring of peaking factors.

2.7.3 SCORPIO

The SCORPIO system [68, 69] was elaborated in the early 1980s, it has been operating in nine PWR units [70] in Sweden, UK, USA, Czech Republic. The version operating in Dukovani NPP (Czech Republic) operates in two modes [70]:

- core follow regime—in which the actual core state is evaluated by combining the instrumentation signals and the theoretical calculation. The operator is provided with information on core status through a graphical interface containing trend curves, core maps, diagrams and tables displaying information on the actual core state including actual measured values reserve to limits in the Technical Specifications.
- predictive regime—the operator sees core characteristics during transients predicted for the coming hours. Quick forecasts realized by the strategy generator could be deeply analyzed by the predictive simulator. Just like in the core follow

mode, characteristics of the evaluated states can be compared to Technical Specifications, and the predicted behavior of the core can be analyzed through the number of dedicated screens.

Main features of the SCORPIO system implemented in Dukovani NPP are as follows. In the core follow regime:

1. Communication with plant data sources and data acquisition is continual.
2. SCORPIO validates measured data and identifies sensor failures.
3. Furthermore calibrates temperature measurement sensors and identifies isothermal core states.
4. SCORPIO carries out on-line 3D power distribution calculation with pin power reconstruction, based on the validated outlet temperatures of thermocouples, SPND measurements and from the results of core Simulator.
5. On-line core calculation is carried out by Moby-Dick code [64].
6. Check on limit and thermal margin violation (DNBR, sub-cooling margin, FdH and other peaking factors) is carried out cyclically.
7. SCORPIO also carries out SPND monitoring, evaluation, interpretation and transformation to linear power.

In the predictive regime, SCORPIO makes it possible:

- To use an integrated module for monitoring fuel performance and conditioned power distribution.
- Integrated module is available for coolant activity monitoring and to identify fuel failures.
- To monitor conveniently and predict the approach to criticality during reactor start-up.
- Predictive capabilities and strategy planning, allows for checking the consequences of operational maneuvers in advance, predicting critical parameters and detect end of fuel cycle, etc.
- Automated transition between cycles (fuel reload).
- Logging functions with archive for all calculated and main measured data.
- User definable printer output for protocols and forms.

SCORPIO screen with the fuel assembly exit temperatures and axial profile in selected fuel assembly at position (10–49) (Dukovani NPP, Czech Republic) are shown in Fig. 2.39. An extra function called *CoreCreate* is available [69] to construct a new core map from assembly cell objects. Figure 2.40 also shows application of SCORPIO to BWR units.

2.7.4 VERONA

VERONA is one of the first in-core signals based operator assisting systems for VVER-440 NPPs. The first VERONA version was implemented in early 1980's at



Fig. 2.39 An example of a core map picture in the SCORPIO-VVER system

the Paks NPP (Hungary). The computer capacity accessible that time in Hungary was rather limited. In the mean time several upgrade processes have been implemented on VERONA. The present description is based on Ref. [57].

Neutron physics studies performed to assess the possibility to raise the original 1375 MW core thermal power of the Paks VVER-440 units to 1485 MW (108%) have shown that the target power level can only be achieved by using a new fuel type. A radially profiled fuel assembly (with 3.82% average enrichment) having a fuel rod lattice pitch of 12.3 mm was selected as the new fuel: in 2006 this fuel type was used at Unit 4 when 108% was achieved. Considering fuel economy this fuel type is not yet optimal, therefore later it will be gradually replaced by assemblies with higher enrichment and containing burnable poison.

The plant and the safety authority wanted to achieve 108% power without changing core safety limits and it was quite obvious that this requirement could only be achieved by the introduction of a more detailed and more accurate on-line core analysis. As the old core analysis computers (MicroVAX-3100 machines installed some 10–12 years ago, see [58, 59] for details) were already overloaded by their tasks, it was also obvious that this could be achieved only by using new computers with much higher resources (in terms of CPU speed, memory size, disk capacity and network bandwidth).

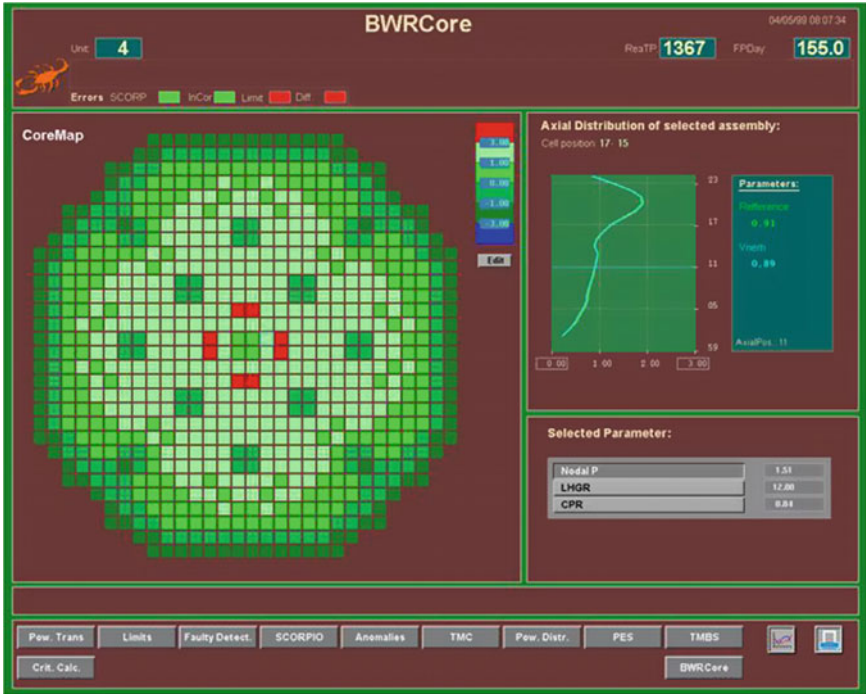


Fig. 2.40 An example of a generated core map picture using the “CoreCreate” tool

In 2002 the NPP decided to carry out a two-step upgrading project. The first step was aimed to incorporate additional computer resources into the old architecture, in order to ensure that the old version of the VERONA was able to run and work properly until the new system would be installed at all units. The main goal of the second step was to create an entirely new system with higher accuracy, with much larger resources and with advanced services. The two steps contained the following major items:

1. Limited-scope upgrading of old core analysis tools (completed in 2003 for all units):
 - a. Replacement of the old Model80 MicroVAX-3100 machines by more powerful Model96 computers (this ensured four times faster CPU and double RAM size plus some extra disk space).
 - b. Replacement of the obsolete graphic workstations by Windows-NT 4.0-based PCs.

The advantage of this upgrading step was that the Open-VMS operating system and the application software on the VAX computers were not changed at all (this was essential to achieve a smooth licensing procedure and an easy transition).

2. Full replacement of the old system (completed in 2008 for all units):

- a. Modernization of system architecture and replacement of application software.
- b. Development of a new, advanced version of the reactor physics calculations.
- c. Partial upgrading of the PDA in-core data acquisition computers.
- d. Full replacement of the VERONA local area network.

2.7.4.1 New System Architecture and New Software Tools

The software running formerly on the VAX computers, was split into two main parts: the reactor physics calculation part was separated and moved to a powerful PC called RPH server. The rest of the software remained unchanged and stayed on the VAX machines (Fig. 2.41).

The following major software items were fully redesigned and recoded:

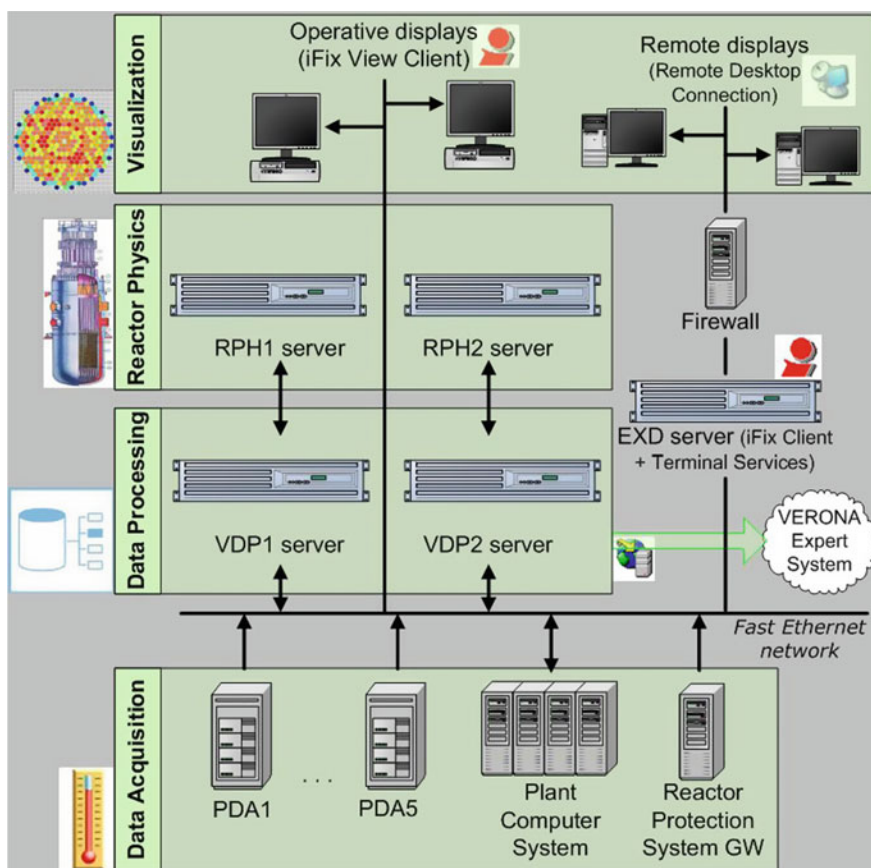


Fig. 2.41 Schematic architecture of the new VERONA system as installed at unit 3

- Database and data archive management tools: Structured Query Language (SQL) compatible, standard relational database management tools were applied.
- Data visualization: a professional picture editor plus display program was applied.
- Serving external users with visual information and data: this task was accomplished by creating a dedicated external display server functioning as multi-user display station.
- System management: reliable system supervision programs and graphic management tools were applied for all important system management tasks.
- System expansion: the new architecture was designed to support seamless system expansion by providing ample reserves and built-in expansion possibilities.

Installation of A new *VERONA* network of speed 100 Mbit/s has been installed, along with extending the in-core data acquisition system. The new *LAN*²² is a redundant Fast Ethernet network using optical media; active components were manufactured by Hirschmann. The new server computers are professional HP *ProLiant* machines with dual *AMD* processors and running Windows 2003 Server operating system. Two redundant VDP (data processing) servers are responsible for storing on-line and archive databases, signal processing, serving the display stations with data, and performing other administrative tasks. Two RPH (reactor physics) servers are responsible for running the core calculations periodically. Further details on system hardware and software structure are outlined in [60, 61].

2.7.4.2 User Interface and Testing

The graphic outlay of the basic screen sections (core map, axial distribution display, reactor and loop parameter summary have remained unaltered. Notwithstanding, new graphic tools were applied and several new functions were introduced. The new core analysis method combines on-line measured and on-line calculated information. However, modules applied to determine pin-wise (i.e. intra-assembly) flux distributions still use a large amount of off-line calculated information (in the form of so-called C matrices [57]). Core calculations are organized into two main cycles: the 2 s cycle is called synchronous, while the 5 min cycle is called asynchronous (Fig. 2.42).

1. First the C-PORCA code is run; it uses actual reactor power, control rod positions and assembly inlet temperatures as input. The code updates nodal isotope concentrations, burnups and determines a 3D (nodal) flux map of the core.
2. By using on-line calculated C-PORCA results and measured SPND currents an axial fitting procedure is performed in order to obtain the actual fast-flux distribution.
3. Afterwards a 2D perturbation calculation is performed on the fast-flux field by using calculated C-PORCA data, fitted axial fast-flux values and measured assembly outlet temperatures.

²²LAN = Local Area Network.

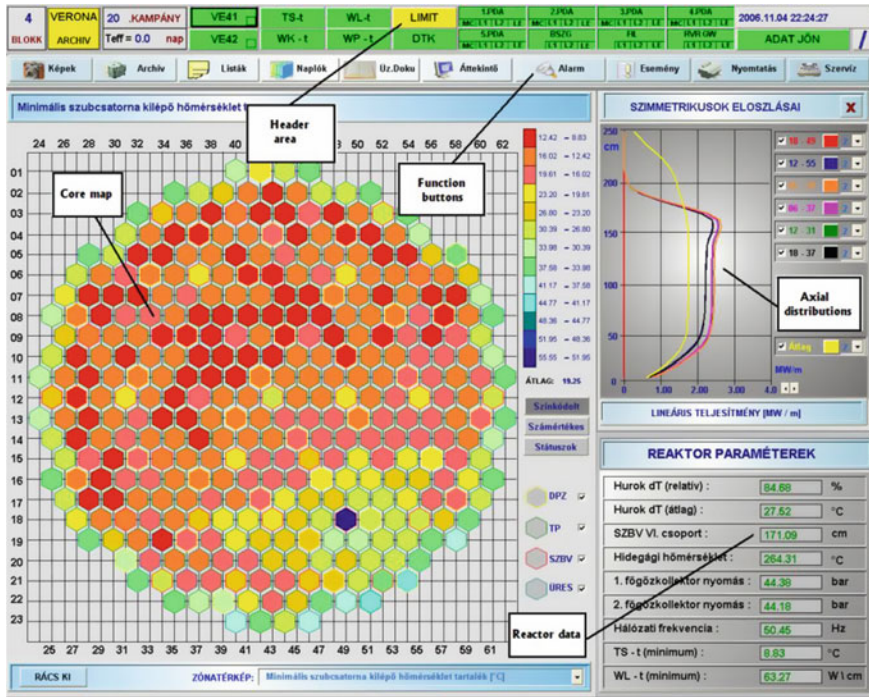


Fig. 2.42 Main display format of the new VERONA HMI (it shows an archive replay)

4. A new adaptation vector is determined (it is used by the synchronous programs).
5. A pinwise core analysis is then performed by using the 3D fast-flux field and the C interpolation matrices. In this step the 3D linear power distribution and individual fuel rod powers are determined.
6. Subchannel outlet temperatures are determined for all fuel assemblies (the model takes into account the coolant mixing between subchannels).
7. Finally important parameters (e.g. adaptation vector, nodal isotope concentrations and burnups) are stored in a special file system called RAR (reactor physics archive) for later retrieval.

Synchronous calculations carry out the following tasks in every cycle:

1. First global core and primary loop parameters are determined (e.g. loop and core coolant flows, powers).
2. The next step contains a 2D extrapolation procedure using measured assembly outlet temperature (the algorithm is the same as in the old version).
3. Then 3D extrapolation is performed using measured SPND currents as input (the axial fast-flux extrapolation algorithm is the same as in the old version).
4. The extrapolated 3D fast-flux is then corrected according to the adaptation vector determined by the asynchronous calculation.

5. A pin-wise core analysis is then performed by using the 3D fast-flux field and the C interpolation matrices. In this step the 3D linear power distribution and individual fuel rod powers are determined.
6. Subchannel outlet temperatures are determined for all fuel assemblies.
7. Finally all measured inputs and calculated outputs are stored in the RAR.

The new core analysis modules have been carefully tested, see [57]. Correctness of the new 2D extrapolation model was extensively checked by using a large number of measured ΔT distributions. In-core measurements were taken from Unit 4, collected through fuel cycles 10–17. The investigated reactor states had the following characteristics:

- Altogether 170 measured distributions were evaluated (each measured field contained 210 measured assembly ΔT values).
- Measured ΔT fields corresponded to a wide variety of core load patterns with different fuel assembly types (2.40, 3.60 and 3.82% enrichment, normal and low-leakage cores, etc.).
- Investigations were restricted to stationary reactor states close to nominal power.

The basic method of the investigations was the following: the 2D extrapolation model was applied for each measured ΔT field and then differences between the calculated and measured distributions were determined. The differences distributions were then statistically analyzed and evaluated. A detailed description of methods and results is given in [63].

Here we show two figures. The first one shows the linear power deviations from the reference, see Fig. 2.43.

Figure 2.44 shows the distributions of the Student fractions. The most important result was the average deviation between extrapolated and measured ΔT values at

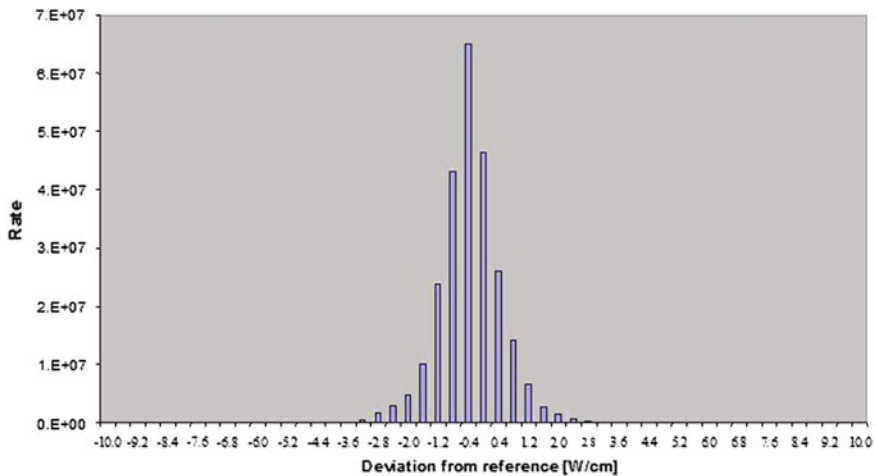


Fig. 2.43 Distribution of linear power deviations from reference (new model)

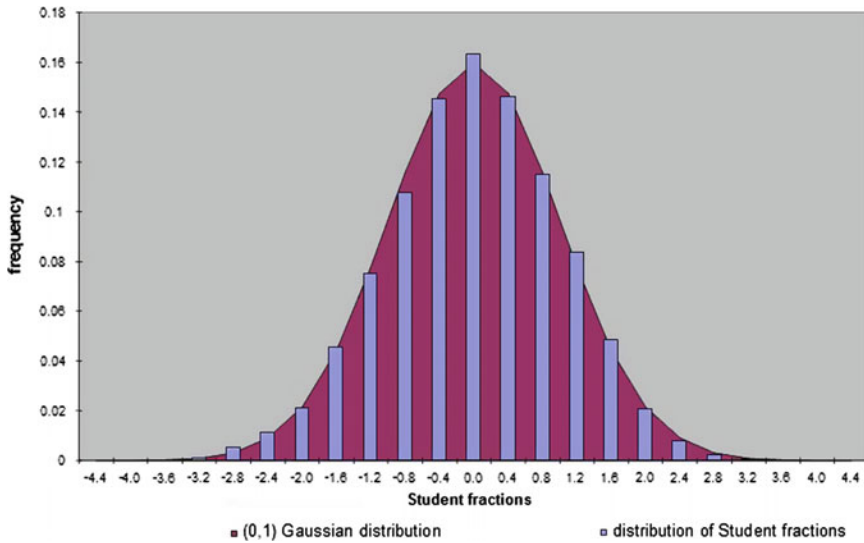


Fig. 2.44 Frequency distribution of Student fractions calculated for the differences between measured and extrapolated assembly ΔT values

the measured points. The accuracy of the extrapolation was obtained as $0.37\text{ }^{\circ}\text{C}$ (variance, 1σ) and the distribution of deviations practically followed a Gaussian distribution (see Fig. 2.44). This means that the new 2D extrapolation is unbiased and is free from systematic errors. Its validated accuracy is very close to the target value ($0.35\text{ }^{\circ}\text{C}$) defined in the requirements' specification document.

2.7.4.3 VERONA-e Expert System

The new architecture and the new high-speed network made the introduction of a new form of reactor physics analysis possible at the plant. The Paks NPP Reactor Physics Department now has access to a so-called VERONA expert system (VERONA-e): this system consists of dedicated workstations running the same software as the reactor physics servers working in the unit configuration. On-line and archive process data can be transferred to these computers via the EXD server and reactor physics experts can perform their own core analysis locally. The expert system is extensively used for collecting long-term core parameter trends, to perform special core calculations and for report generation. These computers may host additional software modules, i.e. programs which are not yet present in the unit configurations. These modules can be used for various tasks, such as long-term trend monitoring and statistical analysis of in-core measurements (for signal validation purposes), application of a detailed core hydraulic model for core anomaly interpretation. Further details are given in [62].

It is now proven by everyday experience that this new, more open system architecture combined with built-in data server functions supports reactor physics experts to a great extent, by providing convenient tools for off-line analysis and report generation.

2.7.5 Recent VVER Development

In the approach to be discussed [71], an important moment is the separation of core design (or follow) calculations from the evaluation of in-core measurement. The reason is: in this manner a common cause failure can be eliminated. In this way the reconstructed power and temperature field depends only on the temperature and neutron detector signals.

In Ref. [71], the goal of the development is summarized as follows:

- to shorten the response time in monitoring neutron physical (power, flux) and thermal hydraulics (coolant, clad and fuel temperature) parameters;
- early detection of anomalies in the operation and to provide smooth reactor operation.

In-core measurement should provide adequate means to indicate anomalies or malfunctions at an early stage.

Structure of the modern VVER in-core instrumentation has two levels. SPNDs are installed at seven axial elevations.

On the low level (LL), at each of the seven elevations, the power density is determined within 0.5 s for each fuel assembly. In that calculation, calibration coefficients are used c.f. Sect. 2.2.1 and the calculated local power densities are used to detect any actual control rod position change, or unplanned change in the actual core state. Also at the low level, local parameters, like linear power density, DNBR; are calculated and compared against the limit values.

On the upper level, further calculations are carried out with an error below 2–2.5% to determine:

- the actual power density distribution and related quantities in every fuel assembly at 16 elevations;
- lower level calibration coefficients are recalculated, and core calculations to assist transient management and predict dynamic behavior of the reactor.

The coefficients used in transforming the SPND currents into linear thermal power in the neighboring fuel elements were determined experimentally at such reactors as VVER-440 (Loviisa, Paks, Dukovany, and Bohunice nuclear power plants) and VVER-1000 (the 5th block of the Novovoronezh nuclear power plant).

In core monitoring of a VVER-1000 unit, the core is usually equipped with [71]:

- 448(= 7×64) SPNDs in 64 fuel assemblies;
- 95 thermocouples (TC);
- 16 TC and 8 resistance thermometers (TR) at primary circuit hot and cold legs.

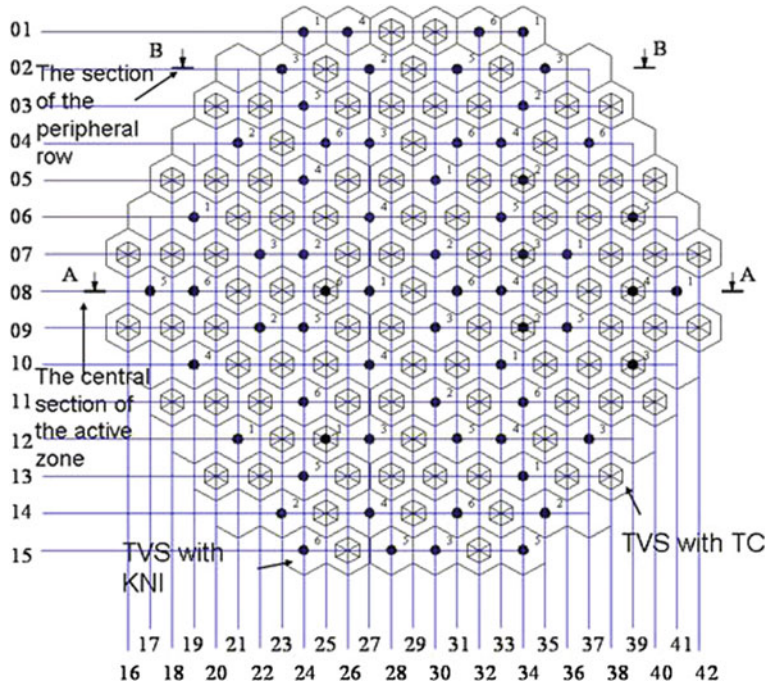


Fig. 2.45 Locations of SPNDs (KNI), control rods, and thermocouples (TC)

Figure 2.45 shows the core map of a VVER-1000 unit with the location of SPNDs (on Fig. 2.45. KNI), control rods and thermo-couples (TC). The total thermal P_{th} power of the reactor is calculated as weighted sum of five evaluation ways:

$$P_{th} = \frac{\sum_i N_i w_i}{w_i}, \quad (2.112)$$

where w_i -the weight of evaluation way i ; N_i -the thermal power of the reactor in evaluation method i .

1. The first evaluation method estimates the power N_1 from the readings of ionization chambers, which are part of the neutron flux monitoring equipment;
2. The second evaluation method estimates N_2 from the SPND readings;
3. Power estimate N_3 is obtained from the readings of the primary loop monitoring;
4. Power estimate N_4 is obtained from the readings of the secondary loop monitoring;
5. N_5 is estimated from the flow rate in the core.

Each of these methods may involve systematic and/or random, unknown errors of the measured values. Systematic deviations caused by failures of a sensor or equipment, or by measurement error, flow adjustment, etc. are eliminated at the start of a new fuel cycle. To avoid the subjectivism and voluntarism in determining the statistical

weights assigned to the aforementioned methods, a special statistical technique was developed [81].

The software and hardware of the lower level meets the recent requirements of the Russian Federation's standards, furthermore, IEC and IAEA norms for safety. The equipments are seismic resistant, environment and human interactions can't do harm in it.

Measuring, processing and information transfer cycle on the upper level is 1 s. The methods applied on the lower level provide the following reliability parameters: Minimal value of mean-time-between-failures (in hours):

1. protection signal formation on heat exchange crisis margin (DNBR):
 - “false” signal generation: $1.7 \cdot 10^6$;
 - missing of generation: $2.7 \cdot 10^{11}$;
2. Protection indication forming on linear power release:
 - “false” signal generation: $2.3 \cdot 10^7$;
 - missing of signal generation: $2, 7 \cdot 10^{11}$.

The lower level application software carries out the following functions: from SPND currents and coefficients, sent from the upper level, it calculates the linear power of maximal loaded fuel element in each fuel assembly on seven levels, compares with permissible settings and in case of limit violation, sends a preventive protection signal PP-2 to the reactor protection system.

On the lower level, when SPND signal calls for automatic protection, it is provided that the response time delay remains below 0, 5 s, and with Kalman filter with Tsimbalov's modification, with delay below 2 s.

The upper level software and hardware features:

1. software and hardware work in operational environment “Unix” (SUN “Solaris”, “Linux” etc.);
2. sample architecture of open systems, which enables creation of modern and prospective decisions on the base of widely used standards (standards—POSIX 1, 1.b, 1.c and others);
3. the most technological industrial constructive (reliability, repair ability, assembling decision spectrum);
4. high productivity—processor modules with operating speed, enough for analysis of the reactor unit state, including modeling of core neutron-physical and thermo-hydraulic processes in real time;
5. system reliability with application of new structural decisions, including some components of control and monitoring, and also support of cluster technologies for full use of computing resources together with automatic resources reconfiguration in case of components or modules failure.

The upper level software includes the reactor physics modules: TVS-M [75], charged particle emergence from the detector is calculated by [76], the energy release from fuel assemblies are calculated by [77–80, 82]. Here we mention only one topic [71, 82].

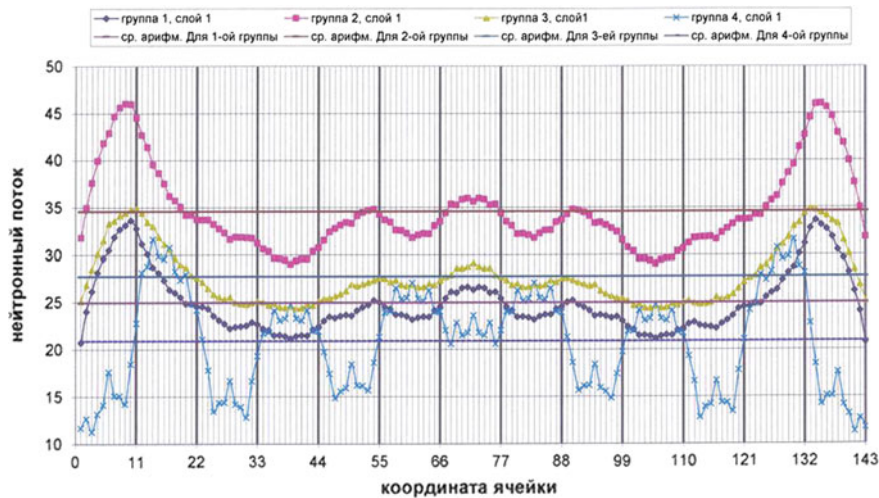


Fig. 2.46 The central section of the active zone A–A. The top layer

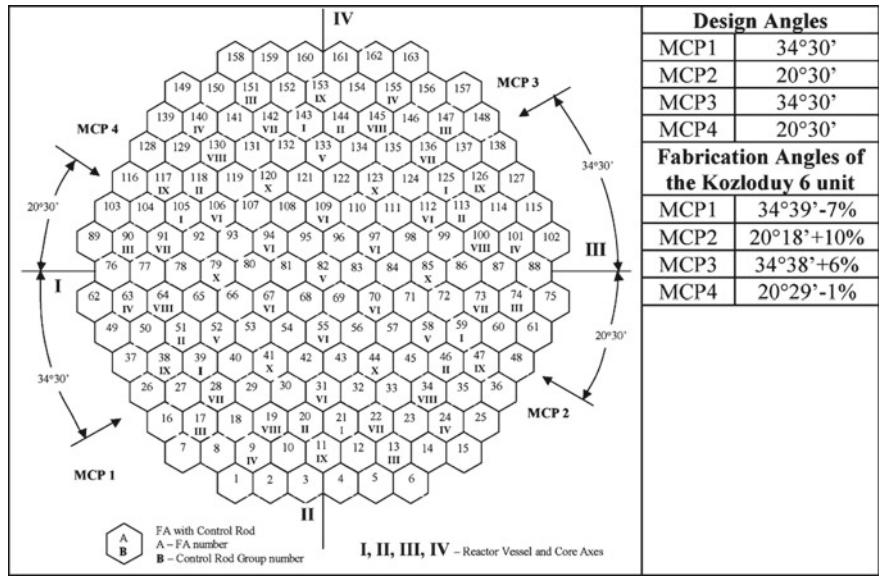


Fig. 2.47 Numbering of the core assemblies and angles of the cold legs coming from the four MCP

The neutron flux satisfies the diffusion equation, see Appendix A for details. The goal is to find an approximation for the space dependent flux to allow for a simple but reasonable representation of the space dependent flux. To this end, calculations with four energy groups have been carried out, the results can be seen in Fig. 2.46, where the fluxes in the four energy groups are shown along a line in the core. Blue

squares are fluxes in the fast group, magenta squares are fluxes in the second, yellow triangles in the third, and blue x stands for thermal fluxes. The goal is to find a smooth space dependent function to represent the flux.

The calculations confirmed the theoretical prediction concerning the maximum “smoothness” of the spatial distribution of the flux corresponding to the slowing-down (i.e. third energy group) neutrons in the core of VVER reactors. This determined the choice of such a group of neutrons as the most suitable one for performing the interpolation. We omit further details [71–74], spatial dependence is represented by the flux of the third energy group.

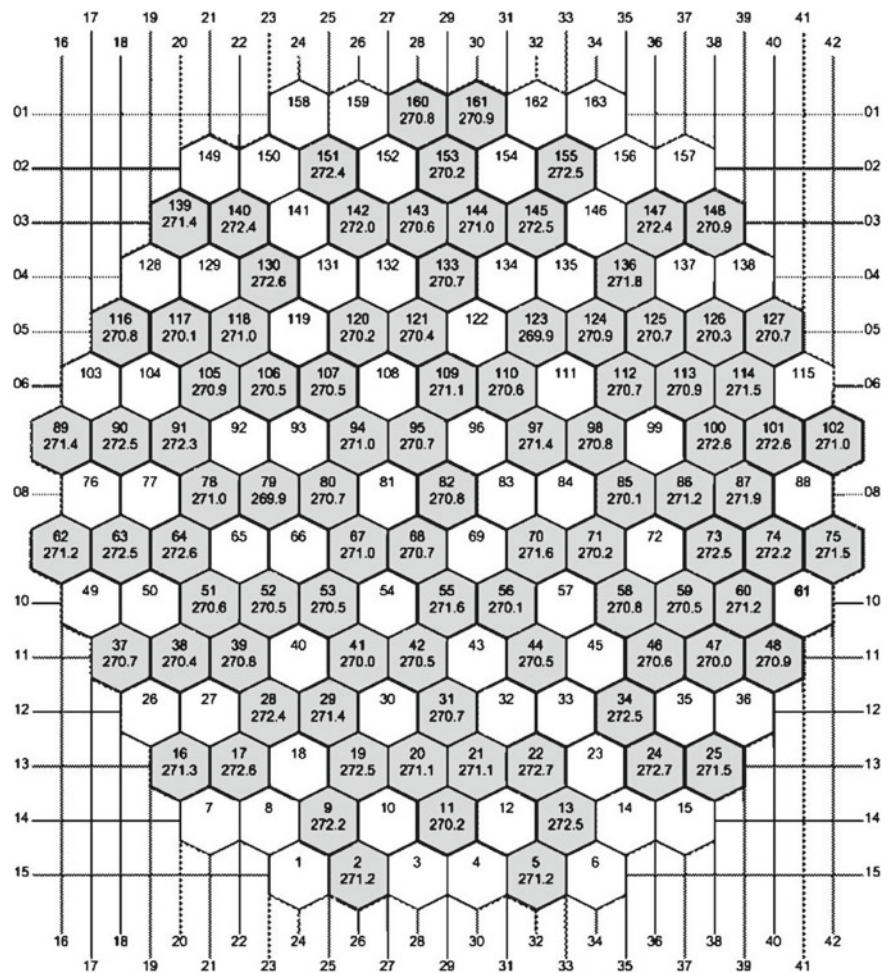


Fig. 2.48 Numbering of the core assemblies and measured coolant temperature at the core outlet in the initial state

We mention one general topic in connection with the VVER cores: the role of the coolant flow distribution in the core has been mentioned in Sect. 2.3.6 in relation with the coolant flow rates of assemblies equipped with thermocouples. In connection with the VVER-1000 unit Kozloduy-6 (Bulgaria), an OECD/NEA benchmark was established [83, 84] and below we briefly mention the conclusions.

The experiment took place on 29th of June 1991 during reactor stat-up of Cycle 1. The goal of the experiment was to determine the mixing coefficients, i.e. the rate of mass exchange, between cold and hot legs and from cold legs to the inlet of fuel assemblies.

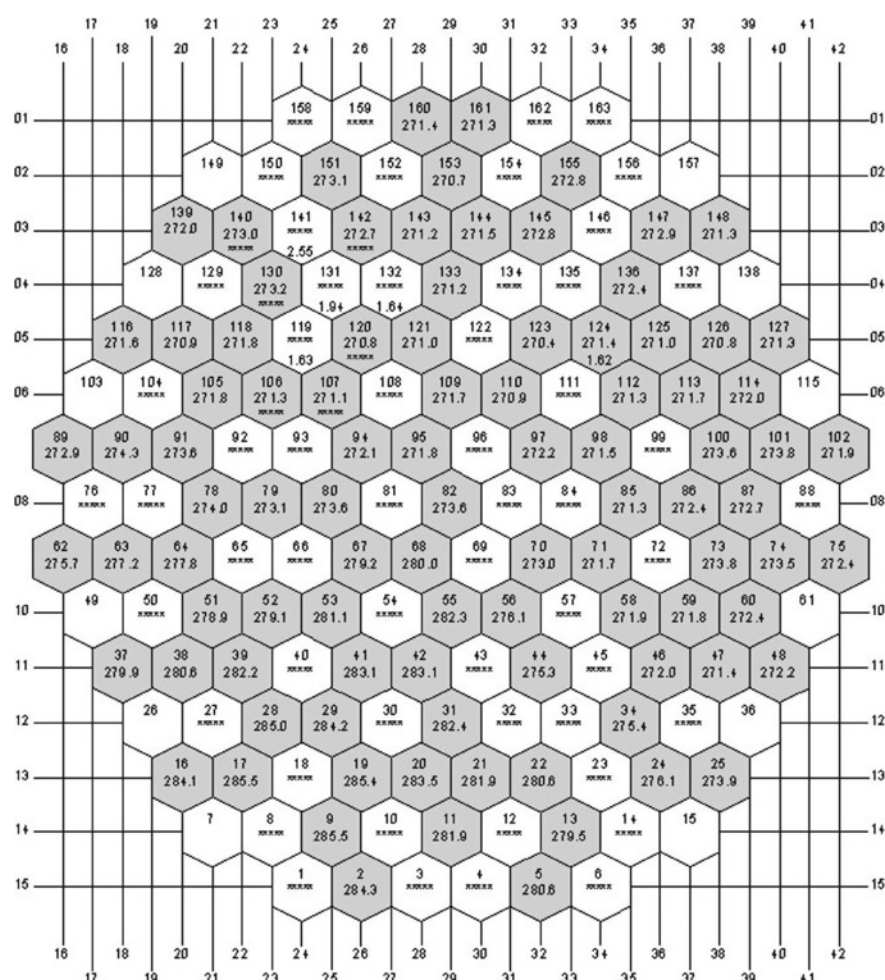


Fig. 2.49 Measured coolant temperature at the core outlet in the final state

Kozloduy unit 6 has four main circulating pumps and the flow rate of a given assembly is a function of those flow rates. Figure 2.47 shows the contributions of the four Main Circulating Pumps (MCPs) in the sectors of the reactor core. The azimuthal distribution of the inlet and outlet nozzles is non uniform, see Fig. 2.47, where the design angles and the measured fabrication angles are also given in table form.

At the beginning of the experiment, four MCP and four SG worked. Thermal power of the unit was 281 MW, this corresponds to 9.36% of the nominal power. Pressure above the core was 15.59 MPa, the nominal value being 15.7 MPa. Coolant temperature at the inlet was 268.6, 19.1 °C below the nominal cold leg temperature. SG levels were at nominal values. For this initial state the temperature rise of each assembly equipped with thermocouples was calculated from measured cold leg and assembly outlet temperatures. Figure 2.48 shows the temperature distribution at the core outlet. The average fuel assembly heat-up was 3.2 °C.

Transient state was initiated at 4:31:00 (EET) by closing the steam isolation valve of SG-1, and isolating SG-1 from feed water. In SG-1 pressure started to grow and stabilized at 6.47 MPa after 20 min. In loop No. 1 the coolant temperature rose by 13–13.5 °C and the mass flow rate reduced by about 3.4%.

The stabilized state of the experiment at 05:06:00 EET is regarded as final state and it has been reached 35 min after the separation of SSG-1. Figure 2.49 shows the the measured assembly outlet temperatures in the final state. The core inlet temperature in the final state is estimated from the measured core outlet temperatures and the estimated average fuel assembly rise of the initial state.

In the frame of the project, a thermal hydraulic code called *TrioU* has been developed at CEA Grenoble. The code is designed large eddy simulation for industrial scale applications, for structured and non-structured grids of several tens of millions nodes [85, 86]. We do not discuss technical details here, but *TrioU* has been tested and widely used, among others in the analysis of Kozloduy-6 problem.

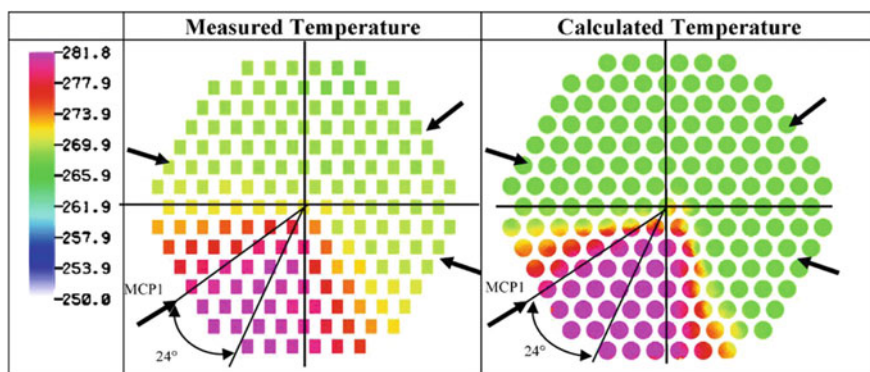


Fig. 2.50 Comparison of measured and calculated temperatures at the core inlet

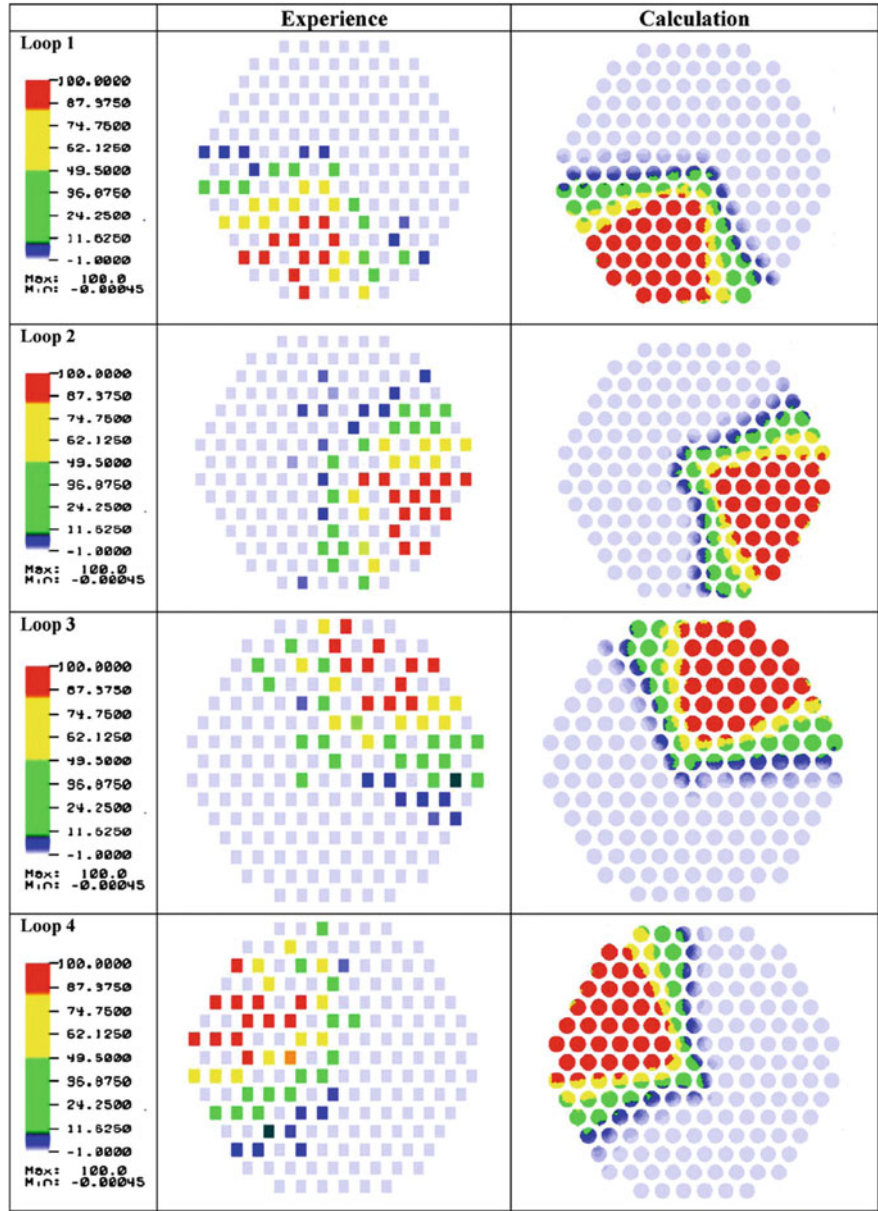


Fig. 2.51 Comparison of loop-to-fuel assembly mixing coefficients measured and calculated for Kozloduy 6

Computational Fluid Dynamics has been dealt with in Subsection A.1.3. *Trio_U* has been designed to model incompressible and low Mach-number flows. The mass, energy, and momentum conservation equations are discretized, the discretization may be structured or unstructured.²³ After discretization the solution of the obtained non-linear algebraic equations are solved by finite element (FE) method. A conjugated gradient method is used to determine the pressure field at each time step. To solve the large volume of calculation, a parallel architecture is used with 256 processors.

Trio_U has been tested on various nuclear safety related applications. Here we mention only calculations concerning the mixing experiment. Figure 2.50 shows the measured and calculated coolant temperatures at the core inlet. Temperature at a non-measured assembly have been obtained by linear interpolation. Small square indicates the measured values, and arrows indicate the axes of the cold leg nozzles. The maximum of the flow center maximum of the flow from MCP1 displaced counter clockwise by appr. 24°. This displacement can be seen also in the *Trio_U* calculations. The correct prediction of the swirl is apparent in the temperatures of assemblies 5, 6, 13, 14, 23, 24.

Another mixing phenomenon is observable between loops and an assemblies. The loop to assembly mixing coefficient K_{ij} is defined as the ratio in percent of coolant from loop i to the flow through assembly j . Calculated and measured K_{ij} coefficients are shown in Fig. 2.51.

References

1. Zernick, W., Currin, H.B., Elyath, E., Previti G.: THINC- a thermal hydraulic interaction code for a semi-open or closed channel. Westinghouse Electric Company, Pittsburgh. WCAP-3704 (1962)
2. Okamoto, Y., Hishida, M., Akino, N.: Hydraulics performance in rod bundles of fast reactor fuel pressure drop vibration and mixing coefficient. Progress in Sodium-Cooled Fast Reactor Engineering, Monaco, IAEA SM-130/5 (1970)
3. Házi, G., Mayer, G., Farkas, I., Makovi, P., El-Kafas, A.A.: Simulation of loss of coolant accident by using RETINA V1.0D code. Ann. Nucl. Energy **28**, 1583–1594 (2001)
4. Baumann, W., Hoffman, H.: Coolant Cross Mixing of Sodium Flowing in Line through Spacer Arrangements. International Heat Transfer Seminar, Trogir, Yugoslavia (1971)
5. Zhukov, A.V., Mouzanov, A.B., Sorokin, A.P. et al.: Inter-Channel Mixing in Cylindrical Pin Bundles. Preprint IPPE-413, Obninsk (1973) (in Russian)
6. Bowling, R.W.: HAMBO A Computer Programme for Subchannel Analysis of the Hydraulic and Burnout Characteristics of Rod Bundles, Part 1, General Description. Report AEEW-R524, London (1968)
7. Plas, R.: FLICA-III-M: Reactors or Test Loops Thermohydraulic Computer Code. Technical Report CEA-N-2418, Saclay (1984)
8. Mironov, Y.V., Shpanski, S.V.: Distribution of two-phase flow parameters over the fuel bundle. Reactors or Test Loops Thermohydraulic Computer Code. Atom. Energy vol. 39 (1975)
9. Zhukov, A.V., Sorokin, A.P., Matyukhin, N.M.: Interchannel Exchange in Fast Reactor Sub-assemblies: Foundation and Physics of the Process. Atomizdat, Moscow (1989). (in Russian)

²³Term regular and irregular mesh is also used.

10. de Groot, S.R., Mazur, P.: Non-Equilibrium Thermodynamics. North-Holland, Amsterdam (1962)
11. Kittel, C.: Introduction to Solid State Physics. Wiley, Amsterdam (2004)
12. Buongiorno, J.: PWR Description. MIT CANES, New York (2010)
13. Papoulis, A.: Probability, Random Variables, and Stochastic processes. McGraw-Hill, Tokyo (1965)
14. Szatmáry, Z.: Evaluation of Measurements, Lecture Note, Budapest Technical University, Budapest, p. 136 (2010) (in Hungarian)
15. Szatmáry, Z.: Data Evaluation Problems in Reactor Physics, Theory of Program RFIT. Report KFKI-1977-43 (1977)
16. On-Line Monitoring for Improving Performance of Nuclear Power Plants, Part 1: Instrument Channel Monitoring, IAEA Nuclear Energy Series No. NP-T-1.1, IAEA, Vienna (2008)
17. Electric Power Research Institute: Cost Benefits of On-line Monitoring. Report EPRI TR-1003572. Palo Alto, CA (2003)
18. Guidelines for the verification and validation of scientific and engineering computer programs for the nuclear industry, an American National Standard, ANSI/ANS-10.4-1987
19. The determination of neutron reaction rate distributions and reactivity of nuclear reactors, an American National Standard, ANS, ANSI/ANS-10.4-1987
20. Thermohydraulics relationships for advanced water cooled reactors, International Atomic Energy Agency, Vienna, IAEA TECDOC-1203 (2001)
21. Raines, K.N., et al.: Effect of pressure, subcooling, and dissolved gas on pool boiling heat transfer from microporous to, square spin-finned surfaces in FC-72. *Int. J. Heat Mass Trans.* **46**, 23–35 (2003)
22. Mardia, K.V., Kent, J.T., Bibby, J.M.: Multivariate Analysis. Academic Press, London (1979)
23. Lucia, D.J., Beran, P.S., Silva, W.A.: Reduced order modeling: new approaches for computational physics. *Progress Aerosp. Sci.* **40**, 51–117 (2004)
24. Holmes, P., Lumley, J.L., Berkooz, G., Rowley, C.W.: Turbulence. Coherent Structures, Dynamical Systems and Symmetry (2012)
25. Makai, M., Temesvári, E.: Evaluation of in-core temperature measurements by the principal components method. *Nucl. Sci. Eng.* **112**, 66–77 (1992)
26. Sorensen, J.M. (ed.): The Reactor Analysis Support Package (RASP), vol. I.: Introduction and Overview, S. Levy Incorporated, Campbell, Calif., Section 5.3 (1986)
27. Siltanen, P., Antila, M., Sorri, V.: Comparison on the HEXBU-3D and BIPR-5 Core Simulation Programs with Measured Data on the LOVIISA-1 Reactor. In: XIth Symposium of VMK, Varna, Sept (1982)
28. Hyman, J.M., Shashkov, M.: Natural discretizations for the divergence, gradient, and curl on logically rectangular grids. *Comput. Math. Appl.* **33**, 81–104 (1997)
29. COBRA-FLX: A Core Thermal-Hydraulic Analysis Code. Topical report, ANP-10311NP, AREVA NP Inc. (2010)
30. Rowe, D.S.: COBRA IIIc: A Digital Computer Program for Steady State and Transient Thermal-Hydraulic Analysis of Rod Bundle Nuclear Fuel Elements. Report BNWL-1695, Pacific Northwest Laboratories, Richland, Washington (1973)
31. Rowe, D.S., Wheeler, C.L., Fitzsimmons, D.E.: An Experimental Study of Flow and Pressure in Rod Bundle Subchannel Containing Blockages, Report BNWL-1771, Pacific Northwest Laboratories (1973)
32. ANSYS CFX Release 12.0, ANSYS Inc. Canonsburg, PA 15317, USA (2009)
33. Tennekes, H., Lumely, J.L.: A First Course in Turbulence. MIT Press, Cambridge (1972)
34. Horelik, N., Herman, B.: MIT Benchmark for Evaluation and Validation of Reactor Simulations, release rev. 1.1.1. MIT Computational Reactor Physics Group, 30 Oct 2013
35. Huang, K.: Statistical Mechanics. Wiley, New York (1963)
36. Orechwa, Y., Makai, M.: Application of Finite Symmetry Groups to Reactor Calculations, INTECH. In: Mesquita, Z. (ed.) Nuclear Reactors, INTECH (2012). <http://www.intechopen.com/articles/show/title/applications-of-finite-groups-in-reactor-physics>

37. Makai, M.: Group Theory Applied to Boundary Value Problems with Applications to reactor physics. Nova Science, New York (2011)
38. Strang, G., Fix, G.J.: An Analysis of the Finite Element Method. Prentice-Hall, Englewood Cliffs, NJ (1973)
39. Hegedüs, C.J.: Generating conjugate directions for arbitrary matrices by matrix equations, I. Comput. Math. Appl. **21**, 71–85 (1991)
40. Palmiotti, G., Lewis, E.E., Carrico, C.B.: VARIANT: VARIational Anisotropic Nodal Transport for Multidimensional Cartesian and Hexagonal Geometry Calculation, Report ANL-95/40, October 1995. Argonne National Laboratory, IL (1995)
41. Laletin, N.I., Elshin, A.V.: Derivation of finite difference equations for the heterogeneous reactor. Report IAE-3281/5, 1, Square fuel assemblies, Kurchatow Institute, Moscow, (1980) and Laletin, N. I. and Elshin, A. V.: *Derivation of finite difference equations for the heterogeneous reactor*, Report IAE-3281/5, 2, Square, triangular, and double lattices, Kurchatow Institute, Moscow (1981) (both in Russian)
42. Arnold, L.: Stochastic Differential Equations: Theory and Applications. Wiley, Amsterdam (1974)
43. Janossy, L.: Theory and the Practice of the Evaluation of Measurements. Oxford University Press, Oxford (1965)
44. Argonne Code Center Benchmark Problem Book, report ANL-7416, Argonne, IL (1975)
45. Szatmáry, Z.: The VVER Experiments: Low Enriched Uranium—Light Water Regular and Perturbed Hexagonal Lattices (LEU-COMP-THERM-016) in OECD NEA International Handbook of Evaluated Criticality Safety Benchmark Experiments, Volume IV
46. TRACE 5.0, Assessment Manual, Appendix A, Report NUREG/IA-0412: Fundamental Validation Cases, US Nuclear Regulatory Commission, Washington DC
47. ROSA-III Experimental Program for BWR LOCA/ECCS Integral Simulation Tests, JAERI-1307 (1987)
48. Szabados, L., Ézsöl, G., Perneczky, L., Tóth, I.: Results of the experiments performed in the PMK-2 facility for VVER safety studies, Vol. I–II. Akadémiai Kiadó, Budapest (2007)
49. Pál, L., Makai, M.: Statistical Considerations on Safety Analysis. [arXiv:physics/0511140v1](https://arxiv.org/abs/physics/0511140v1) [physics.data-an]. 16 Nov 2005
50. Tukey, J.W.: Non-parametric estimation I. Validation of order statistics. Ann. Math. Stat. **16**, 187–192 (1945)
51. Tukey, J.W.: Non-parametric estimation II. Statistically equivalent blocks and tolerance regions-the continuous case. Ann. Math. Stat. **18**, 187–192 (1947)
52. Tukey, J.W.: Non-parametric estimation III. Statistically equivalent blocks and tolerance regions-the continuous case. Ann. Math. Stat. **19**, 30–39 (1948)
53. Fraser, D.A.S., Wormleighton, R.: Non-parametric estimation IV. Ann. Math. Stat. **22**, 294 (1951)
54. Maiorov, L.: The Monte Carlo Codes and Their Applications. Final Reports of TIC, vol. 2, Theoretical Investigations of the Physical Properties of WWER-Type Uranium-Water Lattices, pp. 70–149, Akadémiai Kiadó, Budapest (1994)
55. Gubbins, M.E., Roth, M.J., Taubman, C.J.: A General Introduction to the Use of WIMS-E Modular Program. Report AEEW-R-1329. Winfrith, UK (1982)
56. Guba, A., Makai, M., Pál, L.: Statistical aspects of best estimate method-I. Relat. Eng. Syst. Saf. **80**, 217–232 (2003)
57. Végh, J., et al.: Core analysis at Paks NPP with a new generation of VERONA. Nucl. Eng. Des. **238**, 1316–1331 (2008)
58. Lux, I., et al.: Experiences with the upgraded VERONA-u VVER-440 core monitoring system. In: IAEA Specialists Meeting on Advanced Information Methods and Artificial Intelligence in NPP Control Rooms, Halden, Norway, 13–15 Sep (1994)
59. Végh, J., et al.: Upgrading of the VERONA Core Monitoring System at Unit 2 of the Hungarian Paks NPP. In: Proceedings of the OECD NEA/IAEA International Symposium on NPP Instrumentation and Control, Tokyo, Japan, 18–22 May 1992

60. Major, C., et al.: Development and application of advanced process monitoring tools for VVER-440 type NPPs. In: Proceedings of the IAEA Technical Meeting on On-line Condition Monitoring of Equipment and Processes in Nuclear Power Plants Using Advanced Diagnostic Systems, Knoxville, Tennessee, USA, 27–30 June (2005)
61. Végh, J., et al.: Utilization of modern hardware and software technologies for the creation of process information systems providing advanced services and powerful user interfaces. In: Proceedings of the IAEA Technical Meeting on Impact of Modern Technology on Instrumentation and Control in Nuclear Power Plants, Chatou, France, 13–16 Sept (2005)
62. Pós, I., et al.: An advanced tool of nuclear reactor core analysis for reactor physicists: VERONA-e expert system. In: Proceedings of the 16th Symposium of AER, Bratislava, Slovakia, 25–26 Sept (2006)
63. Patai Szabó, S., Pós, I.: Self power neutron detector model and its validation in the C-PORCA code. In: Proceedings of the 11th Symposium of AER, Csopak, Hungary, 24–28 Sept (2001)
64. Krysl, V., et al.: Theoretical foundation of modular macrocode system MOBY-DICK. Report KFKI-ZR-6-551/1987 (in Russian)
65. Ernst, D., Milisdörfer, L.: 10 years of experience with Westinghouse fuel at NPP Temelin. Prague, 1–3 Nov (2010)
66. William, A.B., et al.: The Whitestar development project: WESTINGHOUSEs next generation core design simulator and core monitoring software to power the nuclear renaissance. In: International Conference on Mathematics, Computational Methods and Reactor Physics, (M & C 2009), Saratoga Springs, New York, 3–7 May (2009)
67. DiGiovine, A.S., No ěl, A.: GARDEL-PWR: studsvik's online monitoring and reactivity management system. In: Proceedings of Advances in Nuclear Fuel Management III (ANFM 2003), Hilton Island, South Carolina, USA, 5–8 Oct 2003
68. Berg, Ø., Hval, S., Scot, U.: The core surveillance system SCORPIO and its validation against measured pressurised-water reactor data. *Atomkernener. Kerntech.* **45**(4), 271–276 (1984)
69. Berg, Ø et al.: User interface design and system integration aspects of core monitoring systems. Core monitoring for commercial reactors: improvements in systems and methods (2000)
70. Molnár, J., Sikora, J.: The SCORPIO-VVER New Upgraded Version with Enhanced Accuracy and Adopted to the IEC Requirements, EHPG 2013, MTO, 10th 15th March 2013. Storefjell Resort Hotel, Norway (2013)
71. Mitin, V.I., Semchenkov, J.M., Kalinushkin, A.E.: Modernization in-core monitoring system of VVER-1000 reactors (V-320) by fuel assemblies with individual characteristics using. In: Proceedings on AER-17
72. Mitin, V.I.: Technical means of in-core control on VVERs. *Atomn. Energy* **60**(1), 7–11 (1986)
73. Mitin, V., Tsimbalov, S.: Power distribution measurement and control for VVER1000 cores. Specialists' Meeting on In-Core Instrumentation and Reactor Core Assessment, Pittsburgh, 1–4 Oct (1991)
74. Mitin, V., Kalinushkin, A., Tsimbalov, S., Tachennikov, V., et al.: IRC system in VVER reactors. History of creation and tendencies of development. Paper at IAAE Task Group Conference, Pen State University (1996)
75. Sidorenko, V.D., et al.: Spectral code TVS-M for calculation of characteristics of cells, supercells and fuel assemblies of VVER-type reactors. In: Proceedings of 5-th Symposium of the AER, Dobogókő, Hungary, 15–20 Oct (1995)
76. Gomin, E.A., Marin, S.V., Tzimbalov, S.A.: Calculation of β emitting Transfer function. Preprint IAE No. 5755/5, Moscow (1984) (in Russian)
77. The MCU-RFF 2000 with Constant Library DLC/VCU Dat, Moscow (2000)
78. Tzimbalov, S.A., Kovel, A.I.: Transfer Function and Material Constant Analysis in the Present State as Function of Reactor Prehistory. Report RNC KI, Moscow (2000)
79. Experience with the Reactor Control System SVRK-M Relating Primary Loop Temperature and Power Distribution Control, Protocoll AES Kozloduy, 19 June 2004
80. Experience with the Reactor Control System SVRK-M Relating Primary Loop Temperature and Power Distribution Control, Protocoll AES Kozloduy, 05 July 2004

81. Mitin, V.I., Mitina, O.V.: A method for determining exact values from several independent measurement types. *Atomn. Energy*. (2007) (in Print)
82. Lizorkin, M.P.: Model problem solutions with using PERMAK. Final Report of TIC, Vol. 2, Theoretical Investigations of the Physical Properties of WWER-Type Lattices, Akadémiai Kiadó (1994)
83. Bieder, U., et al.: Simulation of mixing effects in a VVER-1000 reactor. *Nucl. Eng. Des.* **237**, 1718–1728 (2007)
84. Böttcher, M., Krüßman, R.: Primary loop study of a VVER-1000 reactor with special focus on coolant mixing. *Nucl. Eng. Des.* **240**, 2244–2253 (2010)
85. Bieder, U. et al.: PRICELESS: an object oriented code for industrial LES. In: *Proceedings of the 8th Annual Conference of the CFD Society of Canada*, 11–13 June (2002)
86. Calvin, C., Cueto O., Emonot, P: An object-oriented approach to the design of fluid mechanics software. *Math. Model. Numer. Anal.* **36**(5). <http://www.edpsciences.org/articlesm2an/abs/2002/05/contents/contents>

Reactor Core Monitoring

Background, Theory and Practical Applications

Makai, M.; Végh, J.

2017, XXIX, 423 p. 96 illus., 76 illus. in color., Hardcover

ISBN: 978-3-319-54575-2